Thesis for the Master's degree in chemistry

Viet Hung Nguyen

Development of methods for the determination of rare earth elements as trace impurities in high-purity rare earth oxides and rare earth elements by ICP-MS and HPLC-ICP-MS

60 study points

DEPARTMENT OF CHEMISTRY

Faculty of mathematics and natural sciences

UNIVERSITY OF OSLO 12/2013

Preface

This graduate study has been carried out at the Department of Chemistry, University of Oslo, in the period of January 2012 to December 2013. My supervisors have been Professor Grethe Wibetoe and Ph.D Dejene Kifle.

I would like to thank my supervisors for their excellent guidance and for giving me an interesting task to work with these past two years. I would also like to thank senior engineer Anne-Marie Skramstad for all her much appreciated help with the analysis instruments and helpful discussions.

I would also want to thank my fellow students, Tina and Marian, for all their helpful tips and fun conversations. I especially want to thank my friends for reminding me that there is a life beyond the laboratory, for their moral support and encouragement. Most of all, I want to thank them for all the crazy adventures we have been through and for the future ones to come.

Lastly, I want to thank my family. To my mom and dad for raising me to be the man I am today, and to my brothers and sister for encouraging me to pursue my goals and dreams. Their love and support are invaluable.

Oslo, Norway, December 2013

Viet Hung Nguyen

Table of contents

Abstract

Rare earth elements (REEs) are greatly demanded in modern technology industries and are widely used in several technological applications. The ability of the REEs to carry out their unique properties in their specific applications is dependent on the purity of the respective element, as the presence of impurities can affect both their physical and chemical properties. The main metal-impurities in high-purity REOs are basically trace amounts of REEs. This study focuses on the development of methods in order to determine the purity of standard solutions of Yb and Eu, and high-purity Yb_2O_3 by the impurity approach, utilizing inductively coupled plasma mass spectrometry (ICP-MS) hyphenated with high performance liquid chromatography (HPLC) for online separation of the REEs.

Due to the highly concentrated matrix element, certain spectral and non-spectral interferences are commonly associated with the determination of REEs as trace impurities, such as formation of polyatomic ions causing mass overlaps with REEs of interest, and signal suppression effects which reduce the signal intensity of the REEs. In this study, non-spectral interferences were handled by dilution and were found to be not observable when the matrix element concentration was ≤ 10 µg mL^{-1}. Several attempts were made in order to eliminate the contribution of polyatomic ions to the signal intensities observed at masses of interest. Formation of ^{174}YbH and ^{153}EuO hindered the determination of Lu and Tm in their respective sample solutions of Yb and Eu. By altering the plasma conditions from its standard operational conditions, the signal intensity of ^{174}YbH was reduced, but the reduction was due to an overall decrease in instrumental sensitivity. Separation of the matrix elements from their respective interfered analytes were performed with various separation systems, such as ion pair chromatography (IPC) and extraction chromatography (EXC). IPC utilizing the OS-HIBA and HFBA-HIBA systems were found to be either unsuitable or unsuccessful for online separation of Lu from Yb and Eu from Tm. EXC with the HNO_3-HDEHP system did successfully separate Lu from Yb and Eu from Tm. Methods developed with the HNO_3-HDEHP system can be used for the determination of spectrally interfered REEs and as a diagnostic tool to investigate the contribution of polyatomic ions to the signal intensities of the interfered analytes. The methods developed were able to determine the purity of the standard solutions of Yb and Eu, and high-purity Yb_2O_3, which all were found to be > 99.99 % pure.

Abbreviations

cps	Counts per second
EXC	Extraction chromatography
HDEHP	Dis-(2-ethylhexyl)phosphoric acid
HFBA	Heptafluorobutyric acid
HIBA	α-hydroxyisobutyric acid
HPLC	High performance liquid chromatography
HR	High resolution
HREE(s)	Heavy rare earth element(s)
ICP-MS	Inductively coupled plasma mass spectrometry
ICP-OES	Inductively coupled plasma optical emission spectrometry
ICP RF	ICP radiofrequency
INAA	Instrumental neutron activation analysis
IPC	Ion pair chromatography
IPR	Ion pair reagent
Ln(s)	Lanthanoid(s)
LOD	Limit of detection
LOQ	Limit of quantification
LREE(s)	Light rare earth elements
OS	n-octane sulphonate
PTFE	Polytetrafluoroethylene
QP	Quadrupole
REE(s)	Rare earth element(s)
REO(s)	Rare earth oxide(s)
XRF	X-ray fluorescence

1. Introduction and background

1.1. The rare earth elements

The rare earth elements (REEs) consist of 17 elements; scandium (Sc), yttrium (Y) and the lanthanoids. The lanthanoids (Lns) are comprised of lanthanum (La), cerium (Ce), praseodymium (Pr), neodymium (Nd), promethium (Pr), samarium (Sm), europium (Eu), gadolinium (Gd), terbium (Tb), dysprosium (Dy), holmium (Ho), erbium (Er), thulium (Tm), ytterbium (Yb) and lutetium (Lu) [1]. These elements share many common chemical and physical properties [2]. Although the REEs are widely dispersed, they are found in the Earth's crust and mantel in appreciable amount, hence the term "rare" in rare earth elements may be misleading. All of the REEs have naturally occurring stable isotopes, with the exception of Pm which only have unstable and radioactive isotopes [3, 4]. Henceforth, Pm is excluded in future references of REEs and Lns in this study. The REEs have between 2 to 7 stable naturally occurring isotopes, with the exception of Sc, Y, Pr, Tb, Ho and Tm, which are mono-isotopic.

1.2. Occurrence and application of the REEs

REEs are widely distributed in different mineral classes and structural types, but only a few are recovered for commercial production of rare earth oxides (REOs). The mineral species that are of commercial interest for recovery are xenotime, monazite, bastnasite and rare earth bearing clay. Bastnasite is a carbonate-rich mineral, while xenotime and monazite are phosphate-rich minerals. Although the content of REEs in rare earth bearing clay is low, production of REOs can be achieved by simple processes compared to the other mineral species [4]. Table 1.2.1 shows the typical abundance of the lanthanoids in the different mineral species. As it can be seen from the table, the most abundant REEs in monazite and bastnasite are Y, La, Ce, Pr and Nd. Monazite contains a higher amount of Tb, Dy, Ho, Er, Tm, Yb and Lu compared to bastnasite, of which these elements are present in trace amounts. Xenotime contains high amounts of Y and a significant amount of the REEs from Tb to Lu compared to the other minerals [5]. Generally, the REEs from Sm to Lu are less abundant compared to the other REEs and are also the most expensive of the REEs.

Table 1.2.1: Typical abundance of the lanthanoids in xenotime, monazite and bastnasite. The values are in percentage* [5].

	La	Ce	Pr	Nd	Pm	Sm	Eu	Gd	Tb	Dy	Ho	Er	Tm	Yb	Lu	Y
Monazite	20	43	4.5	16	0	3	0.1	1.5	0.05	0.6	0.05	0.2	0.02	0.1	0.02	2.5
Bastnasite	33.2	49.1	4.3	12	0	0.8	0.12	0.17	**160**	**310**	**50**	**35**	**8**	**6**	**1**	0.1
Xenotime	0.5	5	0.7	2.2	0	1.9	0.2	4	1	8.6	2	5.4	0.9	6.2	0.4	60

*Bold values are in parts per million.

China has the largest production site and one of the largest deposits of REEs, and produces around 97 % of all REEs in the world market. There is a great demand for REEs in modern technology industries. They are of importance for the miniaturization of several technological applications, such as mobile phones and laptops. They are also of key importance for green technology. The REEs from Tb to Lu are generally used in high tech applications such as fibre optics in communication (Er) and as phosphors (Tb) [6], while the elements prior to Tb are mainly used in the production of catalysts for fluid cracking and catalytic converters for automobiles, glass and metallurgical industries, phosphors, batteries for hybrid cars, permanent magnet applications for electric motors, wind turbine generators and much more, as can be seen in table 1.2.2 [7, 8]. Catalysts, glassmaking, lighting and metallurgy consume 59 % of the total consumption of REEs, while battery alloys, ceramics and permanent magnets consume the remaining 41 %. La, Ce, Pr, Nd and Dy constitute the majority of REEs used in their respective fields of applications [7].

Table 1.2.2: Various commercial products and applications where the REEs play a key role [8].

Rare earth product	Application	Primary rare earth elements
Magnets	Motors, power generation, magnetic resonance imaging instruments (MRIs), magnetic storage devices, magnetic refrigeration	Nd, Pr
Phosphors	Cathode ray tubes, liquid crystal displays (LCDs), computers, X-rays, TVs, light bulbs	Eu, Tb, Y
Metal alloys	NiMH* batteries, fuel cells, steel, lighter flints, aluminium, magnesium, cast iron, super alloys	Various REEs
Polishing	LCD and plasma TVs and monitors, silicon wafers and chips	Ce, La, Pr
Catalysts	Petroleum refining, methanol refining, syngas production, ethanol production, diesel additives, industrial pollution scrubbers	Ce, La, Nd, Pr
Glass and mirrors	Optical glass, UV resistant glass, thermal control mirrors	Gd, La, Y

*M is the rare earth element.

1.3. Chemistry and classification of the REEs

The REEs can be divided into light rare earth elements (LREEs) and heavy rare earth elements (HREEs). LREEs consist of Sc and the Lns from La to Gd, while the HREEs consist of the Lns from Tb to Lu [9]. The LREEs have larger ionic (+3) radii compared to the HREEs and consecutively larger coordination number, typically 9. The HREEs have smaller ionic

(+3) radii compared to the LREEs and their coordination number is typically 8 [10]. Although Y is the second lightest of REEs in terms of atomic mass, it is usually grouped with the heavier lanthanides. Y^{3+} has many similar properties as the HREEs in their +3 oxidation state, which is due to similarities of the radii of Y^{3+} (104 pm) and Ho^{3+} (104.1 pm). The similarities in radii also makes the separation of Y and Ho especially difficult [3, 10].

The Lns in their solid state are reactive and electropositive metals. Their reactivity is dependent on their sizes, of which the metals with the largest radii are the most reactive. In aqueous solutions, they yield hydrous oxides and the metals dissolve rapidly in dilute acids to give aqueous solutions of Ln^{3+} salts [3]. Rare earth oxides are strongly basic and are insoluble in water, but absorb water to form hydroxides. When the REOs react with diluted acid and kept at pH $\leq$ 5, they dissolve in solutions which typically yield $[Ln_2(H_2O)_x]^{3+}$ ions [11, 12]. The reaction of REOs with acid gives hydrated salts. When anions can coordinate, a wide variety of species can be obtained. E.g. with nitrate, species such as $[Ln(NO_3)_3.(H_2O)_x]$ are obtained, where x = 5 for La and Ce, and x = 4 for Pr-Yb and Y. The nitrate salt is soluble in water [11].

The Lns share a common and dominating oxidation state of +3, which is the most stable oxidation state in aqueous solutions. However, Ce^{4+} and Eu^{2+} are also stable in aqueous solutions. Oxidation states of +2 and +4 do occur for several lanthanides, especially in their solid states. Ln^{2+} (Nd, Sm, Eu, Dy, Tm, Yb) and Ln^{4+} (Pr, Nd, Tb, Dy) are stable in their solid states, but are unstable in water, with the exception of Eu^{2+} [3, 12]. The +3 oxidation state corresponds to the filling of their 4f-orbitals when going from Ce^{3+} to Lu^{3+} within the group, as can be seen in table 1.3.1. The dominating +3 oxidation state is due to the stabilizing effects exerted on the different orbitals as the ionic charge increases. As successive electrons are removed from a neutral lanthaniod atom, the stabilizing effect on the orbitals in the order of 4f > 5d > 6s, this being the order in which the orbitals penetrate through the inert core of electrons towards the nucleus [3]. 4f-orbitals do not participate significantly in bonding as they do not overlap with ligand orbitals [13].

The hard-soft acid-base (HSAB) theory classifies Ln^{3+} as hard acids [12], or class *a metal ions*, which are characterized by their high charge-to-size ratio where the metal ions are usually in their $\geq$ +3 oxidation states. The general principle of the HSAB-theory states that complex formation between ions prefers the same classes of acids and bases, i.e. hard acids

prefer hard bases. Ln^{3+} forms the most stable complexes with hard bases, or *class a ligands*, which are typically small oxygen-donor electronegative ligands [14].

Table 1.3.1: Electron configurations of Lns and Ln^{3+} taken from [10].

Name	**Symbol**	**Atomic number (Z)**	**Electron configuration (Ln)**	**Electron configuration (Ln^{3+})**
Lanthanum	La	57	$[Xe]5d^16s^2$	[Xe]
Cerium	Ce	58	$[Xe]4f^15d^16s^2$	$[Xe]4f^1$
Praseodymium	Pr	59	$[Xe]4f^36s^2$	$[Xe]4f^2$
Neodymium	Nd	60	$[Xe]4f^46s^2$	$[Xe]4f^3$
Promethium	Pm	61	$[Xe]4f^56s^2$	$[Xe]4f^4$
Samarium	Sm	62	$[Xe]4f^66s^2$	$[Xe]4f^5$
Europium	Eu	63	$[Xe]4f^76s^2$	$[Xe]4f^6$
Gadolinium	Gd	64	$[Xe]4f^75d^16s^2$	$[Xe]4f^7$
Terbium	Tb	65	$[Xe]4f^96s^2$	$[Xe]4f^8$
Dysprosium	Dy	66	$[Xe]4f^{10}6s^2$	$[Xe]4f^9$
Holmium	Ho	67	$[Xe]4f^{11}6s^2$	$[Xe]4f^{10}$
Erbium	Er	68	$[Xe]4f^{12}6s^2$	$[Xe]4f^{11}$
Thulium	Tm	69	$[Xe]4f^{13}6s^2$	$[Xe]4f^{12}$
Ytterbium	Yb	70	$[Xe]4f^{14}6s^2$	$[Xe]4f^{13}$
Lutetium	Lu	71	$[Xe]4f^{14}5d^16s^2$	$[Xe]4f^{14}$

1.3.1. The lanthanide contraction effect

Due to the stability differences of the orbitals, the 4f-orbital has an imperfect shielding effect on the outer electrons located in the d- and s-orbitals. As the nucleus charge increases throughout the Lns, the radii of Ln^{3+} ions decrease, which can be observed in figure 1.3.1. The observed effect of decreasing ion size with increasing atomic number is called the lanthanide contraction effect. The reduction in size from one Ln^{3+} to the next makes their separation possible, but the smallness and regularity of the reduction makes the separation difficult. The common oxidation state combined with the lanthanide contraction effect gives REEs many similar chemical and physical properties [2, 3].

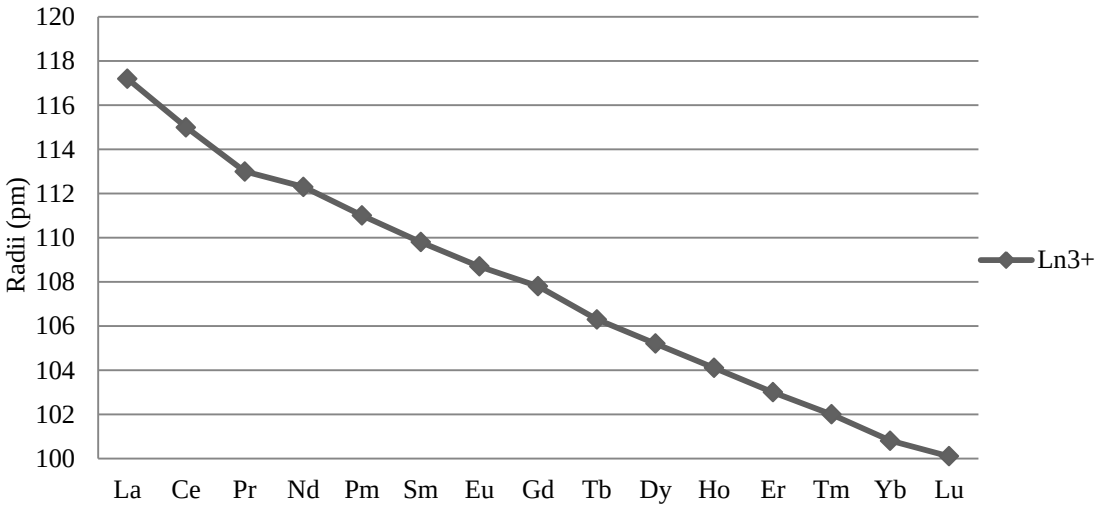

Figure 1.3.1: The lanthanide contraction effect shown by the decreasing Ln^{3+} size with increasing atomic number. Values for the radii of the Lns are taken from [10].

1.3.2. The tetrad effect

In certain liquid-liquid extraction systems where Ln^{3+} undergoes complex formation, a periodic behaviour called the tetrad effect can be observed [15, 16]. Figure 1.3.2 shows that by plotting the logarithm of the stability constants for these complexes in terms of free energy of extraction versus the atomic number Z of the REEs, the tetrad effect can be observed [17]. The tetrad effect is dependent on the stability constants of complex compounds and the atomic number of the Lns [18], and divides the 4f-block elements of which the Lns belong to, into 4 segments, f^0-f^3 (La, Ce, Pr, Nd), f^4-f^7 (Pm, Sm, Eu, Gd), f^7-f^{10} (Gd, Tb, Dy, Ho) and f^{11}-f^{14} (Er, Tm, Yb, Lu) (see figure 1.3.2). Due to the stabilization energy of the inter-electron repulsion energy of the f-electrons, separation of certain neighbouring Lns is more difficult than of other Lns. The 4f-electron configuration has extra stability at quarter (f^3-f^4), half (f^7), three-quarter (f^{10}-f^{11}) and full (f^{14}) electron f-orbital [19]. According to the tetrad effect, separation of the consecutive elements that lie in the zone of the shallowest curvature of each tetrad of the distribution ratios (Pr - Nd, Eu - Gd, Dy - Ho and Yb - Lu) is much more difficult than that of other pairs [17, 19].

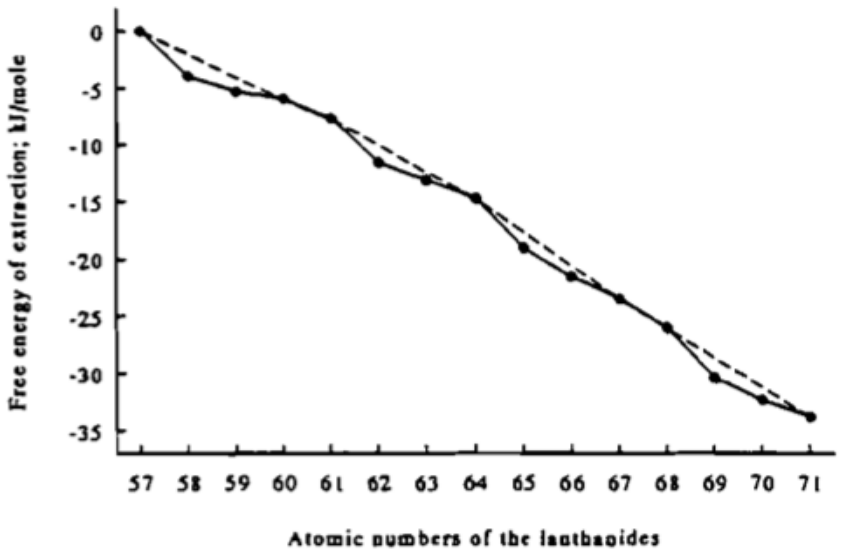

Figure 1.3.2: Stability constants in terms of free energy in extraction of the Lns versus their atomic numbers. The figure is taken from [17].

1.4. State of the art for purity determination of high-purity REEs and REOs

As the REEs are widely used in different applications of modern technology, the ability of these elements to carry out their specific properties in certain product devices is determined by the purity of the element, as the presence of impurities can affect their physical and chemical properties. The tolerated levels of trace-metal impurities in high-purity materials have declined as technology has evolved, where efficiency and minimization are the dominating factors. Manufacturers can provide REOs of high-purity quality up to 99.9999 % pure, where the individual trace metal impurities are in the pg g^{-1} levels [20, 21]. The purity of the REEs depends on their role in their end products; and as a result, prices of these elements greatly depend on their purity.

Direct purity determination of high-purity REOs, which are > 99.95 % pure, requires an analytical method that gives less than 0.05 % measurement uncertainty. This is practically not possible for most analytical techniques. Therefore, the most common method for purity determination of such high-purity materials is performed by the impurity approach, of which the impurities that are most likely to occur are measured by as many different analytical techniques as necessary. The purity of the material is then determined by subtracting the total amount of impurities from the maximum purity of 100 %. The purity of a material can be

characterized by the presence of metallic impurities or total impurities. Total impurities include impurities in the form of metals, non-metals, anions, oxides and residuals, which means that the reported purity of a material characterized only by the presence of metallic impurities can be much higher when compared to the determination of total impurities. The reported purity of a material is therefore determined by how many impurities the operator is investigating [22].

Conventionally, the REEs as trace impurities have been determined by different techniques such as instrumental neutron activation analysis (INAA), X-ray fluorescence (XRF) and inductively coupled plasma atomic emission spectrometry (ICP-OES). These techniques have shown to be unsuitable for industrial applications or have inadequate detection limits [21]. INAA offers high sensitivity and low detection limits for certain REEs, but the technique can only determine a limited number of REEs at a time due to matrix activation and other interferences. INAA requires special equipment, such as a nuclear reactor as the neutron source, produces low-level radioactive waste and is time-consuming, which is unsuitable for routine analysis work [23-26]. XRF also has the capability for multi-element quantification of trace elements in various sample types, but the detection limits for medium- to high-Z elements are typically in the μg g^{-1}-range, but can be enhanced by pre-concentrating the analytes prior to analysis. The detection limits offered by XRF for many metals are inadequate [21, 26-28]. ICP-OES offers rapid multi-element detection over a wide concentration range, but its detection limit is in the μg g^{-1}-area, which is insufficient for the determination of REEs as trace impurities in high-purity materials. The resulting spectra are also more complicated relative to the inductively coupled plasma mass spectrometer and many of the REEs are subjected to severe spectral overlaps [26, 29].

The determination of REEs as trace impurities in high-purity REEs and REOs requires an instrumental technique with low detection limits. Inductively coupled plasma mass spectrometry (ICP-MS) provides rapid analysis time, high sensitivity, multi-element determination capability, wide linear dynamic range and high detection power compared to the former techniques [30]. The ICP-MS is usually equipped with quadrupole (QP) mass analyzers or high-resolution (HR) spectrometers based on the double-focusing magnetic sector design. QP mass analyzers represent approximately 85 % of all ICP-MS systems installed worldwide, but limitations in their resolving power have led to the development of HR double-focusing magnetic sectors. A QP-ICP-MS has typically around 300 resolving power (10 % valley definition), while an HR-ICP-MS offers up to 10 000 resolving power (10

% valley definition). The HR-ICP-MS has the capability of resolving the majority of spectral interferences, but the transmission of ions decreases as the resolving power increases, which results in worsened sensitivity. However, HR-ICP-MS offer higher detection power than the QP-ICP-MS when it is operated at the same resolving power as a QP-ICP-MS. Other benefits of the HR-ICP-MS also include high sensitivity combined with low background levels [31, 32].

Determination of REEs as trace impurities in high-purity REEs and REOs by ICP-MS is often troubled by spectral and non-spectral interferences. Spectral interferences occur in the form of isobaric and polyatomic interferences of which the species have same masses as the analyte masses. Polyatomic ions are usually formed in the cooler regions of the plasma due to the highly concentrated matrix element. The polyatomic ions, such as hydrides and oxides of the matrix element, can cause mass overlaps on analytes of interest. Non-spectral interferences that occur are often signal suppression effects on the analytes due to the extreme difference in concentration between the matrix element and the analytes, which may defocus the ions and lead to reduced signal intensities and inaccurate results. The highly concentrated matrix element can suppress the signal intensity of the REEs, reducing the sensitivity for the analytes [33, 34]. The spectral peak shape, especially at the low-mass and high-mass tail, is determined by the abundance sensitivity of the quadrupole. The abundance sensitivity is defined as the ratio of the maximum ion current recorded at a mass M to the ion current arising from the same species recorded at an adjacent mass (M ± 1) [35]. It is affected by several factors of which the biggest impact is the motion and kinetic energy of the ions as they enter and exit the quadrupole. The abundance sensitivity specification for all quadropoles is always worse on the low-mass side than the high-mass side and is typically 1×10^{-6} at M – 1 and 1×10^{-7} at M + 1, which means that an interfering peak of 1 million counts per second (cps) at M – 1 would produce a background of 1 cps at M, while an interfering peak of 10 million cps at M + 1 would produce a background of 1 cps at M [36].

Formation of polyatomic ions is the most significant problem when determining trace impurities of REEs in high-purity REEs and REOs. The non-spectral interferences in the form of signal suppression of analytes are often handled by diluting the sample solution to an appropriate concentration [33, 37], while spectral interferences have been approached by several different methods such as measuring double charged REEs at their half masses, and by separating the matrix element from analytes of interest, e.g. solvent extraction and chromatographic separation, prior to quantification with ICP-MS. A study which measured

doubled charged REEs at half their masses in highly concentrated REE sample solutions, showed that the sensitivity of the analytes were greatly reduced and certain analytes were not quantifiable at half their masses [38]. Separation of the matrix element from the spectral interfered analytes by solvent extraction and chromatography prior to quantification of trace impurities of REEs with ICP-MS has shown to be more successful. Several studies have determined the purity of high purity REOs, such as La_2O_3, Pr_6O_{11}, Nd_2O_3 and Gd_2O_3, by chromatographic separation of the rare earth matrix element from the analytes prior to quantification with ICP-MS in order to eliminate spectral interferences caused by polyatomic ions. Purities of the different REOs were determined to be > 99.9 % pure [39-42]. In other studies, solvent extraction was used for separating the Ce matrix element from the analytes prior to quantification with ICP-MS, but the total analysis time per sample was 30 minutes, which is relatively high for routine analyses [43].

1.5. Analytical techniques used in the study

The analytical techniques used in this work include both ICP-MS and HPLC-ICP-MS. In HPLC-ICP-MS, two chromatographic separation modes were investigated; ion pair chromatography (IPC) and extraction chromatography (EXC).

1.5.1. Principles of ICP-MS

In ICP-MS, the sample solution is introduced into the nebulizer where it is converted into an aerosol with argon gas. The aerosol is separated from larger droplets by the spray chamber. The aerosol is then vaporized, atomized and finally ionized after it has been transported into the inductively coupled plasma (ICP). This process is achieved by utilizing an ICP operating at a temperature range of 7 000 – 10 000 K. By applying a radiofrequency (RF) signal through a copper coil, an intense magnetic field is produced. The magnetic field interacts with an argon gas that is flowing through a concentric quartz tube, a torch, which ionizes the gas. By applying electrons from a high-voltage spark, a high-temperature plasma is generated, where the temperatures reaches up to 10 000 K. Ions produced in the plasma are directed into the mass spectrometer by its interface region. The interface region consists of two metallic cones, a sampler cone and a skimmer cone, which allows the ions to pass through to the ion optics. The ions are guided by the ion optics into the mass separation device, which separates ions of

interest from the unwanted ions by their mass-to-charge ratio (m/z) and leads them to an ion detector [34].

1.5.2. Principles of ion pair chromatography and extraction chromatography in HPLC-ICP-MS

The use of high performance liquid chromatography (HPLC) for the elimination of spectral interferences in ICP-MS for trace determination of REEs has shown promising results, as discussed in the previous section. Ion pair chromatography is a well-known separation technique in order to separate REEs from each other as it provides a cheap, relatively rapid, precise and accurate separation [44]. The elution order in IPC is from Lu to La, which may give an ideal operational time for the purity determination of high-purity HREEs, as the highly concentrated matrix element would be among those who elute first. In IPC, the packed silica-based hydrophobic columns, such as C8 or C18-columns, function as a support for the ion-pair reagent (IPR). The amphiphilic IPR has a hydrophobic tail that interacts with the hydrophobic stationary phase in the column, forming a monolayer on its surface and exposes its negatively charged part to the analytes, where the rare earth metal ions are adsorbed. The mobile phase is composed of an IPR and a complexing agent. The complexing agent destabilizes the sorption of REEs on the IPR by forming complexes with the metal ions of varying strengths, which elutes along with the mobile phase [45]. The retention of the analytes is dependent on pH of the mobile phase, and its concentration of IPR and complexing agent. By increasing the pH of the mobile phase, there is a larger fraction of HIBA being dissociated along with a larger fraction of the analytes undergoing complexation [46]. The elution order of Lns is from Lu to La as the HREEs tend to form stronger complexes with the complexing agent used for this separation technique.

Extraction chromatography offers the selectivity of solvent extraction in a chromatographic process and the ease of handling ion exchange resins. Similar to IPC, the inert, hydrophobic silica-based columns function as supports for the adsorption of organic liquid extractants, which has complex forming properties. In EXC, the extractant is impregnated into the column support through physical interactions such as adsorption and physical entrapment. The extractant in EXC also contains a hydrophobic and hydrophilic part. Its hydrophobic part interacts with the column support, while the hydrophilic part is exposed for extraction of the analytes. The REEs are partitioned between two immiscible phases, an acidic aqueous phase

and an organic phase, which is the extractant. Firstly, the hydrated rare earth metal ions are extracted into the organic phase, which is impregnated on the column, forming neutral organophilic metal complexes. Secondly, the complexes are extracted from the organic phase into the aqueous phase through an ion-exchange-like process which occurs between the REE-complex and the mineral acid eluent, e.g. nitric acid [47, 48]. When the nitrate concentration increases in the aqueous phase, the nitrate complex formation competes with extraction of the metal ions. The nitric acid enhances the aqueous solubility of the REEs, which releases the REE-nitrate complexes into the aqueous phase. The REEs form complexes of different strengths with the nitrate. Hydration enthalpies of Ln^{3+} are reduced throughout the series and affect the stabilization constants of the Lns. Heavier lanthanoids are therefore strongly hydrated, and bind less strongly with NO_3^- [19], which results in an elution order of La to Lu.

1.6. Objective of the study

The objective of the study was to develop methods that can be used for routine analyses for the purity determination of high-purity REEs and REOs by utilizing ICP-MS and HPLC hyphenated with ICP-MS for online separation. The goal of the methods is the ability to determine purities over 99.999 % on a trace metal basis with a quadrupole ICP-MS. The main constituents of impurities in high-purity REOs are trace concentrations of other REEs. As the REEs and REOs are typically over 99.95 % pure, the purity was to be determined by the impurity approach, focusing on the trace amounts of REEs. The main focus of this thesis has been to develop methods for the purity determination of ytterbium and europium. Ytterbium belongs to the HREEs, which are generally harder to separate from each other compared to LREEs. HREEs are less abundant than LREEs and the prices of these elements are also higher than of LREEs. Therefore, accurate purity determination is of interest. Europium belongs to the group of LREEs. The occurrence of polyatomic ions in highly concentrated Eu-matrices may cause significant problems to the purity determination of the element compared to Yb, as polyatomic ions of Eu have greater potential to cause mass overlaps to other REEs.

The determination of REEs as trace impurities in high-purity REOs with ICP-MS is mainly troubled by spectral interferences in the form of polyatomic ions whose mass overlaps with analytes of interest. Therefore, methods were developed for the separation of REEs from the matrix element by hyphenating HPLC with ICP-MS. Since the ICP-MS is a specific detector, only elements that interfere with the analytes of interest need to be separated from each other.

HPLC-ICP-MS can be used both as a diagnostic tool to identify the contribution of spectral interferences during the method development and for eliminating these interferences in the determination of REEs as trace impurities. Ion pair chromatography and extraction chromatography were investigated in the study for the separation of matrix element from the analytes. Online separation of the REEs with HPLC-ICP-MS provides both the elimination of spectral interferences and the low detection limits that are needed for accurate purity determinations of high-purity REEs and REOs.

2. Experimental

2.1. Instrumentation

The experiments in this study were conducted on a NexION 300D ICP-MS by PerkinElmer (USA), which was controlled via a computer through the NexION software. The instrument consists of three quadrupole mass analyzers and is equipped with a concentric nebulizer, a cyclonic spray chamber and a peristaltic pump. All experiments were performed in the standard mode of the ICP-MS.

The HPLC instrument used for these experiments was a quaternary Flexar HPLC pump combined with a vacuum degasser and a Flexar HPLC Autosampler by PerkinElmer (USA). Control of the HPLC was achieved through a computer by the Chromera software. The HPLC was connected to the ICP-MS by a switching valve, which leads the mobile phase to waste during conditioning and rinsing steps. The chromatographic columns used for the separation were two Eclipse XDB-C18 (4.6 x 150 mm, 5 µm) columns and an Eclipse XDB-C18 (4.6 x 100 mm, 2.7 µm) column purchased from Agilent Technologies (USA).

A temperature programmed Milestone ETHOS 1600 microwave oven (Italy) equipped with PTFE vessels were used in order to digest 99.9 % pure Yb_2O_3.

2.2. Reagents and materials

Sample and calibration solutions of the REEs for the method development were prepared from standard solutions of Yb (10041 ± 23 µg mL^{-1}) and Lu (9985 ± 29 µg mL^{-1}), obtained from Teknolab AB (Kungsbacken, Sweden), while standard solution of Eu (1000 ± 3 µg mL^{-1}) was obtained from Spectrapure Standards AS (Oslo Norway). A multi-elemental solution containing all REEs (100 ± 0.1 µg mL^{-1}) was obtained from Teknolab A/S (Drøbak, Norway). 99.9 % pure ytterbium oxide, Yb_2O_3, based on trace metals was purchased from Sigma Aldrich (USA). 99 % pure α-hydroxyisobutyric acid (HIBA) was obtained from Sigma-Aldrich (Norway). 99 % pure di-(2-ethylhexyl)phosphoric acid (HDEHP) was purchased from Alfa Aesar (Karlsruhe, Germany). 99 % pure heptafluorobutyric acid (HFBA), sodium n-octane sulphonate (OS) and extra pure NaOH pellets were obtained from Merck (Darmstadt,

Germany). 65% (w/w) suprapur HNO_3 was also obtained from Merck (Germany) and will be referred to as 65 % HNO_3 in future references. All solutions and mobile phases prepared for analysis were diluted to their appropriate concentrations with ultra-pure, deionised type 1-water (18MΩ cm) provided by Millipore Milli-Q system (Bedford, USA), which will be referred to as type 1-water in future references.

2.3. Preparation of sample and calibration solutions, and mobile phases

All sample and calibration solutions containing REEs were added nitric acid in order to keep the REEs dissolved at pH ≤ 5 [11]. HNO_3 is generally the preferred acid to use in ICP-MS as it produces less severe spectral interferences and low background signals compared to e.g. HCl [49]. The different molarities of nitric acid were prepared by adding the appropriate amount of 65 % HNO_3 with type 1-water in the respective volumetric flasks. Calculation procedures for the preparation of sample and calibration solutions as well mobile phases are described in section A.1 in the appendix.

2.3.1. Sample preparation for the investigation of signal suppression of REEs and formation of polyatomic ions

Two sets of sample solutions for the investigation of signal suppression of the REEs and the formation of polyatomic ions in different concentrations of Yb by the ICP-MS were prepared.

The first set was prepared by diluting the standard solution of Yb (10041 ± 23 µg mL^{-1}) to 5, 10, 50 and 100 µg mL^{-1}, which were added appropriate amounts of the standard solution containing all REEs (100 µg mL^{-1}) prior to dilution with 0.2M HNO_3. The second set followed the same procedures as the first, but the standard solution of all REEs was not added. The final contents of the sample solutions are presented in table 2.3.1 and 2.3.2.

Table 2.3.1: Final contents of sample solutions for the investigation of signal suppression of REEs in different concentrations of Yb by ICP-MS.

Sample set 1	Yb (µg mL^{-1})	REEs (ng mL^{-1})	HNO_3
Sample solution 1	0	2.5	0.2 M
Sample solution 2	5	2.5	0.2 M
Sample solution 3	10	2.5	0.2 M
Sample solution 4	50	2.5	0.2 M
Sample solution 5	100	2.5	0.2 M

Table 2.3.2: Final contents of sample solutions for the investigation of signal suppression of REEs and formation of polyatomic ions in different concentrations of Yb.

Sample set 2	Yb (µg mL^{-1})	REEs (ng mL^{-1})	HNO_3
Sample solution 1	0	0	0.2 M
Sample solution 2	5	0	0.2 M
Sample solution 3	10	0	0.2 M
Sample solution 4	50	0	0.2 M
Sample solution 5	100	0	0.2 M

2.3.2. Sample preparation for the determination of REEs as trace impurities in standard solution of Yb by method of standard additions with ICP-MS

Sample and calibration solutions were prepared for the determination of REEs as trace impurities in the standard solution of Yb by the method of standard additions with ICP-MS.

Three calibration solutions were prepared by spiking diluted standard solutions of Yb with known concentrations of all REEs. The calibration solutions were prepared by adding appropriate amounts of the standard solution of Yb to each of their respective volumetric flasks, which was spiked with known concentrations of the multi-elemental standard solution. The calibration solutions were diluted with 0.2 M HNO_3. Three sample solutions were prepared by diluting the standard solution of Yb to 10 µg mL^{-1} with 0.2 M HNO_3. Table 2.3.3

lists the final concentration of the sample and calibration solutions. A blank sample was also prepared, which contains 0.2 M HNO_3 and was not added any of the REE-containing standard solutions.

Table 2.3.3: Final concentration of sample and calibration solutions for the determination of REEs as trace impurities in a standard solution of Yb by method of standard addition with ICP-MS.

Solution	**Yb (µg mL^{-1})**	**REEs (pg mL^{-1})**	**HNO_3**
Blank	0	0	0.2 M
Calibration 1	10	50	0.2 M
Calibration 2	10	150	0.2 M
Calibration 3	10	250	0.2 M
Sample 1	10	0	0.2 M
Sample 2	10	0	0.2 M
Sample 3	10	0	0.2 M

2.3.3. Sample preparation for the determination of REEs as trace impurities in standard solutions of Yb and Eu by external standardisation with ICP-MS and HPLC-ICP-MS

Sample and calibration solutions were prepared for the determination of REEs as trace impurities in standard solutions of Yb and Eu by external standardisation with ICP-MS and HPLC-ICP-MS. The Yb-sample solutions were also used for the investigation of the signal intensity at mass 175 with altered plasma conditions.

The calibration solutions covered a concentration range of 25 – 250 pg mL^{-1} for each REE, and was prepared by diluting appropriate amounts of the multi-elemental standard solution with 0.2 M HNO_3. The three sample solutions of Eu and Yb, respectively, were prepared by diluting their respective standard solutions to 10 µg mL^{-1} with 0.2 M HNO_3. Table 2.3.4 lists the final concentrations of the sample and standard solutions that were prepared.

Table 2.3.4: Final concentrations of sample and calibration solutions for the determination of REEs as trace impurities in the standard solutions of Yb and Eu by external standardisation with ICP-MS and HPLC-ICP-MS.

Solution	REEs (pg mL^{-1})	HNO_3
Calibration 1	25	0.2 M
Calibration 2	75	0.2 M
Calibration 3	150	0.2 M
Calibration 4	250	0.2 M
	Eu (µg mL^{-1})	
Sample 1	10	0.2 M
Sample 2	10	0.2 M
Sample 3	10	0.2 M
	Yb (µg mL^{-1})	
Sample 1	10	0.2 M
Sample 2	10	0.2 M
Sample 3	10	0.2 M

2.3.4. Sample preparation for the separation of Lu from Yb and Eu from Tm by HPLC-ICP-MS

Sample solutions of Yb and Eu were prepared for analyses with HPLC-ICP-MS. The sample solutions were prepared from their respective standard solutions and diluted with HNO_3. The final concentration of the different sample solutions is listed in table 2.3.5 and 2.3.6.

Table 2.3.5: Final concentration of sample solutions used for the separation of Lu and Yb in an OS-HIBA and HFBA-HIBA system.

Solution	Concentration of Yb	Concentration of Lu	Concentration of HNO_3
Sample 1	250 pg mL^{-1}	250 pg mL^{-1}	0.4 M
Sample 2	10 µg mL^{-1}	0	0.4 M

Table 2.3.6: Final concentration of the sample solutions analysed by an HNO_3-HDEHP system.

Solution	Yb (µg mL^{-1})	Eu (µg mL^{-1})	REEs (ng mL^{-1})	HNO_3
Sample 1	10	0	0	0.2 M
Sample 2	0	0	1	0.2 M
Sample 3	0	10	0	0.2 M
Sample 4	0	10	2	0.2 M

2.3.5. Preparation of mobile phases for HPLC-ICP-MS

Three chromatographic systems were investigated for the separation of Lu from Yb and Eu from Tm; OS-HIBA, HFBA-HIBA and HNO_3-HDEHP. OS and HFBA are ion pair reagents that act as stationary phases, but are added into the mobile phase. HDEHP is the extractant in extraction chromatography and is impregnated on the column. All of the mobile phases for the different systems consist of two reservoirs in order to perform gradient elution.

The mobile phase for the OS-HIBA system was prepared by adding appropriate amounts of OS and HIBA to their respective 1000 mL bottles, prior to dilution with type 1-water. The pH of the mobile phase reservoir B was adjusted to 3.5 with 10 M NaOH. 10 M NaOH was prepared from extra pure NaOH pellets. The final composition of the mobile phase for the OS-HIBA system is listed in table 2.3.7. Mobile phase reservoir B had its pH adjusted closely to the pK_a of HIBA. The pK_a value of HIBA is 3.77.

Table 2.3.7: Composition of mobile phase reservoir A and B for the separation of Lu from Yb by ion pair chromatography in an OS-HIBA system.

Mobile phase reservoir	Concentration of OS	Concentration of HIBA	pH
A	40 mM	0	Unadjusted
B	40 mM	0.5 M	3.5

The mobile phase for the HFBA-HIBA system was prepared by diluting appropriate amounts of HFBA in each of its 1000 mL bottle. Appropriate amounts of HIBA was added to mobile phase reservoir B and diluted with type 1-water. The pH of mobile phase reservoir B was

adjusted with 10 M NaOH. Table 2.3.8 lists the final composition of the mobile phase for the HFBA-HIBA system.

Table 2.3.8: Composition of mobile phase reservoir A and B for the separation of Lu from Yb by ion pair chromatography in an HFBA-HIBA system.

Mobile phase reservoir	Concentration of HFBA	Concentration of HIBA	pH
A	20 mM	0	Unadjusted
B	20 mM	0.5 M	3.5

The mobile phase reservoirs for the HNO_3-HDEHP system consist of 2.25 M HNO_3 and type 1-water. 2.25 M HNO_3 was prepared from 65 % HNO_3. The final composition of the mobile phase for the HNO_3-HDEHP system is listed in table 2.3.9.

Table 2.3.9: Composition of mobile phase reservoir A and B for the separation of Yb from Lu and Eu from Tm by extraction chromatography with an HNO_3-HDEHP system.

Mobile phase reservoir	Component
A	Type 1-water
B	2.25 M HNO_3

2.4. Sample decomposition of 99.9 % pure Yb_2O_3

Three samples were prepared from 99.9 % pure Yb_2O_3, which was digested and diluted to 8.7 µg mL^{-1} Yb for each sample. Three samples of 0.5 g ytterbium oxide were weighed into their respective PTFE vessels and added 10 mL 65 % suprapur HNO_3. Three blank solutions were also prepared by following the same procedure as the sample solutions, without adding ytterbium oxide. The vessels were placed in the ETHOS 1600 microwave oven and by following the temperature program listed in table 2.4.1, the samples were digested. After the vessels have been cooled to room temperature, the content of each vessel were transferred to their respective 100 mL volumetric flasks and diluted with type 1-water. The final concentration of Yb in the sample solutions after decomposition was 4.4 mg mL^{-1}. From these flasks, 200 µL of each sample solution were added to their respective 100 mL volumetric flasks and diluted with 0.2 M HNO_3 for analysis with the HPLC-ICP-MS and ICP-MS. Table

2.4.2 shows the final concentration of Yb that was digested and diluted from 99.9 % pure Yb_2O_3. For accurate calculations of the final concentration of Yb, see section A.1.3 in the appendix.

Table 2.4.1: Temperature program for decomposition of 99.9 % pure Yb_2O_3.

	Time (min)	**Temperature (^oC)**
Ramping step	5	20 – 200
Holding step	15	200

Table 2.4.2: Final concentration of Yb prepared from digested and diluted sample of 99.9 % pure Yb_2O_3.

Solution	**Concentration of Yb**	**Concentration of HNO_3**
Sample solution 1	8.7 µg mL^{-1}	0.2 M
Sample solution 2	8.7 µg mL^{-1}	0.2 M
Sample solution 3	8.7 µg mL^{-1}	0.2 M

3. Method development

Two analytical techniques were used in this work, ICP-MS and HPLC-ICP-MS, in order to determine the purity of standard solutions of Eu and Yb, and 99.9 % pure Yb_2O_3. The ICP-MS provides detection limits that are needed for the determination of REEs as trace impurities in high-purity REEs and REOs, while the HPLC-ICP-MS was used in order to prevent spectral interferences from hindering the determination of certain REEs of interest. Three different chromatographic systems were investigated, whereas the chromatographic separation modes were ion pair chromatography and extraction chromatography.

3.1. Limit of detection and limit of quantification

The degree of purity to be determined is depended on the limit of detection for the analytes of interest. LOD is often defined as the concentration of an analyte that gives an instrument signal significantly different from the background signal. A common way to determine the LOD is by the blank method [50, 51]. The blank method used in this study determines the LOD from the reproducibility of the measurement of the background, with at least 10 measurements. The LOD is calculated by

$$c_{LOD} = k \times s_{bg} \quad (1)$$

where c_{LOD} is the concentration of the LOD, s_{bg} is the standard deviation of the background measurement, while k is the statistical factor for the probability of which the measurement is different from zero. k is normally set to 3.

The LOQ is regarded as the lower limit for precise quantitative measurements. LOQ can be determined simultaneously with the LOD by the blank method, and is calculated as

$$c_{LOQ} = 10 \times s_{bg} \quad (2)$$

The blank solutions for the determination of LOD and LOQ undergo the same preparation procedures as the sample solutions and contain the same reagents, but the analytes are not added.

3.2. ICP-MS method development

The signal intensity (cps) of the ICP-MS is optimized and calibrated on a daily basis by applying a multi-elemental solution provided by PerkinElmer (USA), which covers a wide range of isotope masses with known concentrations. The instrument is also optimized for the ratio between formation of CeO to Ce and Ce^{2+} to Ce^{+}. Table 3.2.1 lists the different species and their target criteria of the daily performance checks, which are achieved by optimizing the inductively coupled plasma radiofrequency (ICP RF)-power, nebulizer gas flow rate, torch alignment and auto lens voltage to maximize ion transmission.

Table 3.2.1: Daily performance criteria for the optimization of the ICP-MS.

Analyte species	Mass (amu)	Comparator	Target
Be	9.0122	>	3000 cps
Mg	23.985	>	20000 cps
In	114.904	>	50000 cps
U	238.05	>	35000 cps
Bkgd	220	≤	1 cps
CeO/Ce	155.9/139.905	≤	0.025 %
Ce^{2+}/Ce	69.9527/139.905	≤	0.03 %

As formation of REE-based polyatomic ions are related to the ICP RF-power and the nebulizer gas flow rate, the two parameters were held constant for all daily performance checks, while only the torch alignment and auto lens voltage were optimized. Table 3.2.2 presents the standard operational conditions and parameters of the ICP-MS used throughout all experiments, unless stated otherwise, which fulfilled the daily performance check criteria. The results in table 3.2.2 were achieved by subjecting a Smart Tune solution from PerkinElmer (USA) consisting of 1 µg mL^{-1} Be, Ce, Fe, In, Li, Mg, Pb and U in 1 % HNO_3 to the daily performance check. The ICP RF-power and nebulizer gas flow rate presented in the table was found to be optimal for the first daily performance check that was performed. The two parameters were held constant for all future daily performance checks.

Sampling parameters listed in table 3.2.2 were chosen in order to assure that the sample to be analysed is free of memory effects from the previous sample. The sampling time in table 3.2.2

had shown to be sufficient for this purpose. The timing parameters chosen are the same as the default values of the standard quantitative analysis method included in the NexION software. The instrument measured 6 replicates of each isotope per sample instead of the default value of 3. 6 replicates were chosen in order to verify the reproducibility of the measurements under unchanged conditions. The total analysis time per sample is affected by the amount of isotopes selected for analysis and both the timing and sampling parameters.

Table 3.2.2: Standard operational conditions and parameters of the ICP-MS.

Parameter	**Value**			
ICP RF-power	1000 W			
Nebulizer gas flow rate	0.94 L min^{-1}			
Auxiliary gas flow rate	1.2 L min^{-1}			
Plasma gas flow rate	13.0 L min^{-1}			
Typical running vacuum	7.3 x 10^{-7} torr			
Timing parameters		**Sampling parameters**		
Sweeps/reading	20		Seconds	RPM
Readings/replicate	1	Sample flush	25	30
Replicates	6	Read delay	25	20
Dwell time per amu	50ms	Analysis	-	20
Integration time	1000ms	Wash	30	30
Scanning mode	Peak hop transient			

3.2.1. Isotope selection and possible interferences

Spectral interferences occur in the form of isobaric interferences and polyatomic ion interferences. For the purity determination of Yb and Eu by the impurity approach, polyatomic ions are formed from the highly concentrated matrix element. Polyatomic ions of Yb are less problematic compared to Eu, as Yb is one of the last REEs in the series. Eu belongs to the LREEs and its polyatomic ions may cause mass overlaps to several REEs. An overview of all the naturally occurring stable isotopes of the REEs can be seen in figure A.2.1 in the appendix. The isotopes chosen for the different analyses were selected accordingly to figure A.2.1 in the appendix.

3.2.1.1. Isotope selection for Yb-analyses

Yb has seven naturally occurring stable isotopes, which are listed in table 3.2.3. The polyatomic ions of Yb that may cause mass overlaps with isotopes of interest are also presented in the table.

Table 3.2.3: Isotopes of Yb, their natural abundances and potential spectral interferences.

Isotopes of Yb	Natural abundance	Polyatomic ions	Interfered isotopes
^{168}Yb	0.1 %	$^{168}YbH^+$, $^{168}YbO^+$, $^{168}YbOH^+$	$^{168}Er^+$, $^{169}Tm^+$
^{170}Yb	3.0 %	$^{170}YbH^+$, $^{170}YbO^+$, $^{170}YbOH^+$	$^{170}Er^+$
^{171}Yb	14.3 %	$^{171}YbH^+$, $^{171}YbO^+$, $^{171}YbOH^+$	-
^{172}Yb	21.8 %	$^{172}YbH^+$, $^{172}YbO^+$, $^{172}YbOH^+$	-
^{173}Yb	16.1 %	$^{173}YbH^+$, $^{173}YbO^+$, $^{173}YbOH^+$	-
^{174}Yb	31.8 %	$^{174}YbH^+$, $^{174}YbO^+$, $^{174}YbOH^+$	$^{175}Lu^+$
^{176}Yb	12.8 %	$^{176}YbH^+$, $^{176}YbO^+$, $^{176}YbOH^+$	$^{176}Lu^+$

Table 3.2.3 shows that Er, Tm and Lu are affected by spectral interferences caused by Yb as the matrix element. Er has 6 naturally occurring stable isotopes where two of them, ^{166}Er and ^{167}Er, are both free from both isobaric interferences and Yb-based polyatomic ions. Spectral interferences can be avoided by selecting ^{166}Er. Tm is mono-isotopic and is spectrally interfered by ^{168}YbH, which has the same mass as ^{169}Tm, but the natural abundance of ^{168}Yb is too low in order for ^{168}YbH to be formed in the plasma at the matrix concentration chosen for the purity determination, which will be discussed later in section 4.2 in chapter 4. Lu has only two naturally occurring isotopes of which both of them are interfered by spectral interferences, as shown in table 3.2.3. The natural abundance of the isotopes of Lu is 97.4 % for ^{175}Lu and 2.6 % for ^{176}Lu. ^{175}Lu was chosen as the isotope of interest for Lu as it is the most abundant isotope, even though the formation of hydride may affect its determination.

Isotopes of the remaining REEs selected for the different investigations of Yb with the ICP-MS are the most abundant isotopes that are free of both isobaric and polyatomic interferences. Table 3.2.4 shows the monitored isotopes for all analyses of the standard solution of Yb and the 99.9 % pure ytterbium oxide, unless stated otherwise.

Table 3.2.4: Isotopes selected for all analyses of Yb, unless stated otherwise. The selected isotopes are free from spectral interferences, with the exception of ^{175}Lu.

Analyte isotope	Natural abundance (%)
^{45}Sc	100
^{89}Y	100
^{139}La	99.9
^{140}Ce	88.5
^{141}Pr	100
^{143}Nd	12.2
^{147}Sm	15.0
^{153}Eu	52.2
^{157}Gd	15.7
^{159}Tb	100
^{163}Dy	24.9
^{165}Ho	100
^{166}Er	33.6
^{169}Tm	100
^{175}Lu	97.4

3.2.1.2. Isotope selection for Eu-analyses

Eu has two naturally occurring isotopes, ^{151}Eu and ^{153}Eu, which have natural abundances of 47.8 % and 52.2 %, respectively. Eu belongs to the group of LREEs and occurs in the middle of the lanthanoid series. Its polyatomic ions have the potential of causing mass overlaps to several isotopes of the REEs that occur later in the group, which complicates the purity determination of Eu by ICP-MS [37]. Table 3.2.5 illustrates the potential problems caused by Eu and its polyatomic ions.

Table 3.2.5: Isotopes of Eu and their potential spectral interferences and abundance sensitivity.

Interfering ions	Type of interference	Interfered isotopes
$^{151}Eu^{+}$	Abundance sensitivity	$^{150}Sm^{+}$, $^{150}Nd^{+}$
$^{153}Eu^{+}$	Abundance sensitivity	$^{152}Sm^{+}$, $^{152}Gd^{+}$
$^{151}EuH^{+}$	Mass overlap	$^{152}Sm^{+}$, $^{152}Gd^{+}$
$^{153}EuH^{+}$	Mass overlap	$^{154}Sm^{+}$, $^{152}Gd^{+}$
$^{151}EuO^{+}$	Mass overlap	$^{167}Er^{+}$
$^{153}EuO^{+}$	Mass overlap	$^{169}Tm^{+}$
$^{151}EuOH^{+}$	Mass overlap	$^{168}Er^{+}$, $^{168}Yb^{+}$
$^{153}EuOH^{+}$	Mass overlap	$^{170}Er^{+}$, $^{170}Yb^{+}$

For all of the interfered isotopes that are affected by abundance sensitivity and polyatomic ions of Eu, it is possible to select isotopes that are free of such interferences, with the exception of ^{169}Tm. The greatest obstacle for determining REEs as trace impurities in Eu is the formation of ^{153}EuO, which has the same mass as ^{169}Tm. Tm is mono-isotopic and cannot be handled by the same approach as the other REEs. Therefore, the determination of REEs as trace impurities solely by ICP-MS may be misleading, as Tm will have its mass of 169 overlapped by ^{153}EuO. The selected isotopes for the analyses concerning Eu are listed in table 3.2.6, and were chosen accordingly to figure A.2.1 in the appendix. The selected isotopes are the most abundant isotopes that are free of both isobaric and polyatomic interferences as well as abundance sensitivity, with the exception of Tm.

Table 3.2.6: Isotopes selected for all analyses of Eu. The selected isotopes are free of isobaric interferences, abundance sensitivity and polyatomic ion interferences, with the exception of ^{169}Tm.

Analyte	Natural abundance (%)
^{45}Sc	100
^{89}Y	100
^{139}La	99.9
^{140}Ce	88.5
^{141}Pr	100
^{143}Nd	12.2
^{147}Sm	15.0
^{157}Gd	15.7
^{159}Tb	100
^{163}Dy	24.9
^{165}Ho	100
^{166}Er	33.6
^{169}Tm	100
^{174}Yb	31.8
^{175}Lu	97.4

3.2.2. LOD and LOQ

LOD and LOQ were determined for the purity determination of Yb and Eu by analysing the blank solution 10 times of which the standard deviation of the concentration found were multiplied with 3 and 10, respectively. The blank solutions contain the same reagents and goes through the same procedures as the sample solutions, but do not contain the analytes. The procedure for measuring the LOD and LOQ of purity determination of 99.9 % pure Yb_2O_3, and standard solutions of Yb and Eu were determined by analysing their respective blank solutions after all sample solutions have been analysed.

Table 3.2.7: LOD and LOQ for the determination of REEs as trace impurities in a standard solution of Yb diluted to 10 µg mL^{-1}.

Analyte	LOD (pg mL^{-1})*	LOQ (pg mL^{-1})*	LOD (pg mL^{-1})**	LOQ (pg mL^{-1})**
^{45}Sc	1.1	3.7	15	51
^{89}Y	0.1	0.4	0.9	2.8
^{139}La	1.0	3.5	0.6	2.0
^{140}Ce	0.1	0.2	0.6	2.1
^{141}Pr	0.2	0.1	0.6	2.0
^{143}Nd	0.3	0.9	5.2	17
^{147}Sm	0.9	3.1	9.2	31
^{153}Eu	0.2	0.6	1.1	3.5
^{157}Gd	0.2	0.8	3.7	12
^{159}Tb	0.1	0.2	0.4	1.3
^{163}Dy	0.2	0.7	1.1	3.6
^{165}Ho	0.03	0.1	0.6	2.1
^{166}Er	0.1	0.3	1.3	4.4
^{169}Tm	0.04	0.1	0.5	1.7
^{175}Lu	0.1	0.3	0.6	2.0

*ICP RF-power set to 1000 W and nebulizer gas flow rate to 0.94 L min^{-1}.

**ICP RF-power set to 1300 W and nebulizer gas flow rate to 0.80 L min^{-1}.

Table 3.2.8: LOD and LOQ for the determination of REEs as trace impurities in a standard solution of Eu diluted to 10 µg mL^{-1} with standard operational conditions and parameters of the ICP-MS.

Analyte	LOD (pg mL^{-1})	LOQ (pg mL^{-1})
^{45}Sc	2.8	9.2
^{89}Y	0.3	0.9
^{139}La	0.2	0.7
^{140}Ce	0.1	0.3
^{141}Pr	0.1	0.2
^{143}Nd	0.5	1.5
^{147}Sm	0.6	2.0
^{157}Gd	0.8	2.5
^{159}Tb	0.1	0.2
^{163}Dy	0.2	0.8
^{165}Ho	0.03	0.1
^{166}Er	0.1	0.3
^{169}Tm	1.2	3.8
^{174}Yb	3.3	11.0
^{175}Lu	0.1	0.2

Three blank solutions were prepared for the purity determination of the digested and diluted sample of Yb_2O_3. The blank solutions went through the same decomposition and dilution steps as Yb_2O_3. LOD and LOQ were determined by analysing each blank solution 10 times after analysing the samples.

Table 3.2.9: LOD and LOQ for the determination of REEs as trace impurities in Yb_2O_3, with a stated purity of 99.9 %, which was digested and diluted to 8.7 µg Yb mL^{-1}. The ICP-MS was operated with its standard conditions and parameters.

Analyte	LOD (pg mL^{-1})	LOQ (pg mL^{-1})
^{45}Sc	1.9	6.4
^{89}Y	1.8	6.0
^{139}La	2.8	9.3
^{140}Ce	1.5	4.9
^{141}Pr	0.04	0.1
^{143}Nd	0.8	2.8
^{147}Sm	2.8	9.3
^{153}Eu	0.5	1.8
^{157}Gd	0.7	2.5
^{159}Tb	0.1	0.3
^{163}Dy	0.4	1.2
^{165}Ho	0.1	0.3
^{166}Er	0.1	0.3
^{169}Tm	0.1	0.2
^{175}Lu	0.9	0.9

3.3. HPLC-ICP-MS method development

Due to the formation of polyatomic ions, the trace determination of Lu and Tm in their respective sample solutions of Yb and Eu solely by the ICP-MS are inaccurate. Polyatomic ions of Yb and Eu, ^{174}YbH and ^{153}EuO, contribute to the registered signal intensity at their respective masses of 175 and 169. The purpose of utilizing HPLC-ICP-MS is to separate Lu from Yb and Eu from Tm in order to accurately determine the concentration of Lu in highly concentrated Yb and Tm in highly concentrated Eu sample solutions absent spectral interferences. The separation can also be used as a diagnostic tool in order to determine the significancy of the contribution of the polyatomic ions to the affected analytes.

Ion pair chromatography and extraction chromatography were utilized in order to separate Yb from Lu and Eu from Tm. In ion pair chromatography, two systems were investigated for the separation of Yb and Lu; the OS-HIBA system and the HFBA-HIBA system. OS and HFBA are added in the mobile phase, but act as the stationary phase in their respective systems, while HIBA is the complexing agent. In extraction chromatography, a method that was used for the separation of REEs utilizing a diode array detector [52] was optimized for the separation of the analytes of interest, Tm and Lu, from their respective interfering matrix-elements, with the ICP-MS as the detector. The organic extractant in the stationary phase of this method is HDEHP, which is impregnated onto the column and was prepared by the research group, whereas the mobile phase is HNO_3.

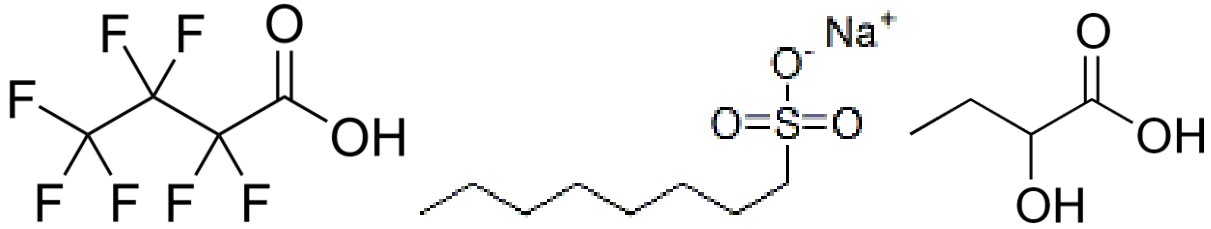

Figure 3.3.1: Molecular structure of HFBA, OS and HIBA.

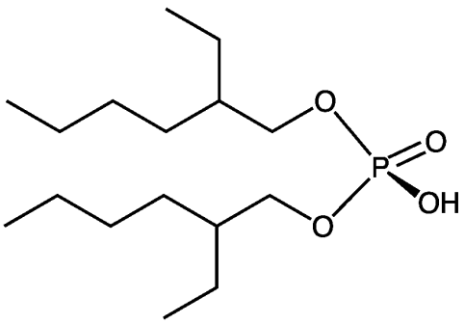

Figure 3.3.2: Molecular structure of HDEHP.

As it has been stated earlier, REEs are classified as *class a metals* according to HSAB-theory, which implies that the most stable complexes are formed with O-donor electronegative ligands. The reagents used for IPC in these experiments include α-hydroxyisobutyric acid, heptafluorobutyric acid and n-octane sulphonate. The sulphonate of OS and deprotonated forms of HIBA and HFBA all contain O-donor electronegative ligands. Figure 3.3.1 and 3.3.2 shows the molecular structures of these reagents.

Sample and calibration solutions were added to a 2 mL-vial designed for the auto sampler of the HPLC-instrument. The injection volume of the sample and calibration solutions was set to

50 µL and the analytes were separated through their respective gradient and isocratic programs at a mobile phase flow rate of 1 mL min^{-1}. The separations were carried out with standard operational conditions and parameters of the ICP-MS, listed in table 3.2.2, unless stated otherwise.

3.3.1. OS-HIBA system for the separation of Lu from Yb

For the OS-HIBA system, an Eclipse XDB-C18 column (4.6 x 150 mm, 5 µm) was conditioned with its mobile phase reservoir A, composed of 40 mM OS, for 7.5 minutes, and another 7.5 minutes of its mobile phase reservoir B, composed of 40 mM OS and 0.5 M α-HIBA, at a mobile phase flow rate of 1 mL min^{-1} prior to injection of samples.

Table 3.3.1: HPLC operating conditions for the separation of Lu from Yb by the OS-HIBA system.

Stationary phase	Eclipse XDB-C18
IPR	40 mM OS
Complexing agent	0.5 M HIBA
Mobile phase flow rate	1 mL min^{-1}
Injection volume	50 µL

3.3.2. HFBA-HIBA system for the separation of Lu from Yb

For the HFBA-HIBA system, an Eclipse XDB-C18 column (4.6 x 100 mm, 2.7 µm) was first conditioned with 20 mM HFBA for 7.5 minutes and another 7.5 minutes with 20 mM HFBA and 0.5 M HIBA, at a mobile phase flow rate of 1 mL min^{-1}, prior to injection of samples.

Table 3.3.2: HPLC operating conditions for the separation of Lu from Yb by the HFBA-HIBA system.

Stationary phase	Eclipse XDB-C18
IPR	20 mM HFBA
Complexing agent	0.5 M HIBA
Mobile phase flow rate	1 mL min^{-1}
Injection volume	50 µL

3.3.3. HNO_3-HDEHP system for the separation of Lu from Yb and Eu from Tm

In extraction chromatography using the HNO_3-HDEHP system, an Eclipse XDB-C18 column (4.6 x 150 mm, 5 µm), which was impregnated with 0.16 mmole HDEHP by the research group, was firstly conditioned for 10 minutes with type 1-water for 10 minutes, and another 10 minutes with 2.25 M HNO_3 prior to injection of samples.

Table 3.3.3: HPLC operating conditions for the separation of Lu from Yb and Eu from Tm by extraction chromatography with the HNO_3-HDEHP system.

Stationary phase	HDEHP modified Eclipse XDB-C18
Organic extractant	0.16 mmole HDEHP
Mobile phase reservoir A	2.25 M HNO_3
Mobile phase reservoir B	Type 1-water
Mobile phase flow rate	1 mL min^{-1}
Injection volume	50 µL

4. Results and discussion

4.1 Investigation of signal suppression effects of REEs in different concentrations of Yb

Non-spectral interferences for the determination of REEs as trace impurities in Yb and Eu are often caused by the highly concentrated matrix element, which may reduce the signal intensity of the REEs. An investigation was carried out in order to determine the signal suppression effects of REEs in various concentrations of Yb. The signal intensity of 2.5 ng mL^{-1} of each REE in various concentrations of Yb, ranging from 0 to 100 µg mL^{-1} was investigated. As it was not possible to obtain a completely pure standard solution of Yb, the measured signal intensities of the REEs in the different concentrations of Yb was subtracted from their signal intensities in sample solutions containing only their corresponding concentrations of Yb. The two sets of sample solutions are referred to as sample set 1 and 2 in section 2.3.1 in chapter 2. This procedure was performed to ensure that the impurities in the standard solution of Yb do not contribute to the observed signal intensities of the added REEs. The signal suppression effects were investigated with standard operational conditions and parameters of the ICP-MS listed in table 3.2.2 in chapter 3. Isotopes selected for monitoring are listed in section 3.2.1.1.

By plotting the signal intensities of 2.5 ng mL^{-1} of each REE versus the increasing concentration of Yb, signal suppression effects can be observed in figure 4.1.1. The figure shows that the REEs' signal intensities increases as the Yb matrix concentration increases from 0 to 10 µg mL^{-1} and reduces as the Yb matrix concentration exceeds 10 µg mL^{-1}. The results are in consistent with several studies, which have shown that signal suppression of the REEs occurs when the matrix element concentration exceeds 10 µg mL^{-1} [41, 42]. The increase in signal intensitis of the REEs in Yb sample solutions from 0 to 10 µg mL^{-1} observed in the figure is most likely caused by systematic errors, such as inaccurate dilution of the sample solutions containing Yb at 0, 5 and 10 µg mL^{-1}.

Table 4.1.1 shows that the signal intensity of all the analytes is reduced by 18-35 %, with the exception of Lu, as the matrix concentration is increased from 10 µg mL^{-1} to 100 µg mL^{-1}. The signal intensity of ^{175}Lu is only reduced by 9 %. Lu suffers the least from the signal

suppression effect, which may be due to the formation of ^{174}YbH, whose mass overlaps with ^{175}Lu. As the concentration of Yb increases, so does the formation of ^{174}YbH, which is simultaneously being affected by the signal suppression effect. In addition to formation of ^{174}YbH, abundance sensitivity may also contribute to the relatively small intensity reduction of ^{175}Lu, which is the consecutive isotope mass to ^{174}Yb, due the extreme difference between the concentration of matrix element and analytes,

The signal suppression effect is not observed in sample solutions of Yb at concentrations of ≤ 10 µg mL^{-1}. Therefore, standard solutions of Yb (10041 ± µg mL^{-1}) and Eu (1000 ± 3 µg mL^{-1}) will be diluted to 10 µg mL^{-1} prior to purity determination by the impurity approach. Samples of 99.9 % pure Yb_2O_3 will be digested and diluted until the final concentration of Yb is ≤ 10 µg mL^{-1}. This investigation also suggests that formation of ^{174}YbH occurs and is causing spectral interferences with ^{175}Lu.

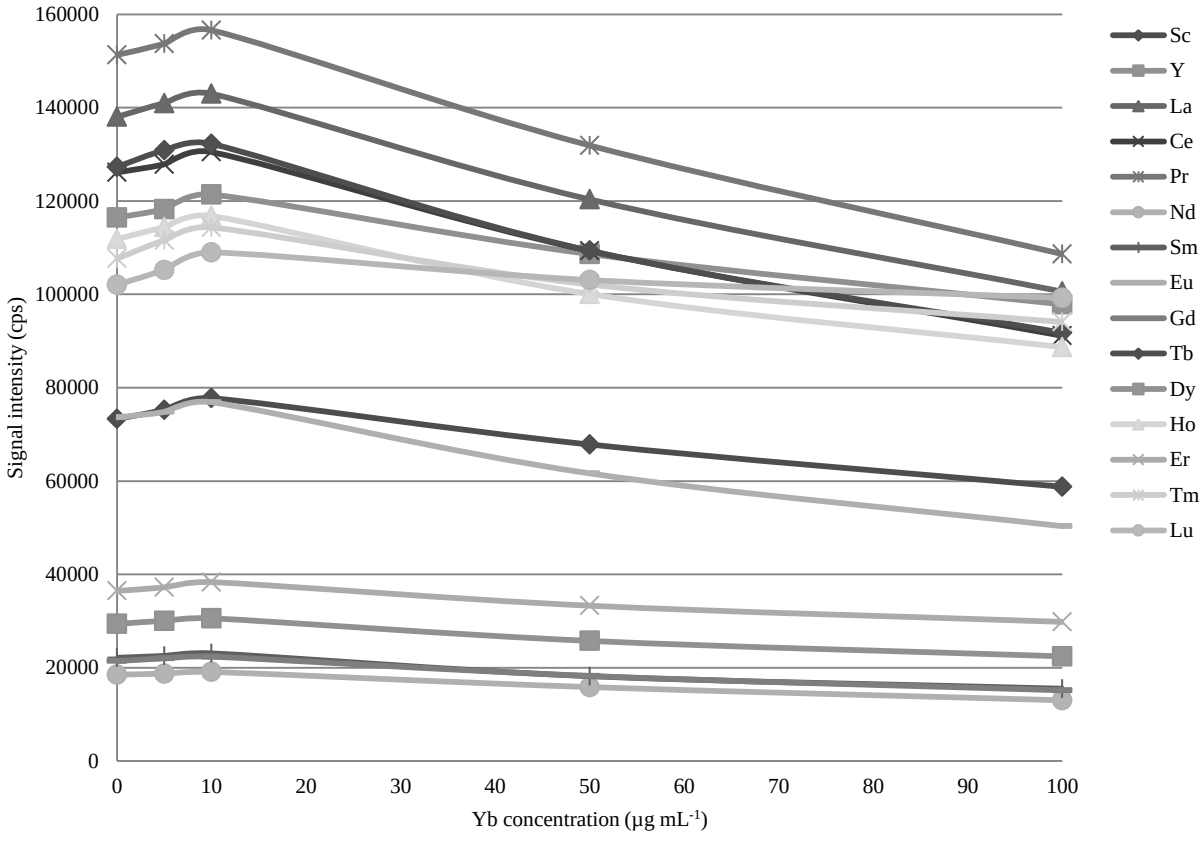

Figure 4.1.1: Signal intensities of 2.5 ng mL^{-1} of each REE in increasing concentrations of Yb (0, 5, 10, 50 and 100 µg mL^{-1}) determined by the ICP-MS with standard operational conditions and parameters as listed in table 3.2.2. The signal intensities of the 2.5 ng mL^{-1} REEs were subtracted from their signal intensities in sample solutions containing only their corresponding concentrations of Yb.

Table 4.1.1: Reduction of signal intensities for 15 REEs by percentage as the matrix concentration of Yb is increased from 10 µg mL^{-1} to 100 µg mL^{-1} determined by the ICP-MS with standard operational conditions and parameters as listed in table 3.2.2. The signal intensities of the 2.5 ng mL^{-1} REEs were subtracted from their signal intensities in sample solutions containing only their corresponding concentrations of Yb.

Analyte Sample	**Signal intensity (cps) 10 µg mL^{-1} Yb**	**Signal intensity (cps) 100 µg mL^{-1} Yb**	**Signal intensity reduction (%)**
Sc	77751	58770	24
Y	121390	97870	19
La	142984	100596	30
Ce	130501	91141	30
Pr	156594	108646	31
Nd	19108	13037	32
Sm	23092	15524	33
Eu	76899	50335	35
Gd	22383	15174	32
Tb	132255	91771	31
Dy	30596	22450	27
Ho	116803	88697	24
Er	38351	29831	22
Tm	114351	94069	18
Lu	108991	99243	9

4.2. Investigation of the formation of Yb-based polyatomic ions

It has been discussed earlier that the purity determination of high-purity REEs and REOs are troubled by formation of polyatomic ions whose masses overlap with the analyte masses. Polyatomic ions of the matrix element are formed in the plasma due to its relatively high concentration compared to the analytes. The investigation of signal suppression of REEs in different concentrations of Yb has shown that the signal suppression effect does not occur when the concentration of the matrix-element is $\leq$ 10 µg mL^{-1}. However, the results did suggest that formation of ^{174}YbH did occur, whose mass overlaps with ^{175}Lu. Since Lu and Yb

occur lastly within the group of Lns, polyatomic ions of Yb do not affect other REEs with the exception of Lu. Formation of ^{174}YbH contributes to the signal intensity observed at mass 175, which makes quantification of Lu inaccurate as long as the hydride formation occurs. It is known from the tetrad effect that Yb and Lu are harder to separate from each other compared to other REEs. Therefore, the standard solution of which the sample solutions were prepared from is most likely to contain a significant trace amount of Lu. The measured signal intensity at mass 175 consists most likely of both ^{174}YbH and ^{175}Lu. It is therefore of interest to determine the concentration of Lu in highly concentrated samples of Yb absent of mass overlap caused by ^{174}YbH, and to determine the contribution of ^{174}YbH to the signal intensity at mass 175.

In order to determine the whether ^{174}YbH is formed in the plasma caused by the relatively highly concentrated Yb-matrix element, the signal intensities of masses, in terms of atomic mass unit (amu), corresponding to ^{176}YbH, ^{172}Yb^{16}O, ^{174}Yb^{16}O and ^{174}Yb^{16}OH were monitored in the sample solutions containing various concentrations of Yb, from 0 to 100 µg mL^{-1}, without any REEs added (see table 2.3.2 in section 2.3.1). The species selected for this investigation do not interfere with any of the analytes of interest listed in table 3.2.4 (section 3.2.1.1), but are chosen to show the degree of polyatomic ion formation at masses absent of trace impurities of REEs. The investigation was carried out with the standard operational conditions and parameters of the ICP-MS as listed in table 3.2.2. Table 4.2.1 lists the masses of the species and the natural abundance of the Yb-isotopes investigated in this section.

Table 4.2.1: Masses of the species chosen for the investigation of polyatomic ion formation in various concentrations of Yb with standard operational conditions and parameters of the ICP-MS, and natural abundance of certain isotopes of Yb.

Species	Mass (amu)	Yb isotope	Natural abundance
$^{176}YbH^{+}$	177	^{176}Yb	12.8 %
$^{172}Yb^{16}O^{+}$	188	^{172}Yb	21.8 %
$^{174}Yb^{16}O^{+}$	190	^{174}Yb	31.8 %
$^{174}Yb^{16}OH^{+}$	191	^{174}Yb	31.8 %

Figure 4.2.1 shows that there is a linear increase for the signal intensity of the above-mentioned polyatomic ions of Yb, indicating that the formation of these ions increases along with the matrix element concentration. It can be seen from the figure that formations of hydrides and hydroxides are less severe than oxides. Formation of ^{176}YbH is observable already at 10 µg mL^{-1} Yb, but its signal intensity is minimal relative to the other polyatomic ions. The signal intensities of these polyatomic ions also appear to be affected by the natural abundance of the isotopes of Yb. The most abundant isotope is ^{174}Yb and the signal intensity of its polyatomic ions are much than the lesser abundant isotope of ^{172}Yb. The figure shows that the signal intensity of ^{174}YbO is much higher than ^{172}YbO. In section 3.2.1.1, it was stated that there is a possibility that the formation of ^{168}YbH could cause a mass overlap on ^{169}Tm. As it can be seen from the results obtained in this section, formation of ^{176}YbH is minimal in a Yb solution of 10 µg mL^{-1}. ^{176}Yb has a natural abundance of 12.8 %, while ^{168}Yb has a natural abundance of 0.1 %. Formation of ^{168}YbH is therefore likely not to occur as the amount of ^{168}Yb being introduced into the plasma is insufficient to form hydrides. If ^{168}YbH does occur, however, its contribution to the signal intensity at mass 169 would be less than the contribution of ^{176}YbH to mass 177.

It can be observed from the figure that formation of ytterbium-based polyatomic ions occurs, which also suggest that the signal intensity at mass 175 in the investigation of signal suppression stems from both ^{175}Lu and ^{174}YbH. In order to accurately determine the concentration of Lu for the purity determinations of Yb, the interfering mass of ^{174}YbH must be eliminated from contributing to the signal intensity registered at mass 175.

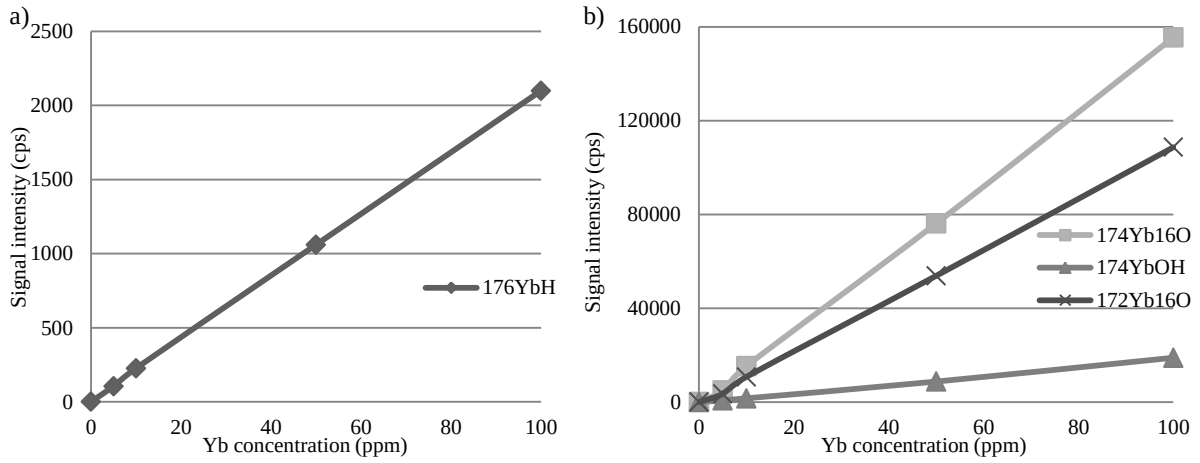

Figure 4.2.1: Signal intensities of a) ^{176}YbH, b) ^{172}Yb^{16}O, ^{174}Yb^{16}O and ^{174}Yb^{16}OH in 0, 5, 10, 50 and 100 µg mL^{-1} Yb determined by the ICP-MS with standard operational conditions and parameters as listed in table 3.2.2.

4.2.1. Formation of polyatomic ions at various ICP RF-power and nebulizer gas flow rate

The possibility of reducing, and ultimately eliminating, the formation of polyatomic ions were investigated by changing the plasma conditions of the ICP-MS. As it has been stated earlier, the formation of polyatomic ions occurs in the cooler regions of the plasma. The formation of ^{174}YbH and the other polyatomic ions of Yb may be reduced by increasing the inductively coupled plasma radiofrequency (ICP RF)-power, which also increases the temperature of the plasma. However, this procedure sacrifices the instrument sensitivity [53]. Formation of the polyatomic ions may also be reduced by altering the nebulizer gas flow rate, as it affects the amount of sample that is introduced into the plasma of the ICP-MS.

By using the standard operational conditions and parameters of the ICP-MS instrument listed in table 3.2.2 in chapter 3, the ICP RF-power of 1000 W and the nebulizer gas flow rate of 0.94 L min^{-1} were used as reference conditions of the plasma for the formation of polyatomic ions. The signal intensities of masses corresponding to ^{174}YbH, ^{176}YbH, ^{174}Yb^{16}O and ^{174}Yb^{16}OH were investigated by altering the plasma conditions through its ICP RF-power and nebulizer gas flow rate in a sample solution of 10 µg Yb mL^{-1}. Table 4.2.2 lists the masses of the species and the natural abundance of the Yb-isotopes investigated in this section. Of the masses selected, only ^{174}YbH with mass 175 is potentially affected by trace amounts of Lu in the sample solution. The other species do not have REEs that might occur at the masses investigated, but were chosen in order to observe the possibilities for reducing polyatomic ion

formation. Two separate investigations were conducted. The first investigation increased the ICP RF-power from 700 W to 1500 W, while keeping the nebulizer gas flow rate constant at 0.94 L min^{-1}. The second investigation increased the nebulizer gas flow rate from 0.75 L min^{-1} to 1.20 L min^{-1}, while keeping the ICP RF-power constant at 1000 W.

Table 4.2.2: Masses of the species chosen for the investigation of polyatomic ion formation in 10 µg mL^{-1} Yb at various ICP RF-power and nebulizer gas flow rate and natural abundance of certain isotopes of Yb.

Species	Mass (amu)	Yb isotope	Natural abundance
$^{174}YbH^{+}$	175	^{174}Yb	31.8 %
$^{176}YbH^{+}$	177	^{176}Yb	12.8 %
$^{174}Yb^{16}O^{+}$	190	^{174}Yb	31.8 %
$^{174}Yb^{16}OH^{+}$	191	^{174}Yb	31.8 %

The results presented in figure 4.2.2 is obtained by increasing the ICP RF-power from 700 W to 1500 W while keeping the nebulizer gas flow rate constant at 0.94 L min^{-1}. The figure shows that the signal intensities of the polyatomic ions are at their highest values when the temperature of the plasma is at its lowest. It can also be observed that the signal intensities of these polyatomic ions are being reduced with increasing ICP RF-power. The signal intensities of these ions, with the exception of ^{174}YbH, are reduced by 60 – 74 % as the ICP RF-power is increased from 700 W to 800 W. The signal intensity of ^{174}YbH at mass 175 was reduced by 25 %.

As explained earlier through the tetrad effect, the standard solution of Yb most likely contains a significant amount of Lu as trace impurity compared to the other REEs. While signal intensities of the polyatomic ions are reduced with increasing ICP RF-power, trace amounts of Lu contribute to the registered signal intensity at mass 175. Figure 4.2.2 shows that the formation of polyatomic ions cannot be completely eliminated by increasing the ICP RF-power. The reduction in signal intensity may also be a result of decreased sensitivity. As the ICP RF-power is increased, the ion kinetic energy is increasing, which may complicate the focusing of ions. Also, by increasing the temperature of the plasma, the chances for formation of doubly charged ions. Reduction in signal intensities may either be a result of reduction in formation of polyatomic ions, increased formation of doubly charged ions, reduced sensitivity, or a combination of those effects.

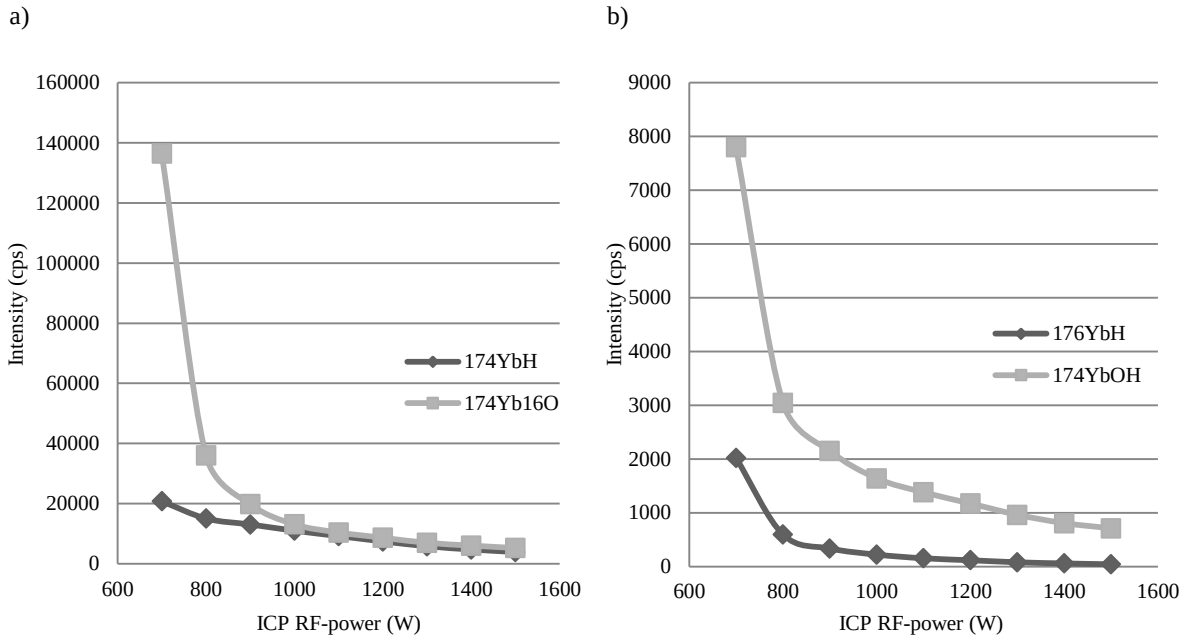

Figure 4.2.2: Signal intensities of masses corresponding to formation of a) ^{174}YbH, ^{174}YbO, b) ^{176}YbH and ^{174}YbOH in a sample of 10 µg Yb mL^{-1} with increasing ICP RF-power. The nebulizer gas flow rate was held constant at 0.94 L min^{-1}.

The formation of polyatomic ions was also investigated by altering the nebulizer gas flow rate. The nebulizer gas flow rate determines the amount of sample that is being introduced into the plasma. As the flow rate increases, so does the amount of sample being introduced into the plasma. The next experiments compared the formation of polyatomic ions as the nebulizer gas flow was increased from 0.75 L min^{-1} to 1.20 L min^{-1}, while the ICP RF-power was held constant at 1000 W.

Figure 4.2.3 shows the signal intensities of the polyatomic ions in table 4.2.2 in a sample of 10 µg mL^{-1} Yb as the nebulizer gas flow rate was increased from 0.75 L min $^{-1}$ to 1.2 L min^{-1}. From the figure it can be seen that the signal intensities of these polyatomic ions are reduced as the nebulizer gas flow rate is reduced from 0.94 L min^{-1} to 0.75 L min^{-1}. The signal intensity of mass 175 reaches its maximum signal intensity at 1.0 L min^{-1} before it is decreasing. It can be observed from figure 4.2.3 that the signal intensity of ^{174}YbO at mass 190 increases exponentially as the nebulizer gas flow rate increases from 1 L min^{-1} to 1.2 L min^{-1}, while the signal intensity of ^{174}YbH at mass 175 decreases. The figure suggests that the increased nebulizer gas flow rate favours the formation of oxides and hydroxides instead of hydrides as more of the sample is being introduced into the plasma.

Signal intensity of ^{176}YbH does not reach its maximum point until the nebulizer gas flow rate is 1.15 L min^{-1}. This is likely due to the natural abundances of the isotopes of Yb, which can be seen in table 4.2.2. ^{174}Yb is the most abundant isotope of Yb, with an abundance of 31.8 %, while ^{176}Yb has an abundance of 12.8 %. The figure suggests that the amount of ^{176}Yb being introduced into the plasma does not reach the corresponding amount of ^{174}Yb at a nebulizer gas flow rate of 1.0 L min^{-1} until the flow rate has passed 1.15 L min^{-1}. The reduction in signal intensities of masses representing formation of polyatomic ions at a nebulizer gas flow rate of 0.75 L min^{-1} is likely due to the small amount of sample being introduced into the plasma, which results in loss of sensitivity as well as less formation of polyatomic ions.

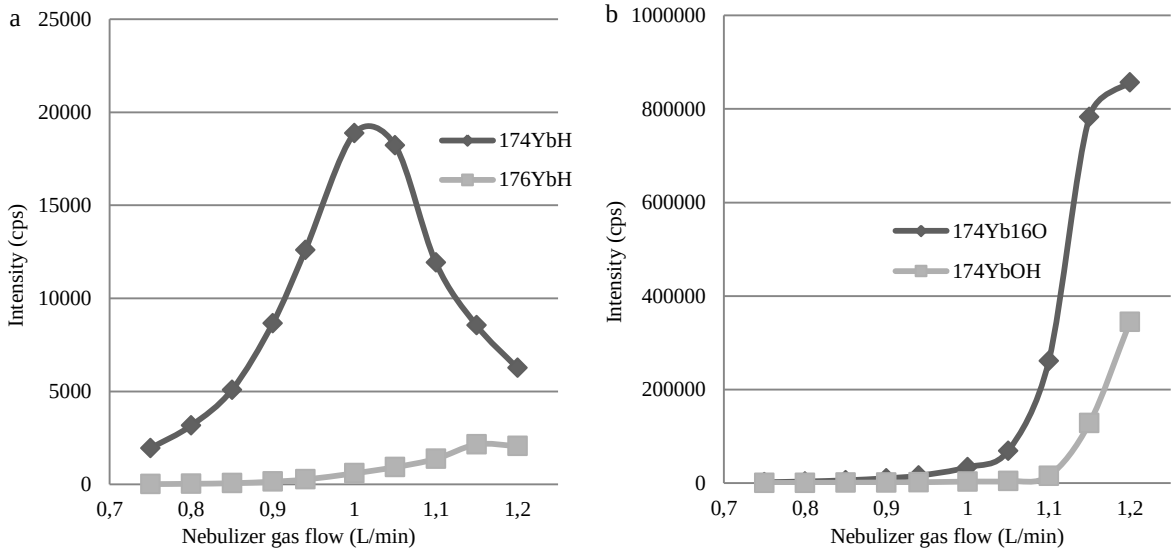

Figure 4.2.3: Signal intensities of masses corresponding to formation of a) ^{174}YbH, ^{176}YbH, b) ^{174}YbO and ^{174}YbOH in a sample of 10 µg Yb mL^{-1} with increasing nebulizer gas flow rate. The ICP RF-power was held constant at 1000 W.

By altering the plasma conditions through the ICP RF-power and the nebulizer gas flow rate it was observed that the signal intensities of the masses corresponding to formation of the above-mentioned polyatomic ions were reduced. From figure 4.2.2 and 4.2.3 it was observed that the nebulizer gas flow rate affected the signal intensity of ^{174}YbH at mass 175 to a higher degree compared to the ICP RF-power. As the nebulizer gas flow rate is reduced from 0.94 L min^{-1} to 0.75 L min^{-1}, the signal intensity of mass 175 was reduced by 90 % of its original intensity, while the increase of ICP RF-power from 700 W to 1500 W reduced the original signal intensity by 80 %. The reduction in signal intensities of the monitored species in figure 4.2.3 may be due to the lesser amount of sample being introduced into the plasma, which reduces the sensitivity of the species. But as a consequence of reduced introduction of sample,

formation of polyatomic ions may also be reduced as the amount of matrix element is insufficient to form polyatomic ions in the plasma.

Although the reduction of signal intensity may be due to both loss in sensitivity and reduced formation of polyatomic ions, it is not possible to determine which plasma conditions may completely remove the formation of ^{174}YbH in the standard solution of Yb, diluted to 10 µg mL^{-1}, as it has the same mass as ^{175}Lu. To find the most ideal plasma condition for the reduction in ytterbium hydride formation, Yb must be separated from Lu in order to determine the contribution of ^{174}YbH to the signal intensity at mass 175.

4.3. Determination of REEs as trace impurities in standard solution of Yb with ICP-MS by the method of standard additions

The method of standard additions was applied to the standard solution of Yb in order to obtain an estimate of its purity when determined by the ICP-MS while being affected by polyatomic ion formation. The standard solution of Yb was diluted to 10 µg mL^{-1} based on the results in section 4.1, as signal suppression of the REEs was not observed at this concentration of the matrix element. It is expected that the Yb standard solution contains a relatively high amount of Lu compared to the other REEs, as a pure standard solution of Yb is not available. The determination was performed with the presence of ^{174}YbH overlapping with ^{175}Lu at the mass of 175, as the method of standard additions does not correct for formation of polyatomic ions. The sample and calibration solutions from section 2.3.2 in chapter 2 were determined. Isotopes chosen for monitoring are presented in table 3.2.4 in chapter 3. Standard operational conditions and parameters of the ICP-MS were used for the determination of REEs as trace impurities in the diluted standard solution of Yb.

The results presented in table 4.3.1 shows that Lu constitutes 62 % of the total REEs as trace impurities found in the diluted standard solution of Yb. The total amount of REEs found in 10 µg Yb mL^{-1} is 376 ± 10 pg mL^{-1} and resulted in a purity of > 99.99 % on a trace metal basis of the standard solution of Yb. But due to the formation of polyatomic ions, the determination of REEs as trace impurities is inaccurate as the formation of ^{174}YbH contributes to the registered signal intensity of ^{175}Lu at mass 175. In order to determine the exact concentration of Lu, the

signal intensity of ^{175}Lu at mass 175 must be distinguished from the signal intensity of ^{174}YbH. See section A.2.1 in the appendix for purity calculation, calibration curves and statistics.

Table 4.3.1: Concentration of REEs determined as trace impurities in the standard solution of Yb, diluted to 10 µg mL^{-1}, by method of standard additions with ICP-MS. The standard operational conditions and parameters of the ICP-MS are listed in table 3.2.2 of chapter 3.

Analyte isotope	**Concentration (pg mL^{-1})**
Sc	0.6 ± 0.2
Y	10.4 ± 0.2
La	8.25 ± 0.04
Ce	1.2 ± 0.1
Pr	11.03 ± 0.03
Nd	38.4 ± 0.7
Sm	19.2 ± 0.7
Eu	2.2 ± 0.1
Gd	7.5 ± 0.3
Tb	1.10 ± 0.03
Dy	9.3 ± 0.2
Ho	0.61 ± 0.04
Er	15.3 ± 0.1
Tm	18.2 ± 0.6
Lu	232.5 ± 10.0
ΣREEs	376 ± 10
Purity of Yb standard solution	99.9962 ± 0.0001 %

4.4. Determination of REEs as trace impurities in standard solution of Eu with ICP-MS by external standardisation

In order to obtain an estimate of the purity of the standard solution of Eu, the REEs as trace impurities were determined by external standardisation with the ICP-MS. Purity determination based on a trace metal basis was performed on the standard solution of

europium, which was diluted to 10 µg mL^{-1} based on the results in section 4.1. As explained in section 3.2.1.2 of chapter 3, the abundance sensitivity and spectral interferences that were presented in table 3.2.5 can be avoided by selecting the isotopes listed in table 3.2.6. Tm is the only analyte that would be affected by spectral interferences in the form of polyatomic ion formation, as it is mono-isotopic. Gd is expected to be the main constituent of the total REEs as trace impurities, as Eu and Gd are much harder to separate from each other relatively to other REEs (see section 1.3.2 in chapter 1). The analysis was performed on sample and calibration solutions from section 2.3.3 in chapter 2 with standard operational conditions and parameters of the ICP-MS.

The results obtained in table 4.4.1 shows the amount of REEs determined in standard solution of Eu, diluted to 10 µg mL^{-1}. The total concentration of REEs determined in the sample solution was 2212 ± 70 µg mL^{-1}. Gd and Tm constitute 95 % of the REEs as trace impurities, where Tm by itself constitutes 74 % of the total impurities. Based on the investigation of polyatomic ions in section 4.2, it was found that the formation of oxides is much more severe than formation of hydrides. The high amount of Tm in the sample solution is therefore most likely caused by the formation of ^{153}EuO, which has the same mass as the mono-isotopic Tm, 169 amu. The results also show that Sc is below its limit of detection. Purity of the standard solution of Eu was found to be > 99.98 % when determined solely by ICP-MS based on trace REEs as impurities. But in order to acquire an accurate purity of the Eu standard solution, ^{169}Tm must be determined absent the contribution of ^{153}EuO to the signal intensity at mass 169. The low detection limits obtained in this method, ranging from 0.03 to 3.3 pg mL^{-1}, give a possibility for determining certain REEs in the concentration range of fg-pg mL^{-1} as trace impurities in REEs and REOs that are > 99.999 % pure. See section A.2.2 in the appendix for purity calculation, calibration curves and statistics, and calculation of the detection limits.

Table 4.4.1: Concentration of REEs determined as trace impurities in the standard solution of Eu, diluted to 10 µg mL^{-1}, by external standardisation with ICP-MS. The standard operational conditions and parameters of the ICP-MS are listed in table 3.2.2 of chapter 3.

Analyte	Concentration (pg mL^{-1})	LOD (pg mL^{-1})
^{45}Sc	< LOD	2.8
^{89}Y	6.0 ± 0.4	0.3
^{139}La	3.2 ± 0.3	0.2
^{140}Ce	1.0 ± 0.3	0.1
^{141}Pr	0.8 ± 0.2	0.1
^{143}Nd	2.9 ± 0.1	0.5
^{147}Sm	76.3 ± 1.5	0.6
^{157}Gd	459.0 ± 8.6	0.8
^{159}Tb	0.4 ± 0.1	0.1
^{163}Dy	1.3 ± 0.02	0.2
^{165}Ho	0.2 ± 0.04	0.03
^{166}Er	0.4 ± 0.1	0.1
^{169}Tm	1642.2 ± 69.7	1.2
^{174}Yb	17.2 ± 4.9	3.3
^{175}Lu	0.6 ± 0.3	0.1
ΣREEs	2212 ± 70	
Purity of Eu standard solution	99.9779 ± 0.0007 %	

4.5. Separation of Lu from Yb by ion pair chromatography with OS-HIBA system

Due to the formation of ^{174}YbH, caused by the highly concentrated matrix element of Yb, whose mass overlaps with ^{175}Lu, accurate purity determination of the standard solution of Yb by ICP-MS is not possible. The attempt of finding the plasma conditions which eliminates the hydride formation is also not possible as the standard solution contains a relatively high amount of Lu as trace impurity. The presence of Lu hinders the conclusion of which plasma conditions the signal intensity of ^{174}YbH was undetectable. Therefore, separation of Lu from

Yb is needed in order to determine the concentration of Lu absent of the interfering polyatomic ion of ^{174}YbH and the contribution of ^{174}YbH to the signal intensity at mass 175.

This section investigated the separation of Lu from Yb by ion pair chromatography, utilizing the OS-HIBA system. The mobile phase composition is described in section 2.3.5 and sample solutions used for the separation of Lu and Yb are presented in section 2.3.4 in chapter 2. All analyses were conducted with standard operational conditions and parameters of the ICP-MS listed in table 3.2.2 in chapter 3. The only masses that were monitored during the chromatographic separations with this system were mass 175, which correspond to ^{175}Lu and the formation of ^{174}YbH in the plasma, and mass 174 corresponds to ^{174}Yb. Since polyatomic ions of Yb do not cause mass overlaps with the remaining REEs, their separation from the matrix element is not needed. Operating conditions of the HPLC is referred to section 3.3.1 in chapter 3. If the desired separation between Lu and Yb is achieved in a sample solution of 10 µg mL^{-1} Yb, mass 175 should have two peaks in the chromatogram, which represent ^{175}Lu and formation of ^{174}YbH in the plasma.

The pH and concentration of OS and HIBA in the mobile phase were optimized until the desired separation of Lu and Yb was achieved. With the mobile phase composition listed in table 4.5.1, Lu and Yb at concentration of 250 pg mL^{-1} were partially separated through a gradient program with an analysis time of 10 minutes per sample as can be seen in figure 4.5.1.

Table 4.5.1: Gradient program for the separation of Lu and Yb in an OS-HIBA system by ion pair chromatography.

Gradient program	Time	Mobile phase composition	Mobile phase flow rate
Equilibration step	5 min	0.05 M HIBA, 40 mM n-OS	1 mL min^{-1}
Gradient step	5 min	0.05-0.5 M HIBA, 40 mM n-OS	1 mL min^{-1}

Although figure 4.5.1 shows that the two elements did not achieve full separation, the retention times of the analytes were found through repeated runs with the gradient program in table 4.5.1 in order to establish its precision. It was found that the retention times of Lu and Yb with the gradient program in table 4.5.1 were 4.1 minutes and 4.3 minutes, respectively. The same method was then applied to the standard solution of Yb, diluted to 10 µg mL^{-1}. The partial separation of Lu and Yb was sufficient to detect the formation of ^{174}YbH as the matrix

element is introduced into the plasma, which can be seen in figure 4.5.2, but insufficient to determine its exact contribution to the signal intensity at mass 175. The formation of ^{174}YbH does occur in a sample of 10 µg mL^{-1} Yb and has the same mass as ^{175}Lu, which is observed in the chromatogram as a shoulder the peak of Lu. From figure 4.5.2 it can be seen that the shoulder peak of Lu reaches it maximum point at 4.3 minutes, which is also the retention time of Yb found with the sample solution containing 250 pg Lu and Yb mL^{-1}. Therefore, the shoulder peak of Lu represents the formation of ^{174}YbH as the matrix element is introduced to the plasma.

The OS-HIBA system gives sharp and symmetrical peaks of the analytes and further optimization of the mobile phase could perhaps improve the separation of Lu and Yb. But the reagents used in this system contain high amount of Na. All of the reagents used for the mobile phase, with the exception of HIBA, contain sodium. The high amount of solids is not ideal for a routine analysis method due to the increased chance of salt deposition on the entrance cones of the ICP-MS, such as the sampler and skimmer cones. The level of total dissolved solids in the sample matrix analysed by ICP-MS is preferably kept below 0.2 % due to the small orifice sizes of the cones. High amounts of salts may therefore lead to deposition of solids on the cones and blocking the orifice, which may result in unstable signals [34]. The deposition of solids while using this system also increased the frequency for cleaning the cones in the interface region, which is not ideal for a routine analysis method. Therefore, a different IPR was tested that did not contain sodium. This IPR is also more volatile, which is more suited for the hyphenation of the HPLC to the ICP-MS for an online separation.

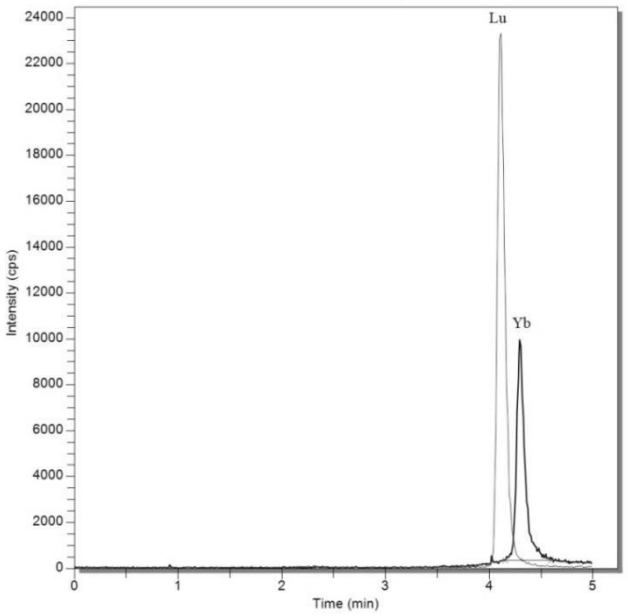

Figure 4.5.1: Chromatogram of Yb and Lu at a concentration of 250 pg mL^{-1} separated by a gradient run of 0.05 M to 0.5 M HIBA over 5 minutes with 40 mM OS as the IPR on a C18-column (4.6 x 150 mm, 5 µm). The ICP-MS was set to its standard operational conditions and parameters as listed in table 3.2.2 in chapter 3. The peaks labelled as Lu and Yb corresponds to the masses 175 and 174, respectively.

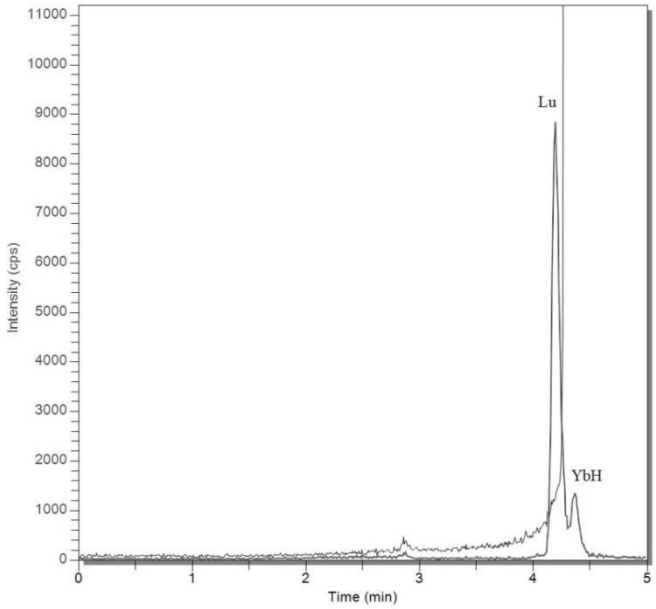

Figure 4.5.2: Chromatogram of Lu and Yb in the standard solution of Yb diluted to 10 µg mL^{-1} and separated by a gradient run of 0.05 M to 0.5 M HIBA over 5 minutes with 40 mM OS as the IPR on a C18-column (4.6 x 150 mm, 5 µm). The ICP-MS was set to its standard operational conditions and parameters as listed in table 3.2.2 in chapter 3. The peak of Yb has been cropped out of the picture. The peak labelled as YbH represents the formation of ^{174}YbH in the plasma, which has the mass of 175.

4.6. Separation of Lu from Yb by ion pair chromatography with HFBA-HIBA system

The OS-HIBA system from the previous section was shown to be unsuitable for a routine analysis method due to the deposition of salts on the entrance cones of the interface region of the ICP-MS. Attempts of separating Lu from Yb through ion pair chromatography were therefore performed with HFBA as the IPR. HFBA is more volatile, does not contain Na as opposed to OS and is therefore more suitable for the ICP-MS. The sample solutions and mobile phase that were analysed are described in section 2.3.4 and 2.3.5 in chapter 2. The masses of 175 and 174 were selected for monitoring. Section 3.3.2 in chapter 3 describes the operational conditions of the HPLC. Standard operational conditions and parameters of the ICP-MS were used throughout all analyses.

The attempt of separating Lu at mass 175 from Yb at mass 174 by the HFBA-HIBA system was unsuccessful. Different concentrations of HFBA and HIBA as well as pH of the mobile phase were tried, but the desired separation was not achieved. The best separation achieved with this system was by a gradient program of which the analysis time per sample is 11 minutes, listed in table 4.6.1. The gradient program did not succeed in the separation of 250 pg mL^{-1} Lu and Yb from each other, as can be seen in figure 4.6.1.

Although HFBA does not contain sodium, the amount of NaOH added to adjust the pH of the mobile phase was enough to cause significant deposition of salts on the entrance cones of the ICP-MS. The pH of this mobile phase system was adjusted by using between 2-5 mL of 10 M NaOH (see section 2.3.5, chapter 2), which greatly contributed to the deposition of salts on the entrance cones of the ICP-MS. It was mentioned in the previous section that the tolerated amounts of salts for the ICP-MS is minimal. Further optimization of this system was therefore not investigated as the entrance cones of the ICP-MS had to be frequently cleaned. Separation of Lu and Yb must be performed without any reagents containing sodium due to the ease of deposition of solids on the entrance cones of the ICP-MS. NH_4OH is a more suitable strong base to adjust the mobile phase's pH compared to NaOH. Further investigations of this system, by using NH_4OH to adjust the mobile phase's pH, are needed to determine its suitability towards the separation of Lu from Yb.

Table 4.6.1: Gradient program for the separation of Lu from Yb with HFBA as the IPR.

Gradient program	Time (min)	Mobile phase composition	Mobile phase flow rate
Equilibration step	5	0.05 M HIBA, 20 mM HFBA	1 mL min^{-1}
Gradient step	6	0.5 M HIBA, 20 mM HFBA	1 mL min^{-1}

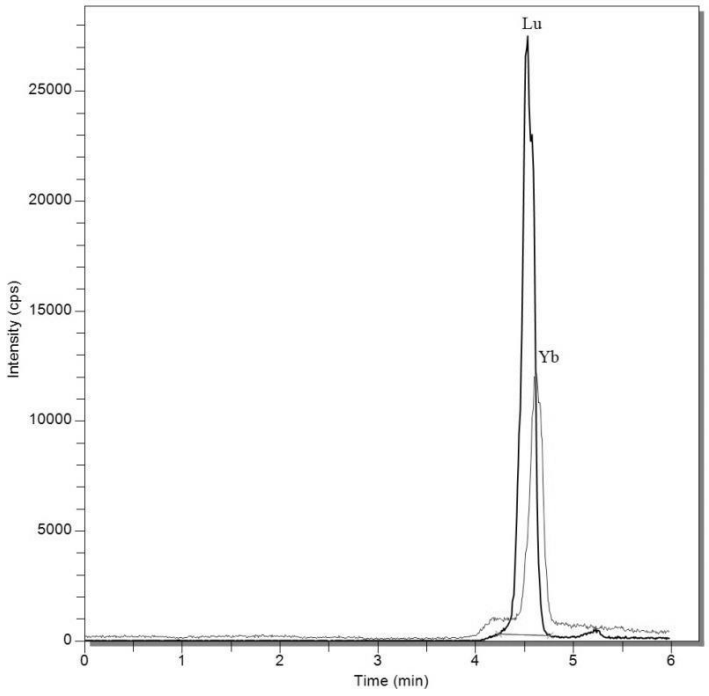

Figure 4.6.1: Chromatogram of an unsuccessful attempt of separating Lu from Yb at a concentration of 250 pg mL^{-1} from each other. The gradient program in table 4.6.1 was used on a C18-column (4.6 x 100 mm, 2.7 µm). Standard operational conditions and parameters of the ICP-MS were used.

4.7. Separation of Lu from Yb by extraction chromatography with HNO_3-HDEHP system

Extraction chromatography with HDEHP as the organic extractant impregnated on a C18-column and HNO_3 as the eluent was investigated for the separation of Lu from Yb. The original method, which these experiments are based on, was designed to separate all of the REEs from each other. From its original gradient program, the retention time of Yb and Lu were found to be 22 and 23 minutes, respectively [52]. The total analysis time per sample of the original method is too long for the purpose of this work. Therefore, several attempts of shortening the total analysis time were made.

The mobile phase for the HNO_3-HDEHP system described in section 2.3.5 were used for the separation of Lu and Yb in sample solutions listed in section 2.3.4 in chapter 2. The sample solution containing each REE at 1 ng mL^{-1} was to be analysed until the desired separation of Lu and Yb was achieved within a reasonable timespan. The appropriate elution program was then to be applied to the standard solution of Yb, which was diluted to 10 µg mL^{-1}. The analyses were performed with standard operational conditions and parameters of the ICP-MS. Operational conditions of the HPLC can be seen in section 3.3.3 in chapter 3. The isotopes that were monitored in the sample of all REEs at 1 ng mL^{-1} are listed in table 3.2.4 (chapter 3). For the diluted standard solution Yb, the masses of 168 and 175 were selected for monitoring. The mass of 168, which corresponds to ^{168}Yb, was chosen since the natural abundance of ^{168}Yb is 0.1 % (see section 3.2.1.1), which is sufficient for detection in a highly-concentrated sample of Yb without overloading the detector of the ICP-MS. If the desired separation between Lu and Yb is achieved in a sample solution of 10 µg mL^{-1} Yb, mass 175 should have two peaks, where one corresponds to ^{175}Lu and the other formation of ^{174}YbH in the plasma. The peak that represents formation of ^{174}YbH will have the same retention time as mass 168 as it is formed when the matrix element Yb is introduced into the plasma.

As a preliminary investigation of the system, the sample of REEs at equal concentration (1 ng mL^{-1}) was subjected to a gradient program of 0.2 M to 2 M HNO_3 over 15 minutes with an additional step of 5 minutes with constant 2 M HNO_3. Figure 4.7.1 shows that the system is able to provide decent separation between LREEs and HREEs. The retention time of Yb and Lu were 13 and 15 minutes, respectively. The gradient program was able to separate Yb and Lu, but the total analysis time is too high for a routine analysis method, and therefore undesirable. In order to shorten the analysis time, an attempt of separating the analytes by an isocratic run was performed with a mobile phase strength of 2.25 M HNO_3. An isocratic program could greatly reduce the total analysis time, provided that it gives the desired separation of Lu and Yb.

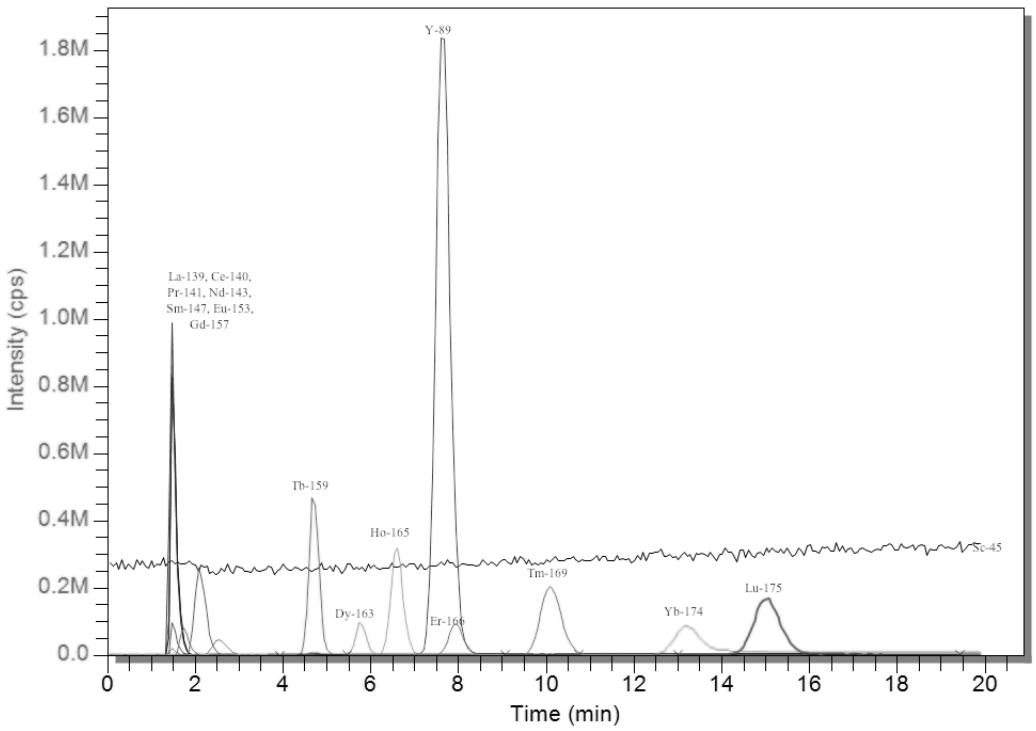

Figure 4.7.1: Chromatogram of the sample solution containing all REEs at 1 ng mL^{-1}, separated by gradient elution of 0.2M – 2M HNO_3 over 15 minutes, with an additional step of 5 minutes with constant 2M HNO_3, on a C18-column (4.6 x 150 mm, 5 µm) impregnated with 0.16 mmole HDEHP. The mobile phase flow rate was 1 mL min^{-1}, while standard operational conditions and parameters of the ICP-MS were used.

Yb and Lu were separated from each other in the sample of 1 ng mL^{-1} of each REE within a 6-minute isocratic run with 2.25 M HNO_3, as shown in figure 4.7.2. Although it also shows that Yb and Lu are not completely separated, the separation achieved may be sufficient for detecting the formation of ^{174}YbH in the plasma. The same isocratic conditions were applied to the same sample, but the masses selected for monitoring were 174 (Yb) and 175 (Lu). The isocratic run had also been reduced to 5 minutes. Table 4.7.1 presents the isocratic program and mobile phase composition for the separation of Lu from Yb. As can be seen in figure 4.7.3, the retention time of Yb and Lu are 2.7 and 3.7 minutes, respectively. The retention times were established by several repeated runs with the same chromatographic conditions.

Table 4.7.1: Isocratic program for the separation of Yb and Lu in 10 µg mL^{-1} Yb by extraction chromatography on a C18-column (4.6 x 150 mm, 5 µm) impregnated with 0.16 mmole HDEHP.

Isocratic program	Time	Mobile phase strength	Mobile phase flow rate
Equilibration step	1 min	2.25 M HNO_3	1 mL min^{-1}
Isocratic step	5 min	2.25 M HNO_3	1 mL min^{-1}

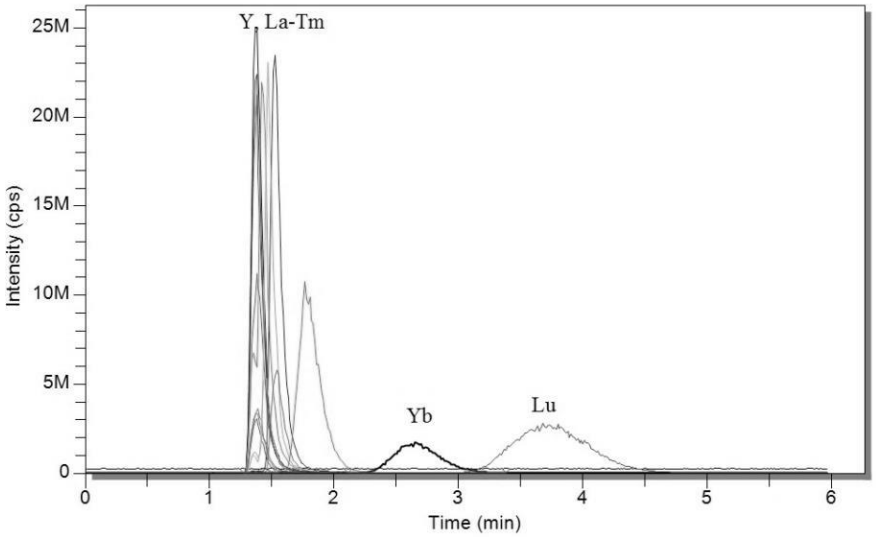

Figure 4.7.2: Chromatogram of 1 ng mL^{-1} of each REE, separated by isocratic elution with 2.25M HNO_3 over 6 minutes on a C18-column (4.6 x 150 mm, 5 µm) impregnated with 0.16 mmole HDEHP. The mobile phase flow rate was 1mL min^{-1}, while standard operational conditions and parameters of the ICP-MS were used.

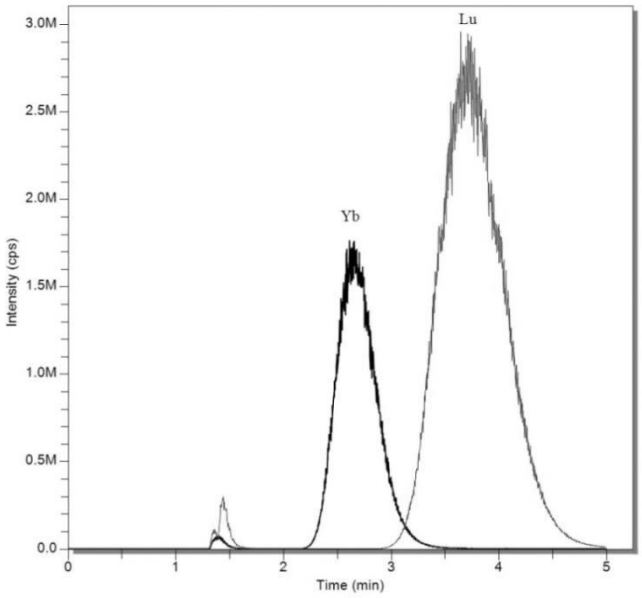

Figure 4.7.3: Chromatogram of 1 ng mL^{-1} of each REE separated by isocratic elution with 2.25M HNO_3 over 5 minutes on a C18-column (4.6 x 150 mm, 5 µm) impregnated with 0.16 mmole HDEHP. The mobile phase flow rate was 1mL min^{-1}, while standard operational conditions and parameters of the ICP-MS were used.

The isocratic program was also applied to the diluted standard solution of Yb of which the masses selected for monitoring were mass 168 and 175. Figure 4.7.4 shows that the separation achieved is sufficient to distinguish the contribution of ^{174}YbH to the signal intensity at mass 175 from ^{175}Lu. The peaks labelled YbH and Lu in the figure have mass 175. It can be

observed that the peak labelled as YbH has the same retention time as mass 168, which indicates that the formation of ^{174}YbH occurs as the matrix element in introduced into the plasma.

The results obtained is consistent with the results from section 4.5, which showed that formation of ^{174}YbH occurs in the plasma in a sample solution of where the concentration of the matrix element Yb is 10 µg mL^{-1}. Baseline separation of the two species was not achieved, but the method can be used for further investigations of which plasma conditions are able to eliminate the formation of polyatomic ions, as the isocratic run greatly reduces the total analysis time compared to a gradient run. The initial equilibration step of each analysis is set to 1 minute as the column is firstly conditioned with type 1-water for 10 minutes, and another 10 minutes with 2.25 M HNO_3 (see section 3.3.3 in chapter 3). This greatly reduces the time spent per analysis as compared to a typical gradient program of which the equilibration step between each sample is much longer. But in order to accurately determine the concentration of Lu in the standard solution of Yb and to determine the exact contribution of ^{174}YbH to the signal intensity at mass 175, Lu must be fully separated from Yb.

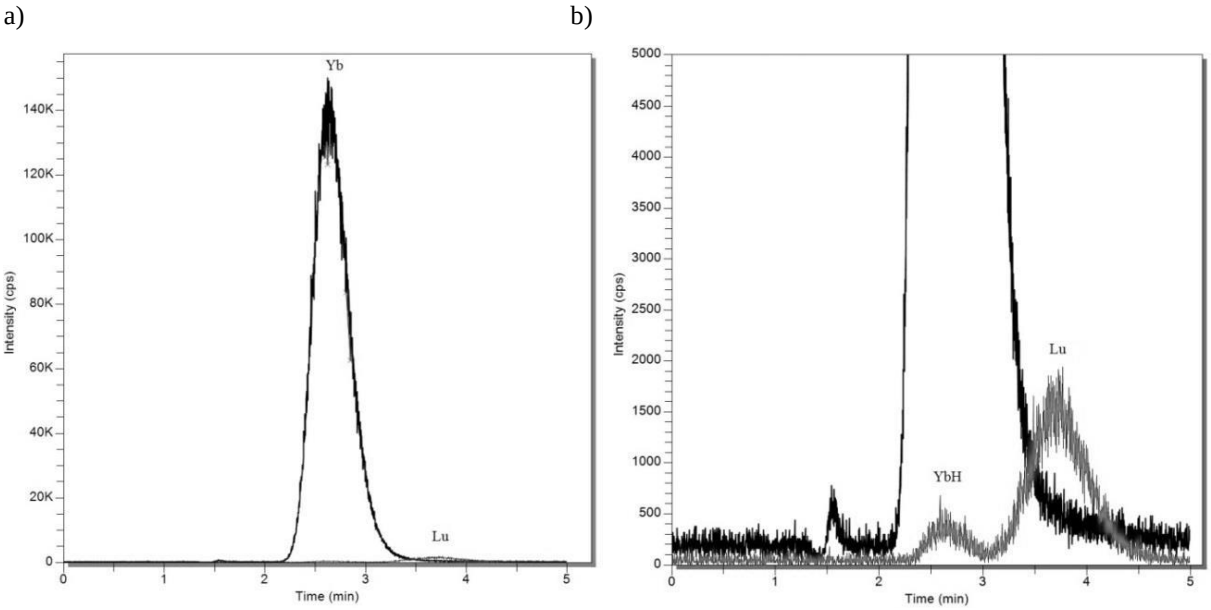

Figure 4.7.4: Chromatogram of standard solution of Yb diluted to 10 µg mL^{-1}. Chromatogram a) shows that mass 168 labelled as Yb is separated from mass 175 labelled as Lu by isocratic elution with 2.25M HNO_3 over 5 minutes on a C18-column (4.6 x 150 mm, 5 µm) impregnated with 0.16 mmole HDEHP. Formation of ^{174}YbH in the plasma can be observed in b), which is caused by the introduction of the highly concentrated Yb matrix to plasma. The mobile phase flow rate was 1mL min^{-1}, while standard operational conditions and parameters of the ICP-MS were used.

As the isocratic elution program was not able to separate the two elements at the baseline, gradient programs were investigated. The desired separation between Lu and Yb was achieved through the gradient program listed in table 4.7.2. Although the total analysis time has increased from 6 minutes to 13 minutes per analysis when going from an isocratic to a gradient program, the desired separation within a reasonable timespan was achieved. The contribution of ^{174}YbH to the signal intensity at mass 175 was found to be distinguishable from ^{175}Lu. Figure 4.7.5 shows the successful separation in the standard solution of Yb diluted to 10 µg mL^{-1} and that the retention times of Yb and Lu were 4.2 and 6.4 minutes, respectively, in this HNO_3-HDEHP system.

By integrating the peak areas via the Chromera software, it was found that ^{174}YbH constitutes 10 % of the total area at mass 175. The contribution of ^{174}YbH to the signal intensity of ^{175}Lu at mass 175 in the diluted standard solution of Yb is relatively small. However, its contribution would have not been able to determine without separating Lu from Yb. In section 4.3, REEs in the standard solution of Yb were determined by the method of standard additions. At a concentration of 10 µg mL^{-1} Yb, Lu was found to be 232.5 ± 10 pg mL^{-1}, including the contribution of ^{174}YbH. Since the ytterbium hydride constitutes 10 % of the total area at mass 175 found by integrating the peak areas, the contribution corresponds to 23.3 pg mL^{-1}. In order to determine the significance of ^{174}YbH to the concentration of Lu found by the ICP-MS, its concentration in the Yb standard solution must also be determined by separating Lu from Yb with HPLC-ICP-MS.

The HNO_3-HDEHP system provided the best separation of the three different chromatographic systems that were investigated for the separation of Lu from Yb, and also proved to be more suitable towards the hyphenation of the HPLC to ICP-MS compared to OS-HIBA due to the absent of dissolved solids in the reagents.

The successful separation of ^{175}Lu and ^{174}YbH, achieved by extraction chromatography on a C18-column (4.6 x 150 mm, 5 µm) impregnated with 0.16 mmole HDEHP with the gradient program listed in table 4.7.2, will be utilized for the purity determination of Yb_2O_3 with a stated purity of 99.9 % based on trace metals and of the Yb standard solution. The isocratic program listed in table 4.7.1 will be used for the investigation of eliminating the formation of ^{174}YbH.

Table 4.7.2: Gradient program for the separation of Yb and Lu by extraction chromatography with HNO_3 as the eluent and 0.16 mmole HDEHP as the extractant impregnated on a C18-column (4.6 x 150 mm, 5 µm).

Gradient program	Time	Mobile phase strength	Mobile phase flow rate
Equilibration step	5 min	1.8M HNO_3	1mL/min
Gradient step	8 min	1.8-2.25M HNO_3	1mL/min

a) b)

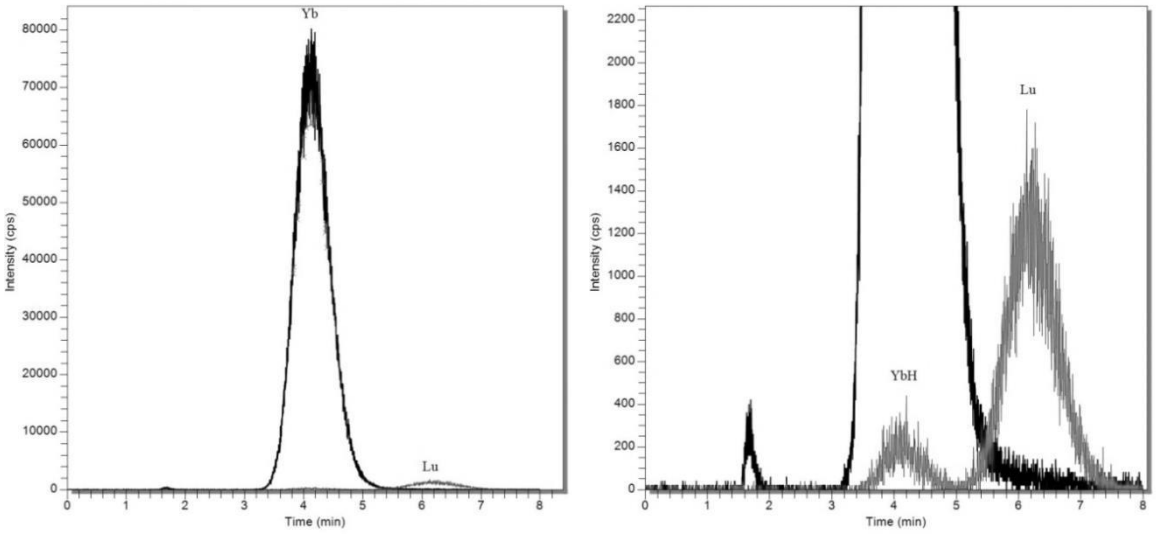

Figure 4.7.5: Chromatogram of standard solution of Yb diluted to 10 µg mL^{-1}. Chromatogram a) shows that mass 168 labelled as Yb is separated from mass 175 labelled as Lu by a gradient run of 1.8 M – 2.25 M HNO_3 over 8 minutes on a C18-column (4.6 x 150 mm, 5 µm) impregnated with 0.16 mmole HDEHP. The mobile phase flow rate was 1mL min^{-1}, while standard operational conditions and parameters of the ICP-MS were used. The formation of ^{174}YbH with mass 175 in the plasma due to the highly concentrated matrix element is observable in chromatogram b) where it is labelled as YbH.

4.7.1. Reducing the formation of ^{174}YbH in the plasma by altering the ICP RF-power and nebulizer gas flow rate

The possibility of eliminating the formation of polyatomic ions by adjusting the ICP RF-power and the nebulizer gas flow rate in a sample of 10 µg Yb mL^{-1} was investigated in section 4.2.1. It was found that the signal intensities of polyatomic ions were reduced with increasing ICP RF-power and decreasing nebulizer gas flow rate. However, it was not

possible to determine whether formation of ^{174}YbH was eliminated or not without distinguishing the signal intensity of ^{174}YbH at mass 175 from ^{175}Lu.

This section utilized the HNO_3-HDEHP system from the previous section, which was able to partially separate Lu from Yb by the isocratic program listed in table 4.7.1, to investigate the signal intensity reduction of mass 175 with various ICP RF-powers and nebulizer gas flow rates. The isocratic program listed in table 4.7.1 was used, as the separation was able to distinguish the signal intensity of ^{174}YbH at mass 175 from ^{175}Lu within a relatively short time compared to the gradient program (table 4.7.2). The attempt of reducing the formation of ytterbium hydride was done by adjusting the ICP RF-power and the nebulizer gas flow rate based on the results obtained from section 4.2.1. The standard operational parameters and conditions of the ICP-MS listed in table 3.2.2 were used as the reference conditions for the formation of ^{174}YbH in the plasma.

A sample solution of 10 µg mL^{-1} Yb (see section 2.3.4 in chapter 2) was subjected to various combinations of nebulizer gas flow rates and ICP RF-powers. Table 4.7.3 shows the various combinations of the ICP-related parameters that were tested, while figure 4.7.6 shows certain chromatograms of the signal intensity at mass 175 with various combinations of the ICP-related parameters. The signal intensity of the first peak of mass 175, which has the same retention time as mass 168 and represents formation of ^{174}YbH in the plasma, was reduced closely to its noise signal with an ICP RF-power of 1300 W and a nebulizer gas flow rate of 0.80 L min^{-1}. It may appear as if the formation of ^{174}YbH was eliminated, but the similar reductions of the signal intensities of Yb and Lu at mass 168 and 175, respectively, rather suggest that the sensitivity has been greatly reduced. Figure 4.7.7 shows the signal intensity of Yb at mass 168 with the corresponding ICP RF-powers and nebulizer gas flow rates as in figure 4.7.6. REEs as trace impurities in the standard solution of Yb will be determined by the ICP-MS with an ICP RF-power of 1300 W and a nebulizer gas flow rate of 0.80 L min^{-1}, and the results will be compared with standard operational conditions and parameters of the plasma after separation of Yb and Lu by the HNO_3-HDEHP whether there is a significant change in the amount of Lu determined by the methods. See section A.3 in the appendix for the remaining chromatograms of the other combinations of ICP RF-power and nebulizer gas flow rate.

Table 4.7.3: Different combinations of ICP RF-power and nebulizer gas flow rate in an attempt of eliminating the formation of ^{174}YbH in the plasma for a sample solution of Yb at 10 µg mL^{-1} by HPLC-ICP-MS.

ICP RF-power	Nebulizer gas flow rate
1000 W	0.94 L min^{-1}
1000 W	0.90 L min^{-1}
1000 W	0.85 L min^{-1}
1100 W	0.85 L min^{-1}
1200 W	0.85 L min^{-1}
1200 W	0.80 L min^{-1}
1300 W	0.80 L min^{-1}

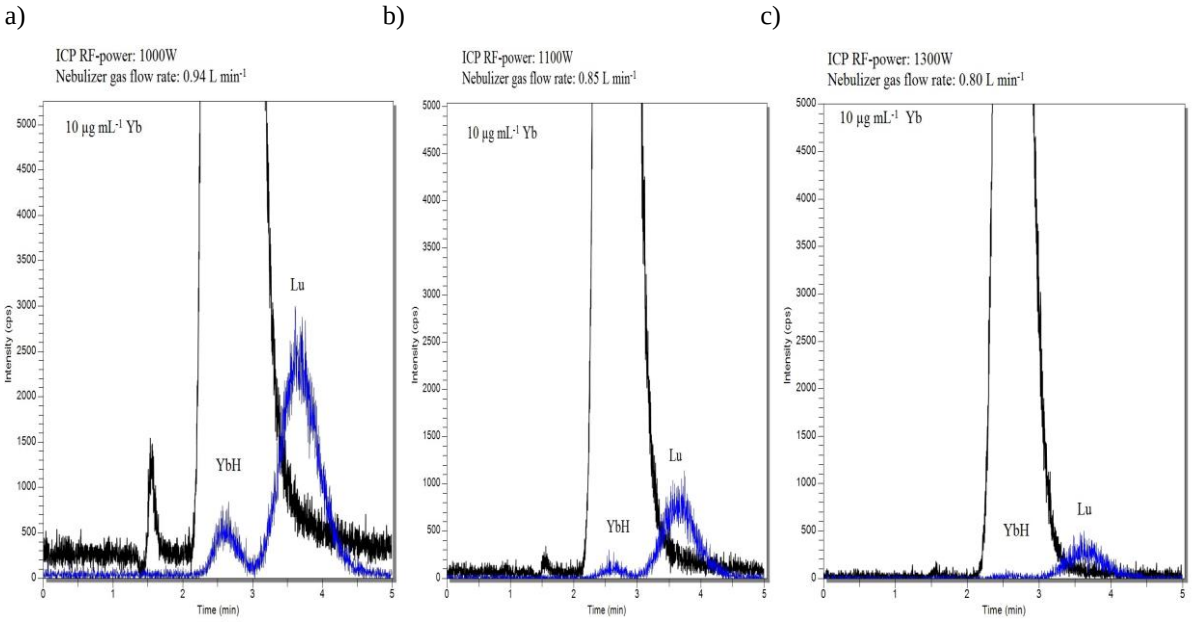

Figure 4.7.6: Chromatograms showing signal intensities of mass 175, which corresponds to ^{175}Lu and formation of ^{174}YbH in the plasma , in a sample of 10 µg Yb mL^{-1} with a) an ICP RF-power of 1000 W and nebulizer gas flow rate of 0.94 L min^{-1}, b) ICP RF-power of 1100 W and nebulizer gas flow rate of 0.85 L min^{-1} and c) ICP RF-power of 1300 W and nebulizer gas flow rate of 0.80 L min^{-1}. The separation of mass 175 and 168 was carried out by the isocratic program listed in table 4.7.1 with the HNO_3-HDEHP system.

a) b) c)

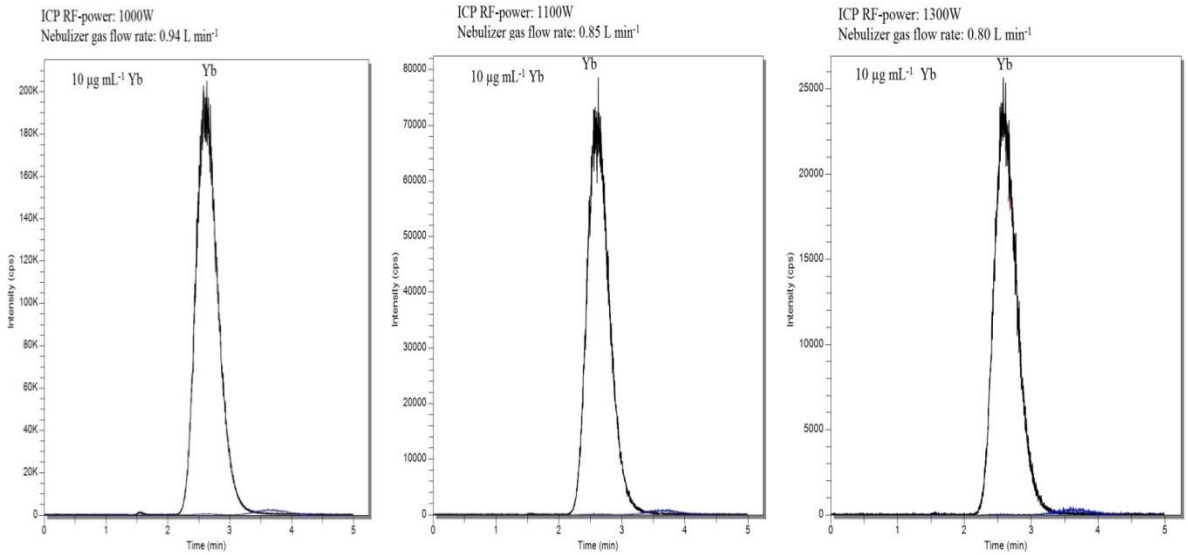

Figure 4.7.7: Chromatograms showing signal intensities of mass 168, corresponding to ^{168}Yb, in a sample of 10 µg Yb mL^{-1} with a) an ICP RF-power of 1000 W and nebulizer gas flow rate of 0.94 L min^{-1}, b) ICP RF-power of 1100 W and nebulizer gas flow rate of 0.85 L min^{-1} and c) ICP RF-power of 1300 W and nebulizer gas flow rate of 0.80 L min^{-1}. The separation of mass 175 and 168 was carried out by the isocratic program listed in table 4.7.1 with the HNO_3-HDEHP system.

4.7.2. Determination of REEs as trace impurities in standard solution of Yb by ICP-MS and HPLC-ICP-MS

By utilizing the methods developed in the previous sections, purity of the standard solution of Yb was determined by the impurity approach. The standard solution was diluted to 10 µg mL^{-1} and the REEs as trace impurities were determined by external standardisation with both the ICP-MS and HPLC-ICP-MS. Lu was determined with HPLC-ICP-MS while the other REEs were determined by the ICP-MS.

Yb and Lu were separated by extraction chromatography with the HNO_3-HDEHP system, using the gradient program listed in table 4.7.2, in order to determine the concentration of Lu absent the contribution of ^{174}YbH to the signal intensity at mass 175. The remaining REEs were determined by the ICP-MS utilizing standard operational conditions and parameters of the ICP-MS, as seen in table 3.2.2 in chapter 3. REEs in the diluted Yb standard solution were also determined with altered plasma conditions based on the findings in section 4.7.1 and the results were compared with the results obtained with standard operation conditions and parameters of the ICP-MS. The altered plasma conditions have an ICP RF-power of 1300 W

and a nebulizer gas flow rate of 0.80 L min^{-1}. Isotopes selected for monitoring in both methods can be seen in section 3.2.1 in chapter 3. In the HNO_3-HDEHP system, the masses selected for monitoring were 168 and 175. Sample and calibration solutions are referred to section 2.3.3 in chapter 2.

The concentrations of REEs as trace impurities in the standard solution of Yb diluted to 10 µg mL^{-1} are presented in table 4.7.4. The results show that the concentrations of REEs found by the two plasma conditions of the ICP-MS are consistent with each other, but the sensitivity for all of the REEs has been decreased when using plasma conditions that reduce the signal intensity of ^{174}YbH. The detection limits of the analytes determined with the altered plasma conditions are increased by several factors.

The concentration of Lu was reduced by 6 % of its original concentration found with the standard plasma conditions, which is in good agreement with the contribution of ^{174}YbH to the signal intensity at mass 175, which was found to be 10 % in the previous section. Although the reduction in signal intensity at mass 175 may seem as if the formation of hydride is eliminated, it is most likely due to an overall decrease in sensitivity. The concentration of Lu determined by HPLC-ICP-MS was found to be reduced by 8 % of its original concentration that was determined by the ICP-MS with standard operational conditions and parameters. In all methods, the purity of the standard solution of Yb was found to be > 99.99 %. By performing a t-test [54] to compare the concentration of REEs determined solely by the ICP-MS operating at standard operational conditions and parameters with REEs determined by the ICP-MS with altered plasma conditions, it was found that the results obtained by the two methods do not significantly differ from each other and that the methods give the same results. The t-test was also used to compare the concentration of Lu determined solely by the ICP-MS with standard operational conditions and parameters, with the concentration determined by HPLC-ICP-MS. It was found that the concentrations of Lu determined by the two methods do significantly differ from each other. The results obtained by utilizing the HPLC-ICP-MS for determining Lu and the ICP-MS for determining the remaining REEs represent more accurate results as the contribution of the interfering polyatomic ion, ^{174}YbH, to the signal intensity at mass 175 has been separated from ^{175}Lu. The purity of Yb found by combining these two analytical techniques is slightly higher than with the results achieved solely by the ICP-MS. Although the contribution of ^{174}YbH to the signal intensity at mass 175 may seem small for the purity determined in this standard solution of Yb, its contribution may be more severe for the analysis of Yb with higher

purities, such as > 99.999 %, by the impurity approach. Calibration curves, statistics, LOD and chromatograms for the purity determination of the Yb standard solution are presented in the appendix under section A.5.1 and A.5.2. Calculations for the t-test can also be seen in section A.5 in the appendix.

Table 4.7.4: Average concentration of REEs found in the standard solution of Yb diluted to 10 µg mL^{-1} by HPLIC-ICP-MS and ICP-MS at standard operational conditions and parameters, and with altered plasma conditions. The values presented are in pg mL^{-1}. Purity of the Yb standard solution is also presented.

Analyte	**Concentration***	**LOD***	**Concentration****	**LOD****	**Concentration*****
Sc	14.2 ± 0.6	1.10	20.9 ± 2.1	15.32	
Y	17.2 ± 0.5	0.13	18.3 ± 0.3	0.85	
La	9.6 ± 0.1	1.04	9.7 ± 0.4	0.60	
Ce	3.0 ± 0.02	0.07	2.3 ± 0.2	0.62	
Pr	11.3 ± 0.2	0.02	12.0 ± 1.0	0.60	
Nd	44 ± 2	0.28	44.1 ± 3.3	5.17	
Sm	99 ± 2	0.93	108.06 ± 8.4	9.19	
Eu	16.5 ± 0.5	0.17	17.3 ± 0.9	1.06	
Gd	23.8 ± 0.6	0.23	26.0 ± 3.8	3.74	
Tb	2.9 ± 0.2	0.07	3.4 ± 0.4	0.39	
Dy	15.1 ± 0.7	0.21	17.1 ± 1.2	1.09	
Ho	1.8 ± 0.1	0.03	1.9 ± 0.2	0.63	
Er	15.5 ± 0.2	0.08	15.0 ± 1.5	1.32	
Tm	17.7 ± 0.5	0.04	17.2 ± 0.2	0.51	
Lu	228 ± 1	0.08	215 ± 5	0.61	210 ± 2
∑REEs	520 ± 3		528 ± 12		501 ± 4
Purity of Yb	99.99480 ± 0.00003 %		99.9947 ± 0.0001 %		99.99499 ± 0.00004 %

*Determined with standard operational conditions and parameters of the ICP-MS. The ICP RF-power was set to 1000 W and the nebulizer gas flow rate was 0.94 L min^{-1}.

**Determined with altered plasma conditions for reducing the signal intensity of ^{174}YbH. The ICP RF-power was set to 1300 W and the nebulizer gas flow rate was 0.80 L min^{-1}.

*** Lu determined with online separation of Lu from Yb by extraction chromatography hyphenated with the ICP-MS at standard operational conditions and parameters.

4.7.3. Determination of REEs as trace impurities in 99.9 % pure Yb_2O_3 by ICP-MS and HPLC-ICP-MS

A commercially available sample of Yb_2O_3 with a stated purity of 99.9 % was decomposed and diluted to 8.7 µg Yb mL^{-1} (see section 2.4 in chapter 2 for sample decomposition procedure). The REEs as trace impurities in the sample solutions were then determined by HPLC-ICP-MS and ICP-MS with standard operational conditions and parameters. Lu was determined with HPLC-ICP-MS by separating Yb and Lu by extraction chromatography with the HNO_3-HDEHP system as in the previous section. The remaining REEs were determined solely by the ICP-MS. Since the previous section has shown that the determination of REEs with altered plasma conditions did not significantly differ from the standard operational conditions and parameters of the ICP-MS, the method was not applied in this analysis. See section A.1.3 in the appendix for the calculations of the final concentration of Yb in the samples that were analysed.

The concentration of REEs as trace impurities found in the decomposed and diluted sample of 99.9 % pure Yb_2O_3 is presented in table 4.7.5. The results show that Yb and Lu constitute 76 % of the total amount of REEs as trace impurities found in the sample of 8.7 µg Yb mL^{-1}. The concentration of Lu found by HPLC-ICP-MS was 8 % lower than the original concentration found by ICP-MS. From figure 4.7.8, it was found that ^{174}YbH constitutes 10 % of the total area at mass 175. The purity of Yb_2O_3 was stated by the manufacturer to be > 99.9 % pure on a trace REEs basis, while its purity was found to be > 99.99 % pure on a trace REEs basis by the methods developed in this work.

By applying a t-test to compare the concentration of Lu determined by the two different methods, it was found that the results obtained do not significantly differ from each other. The standard deviations of the results are relatively high compared to the standard deviations of the results obtained in the previous section (see table 4.7.4), which most likely are caused due to the decomposition procedure of Yb_2O_3. The errors might have aris due to the variations in amount of sample weighed for decomposition and transfer of samples from their PTFE vessels to their volumetric flasks. See section A.5.3 in the appendix for the calibration curves, statistics, LOD and chromatograms for the purity determination of decomposed Yb_2O_3. Calculations for the t-test can also be seen in section A.5.

Table 4.7.5: Average concentration of REEs as trace impurities in 99.9 % pure Yb_2O_3 digested and diluted to 8.7 µg Yb mL^{-1}. The values are in pg mL^{-1}.

Analyte	Concentration*	Concentration**	LOD*
Sc	6 ± 3		1.9
Y	330 ± 23		1.8
La	6 ± 2		2.8
Ce	27 ± 8		1.5
Pr	4 ± 1		0.04
Nd	17 ± 2		0.8
Sm	16 ± 5		2.8
Eu	4 ± 3		0.5
Gd	10 ± 2		0.7
Tb	4.4 ± 0.3		0.1
Dy	13 ± 1		0.4
Ho	5.2 ± 0.5		0.1
Er	32 ± 2		0.1
Tm	54 ± 3		0.1
Lu	314 ± 13	290 ± 9	0.9
∑REEs	843 ± 28	819 ± 27	
Purity of Yb	99.9903 ± 0.0003 %	99.9906 ± 0.0003 %	

*Determined by ICP-MS with standard operational conditions and parameters of the ICP-MS. The ICP RF-power was set to 1000 W and the nebulizer gas flow rate was 0.94 L min^{-1}.

**Determined by HPLC-ICP-MS with the gradient program listed in table 4.7.2. The ICP-MS was operated with standard operational conditions and parameters.

a) b)

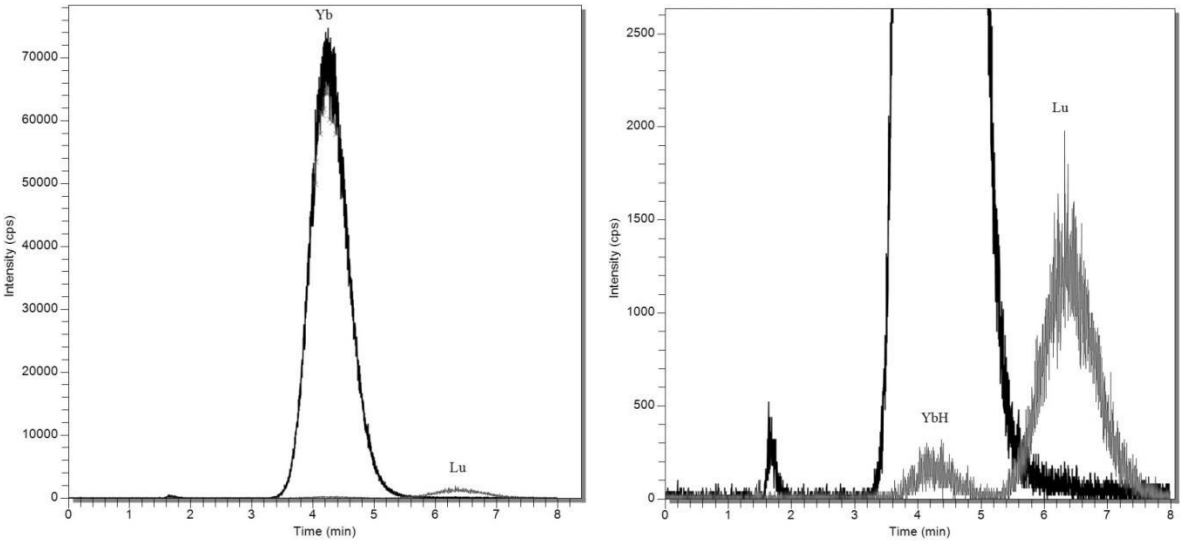

Figure 4.7.8: Chromatogram of 8.7 µg Yb mL^{-1} separated by extraction chromatography with the HNO_3-HDEHP system by the gradient program listed in table 4.7.2. The ICP-MS was operated with standard operational conditions and parameters. The masses selected for monitoring are 168 and 175. Chromatogram a) shows the separation of mass 168 (Yb) and 175 (Lu). Chromatogram b) shows the same separation of mass 175. The peak labelled as YbH represents the formation of ^{174}YbH in the plasma, which has the same mass as the peak labelled as Lu. ^{174}YbH constitutes 10 % of the total area at mass 175 that was found by integration via the Chromera software.

4.8. Separation of Eu from Tm by extraction chromatography with HNO_3-HDEHP system

In section 4.4, the purity of the standard solution of Eu was estimated by external standardisation with ICP-MS by the impurity approach. The determination of REEs as trace impurities in the standard solution of Eu, diluted to 10 µg mL^{-1}, were troubled by the formation of a polyatomic ion whose mass overlapped with the signal intensity of Tm at mass 169. ^{153}EuO was formed due to the highly concentrated matrix element and has the same mass of 169 as the mono-isotopic Tm. Separation of Eu from Tm is therefore needed in order to determine the concentration of Tm without the contribution of ^{153}EuO to the signal intensity at mass 169. Extraction chromatography with the HNO_3-HDEHP system was investigated as the original method of which these experiments are based on [52] provides good separation between the REEs. The preliminary investigations in section 4.7 also showed that LREEs and HREEs are generally well separated from each other.

Sample solutions of Eu that were subjected for separation by this system are listed in section 2.3.4 in chapter 2. The isotopes that were selected for monitoring are presented in section 3.2.2 in chapter 3 unless stated otherwise. Tm is the only element being affected by the polyatomic ions of Eu, therefore, separation of the other REEs is not important as they have isotopes that are free of isobaric and polyatomic interferences (see section 3.2.2 in chapter 3). The goal of the method is to achieve sufficient separation between Eu and Tm within a reasonable time. The experiments were performed with standard operational conditions and parameters of the ICP-MS.

During the first experiments it was discovered that the REEs, with a concentration of 1 ng mL^{-1}, prior to Tm were fully eluted between 1.4 to 1.6 minutes with an isocratic run of 5 minutes with 2.25 M HNO_3, which can be seen in figure 4.8.1. Tm, Yb and Lu are more strongly retained by HDEHP and did not co-elute with the other REEs, however, the peak of Tm did partially overlap with the other REEs. In order to obtain a better separation between Tm and Eu, gradient elution programs were tested.

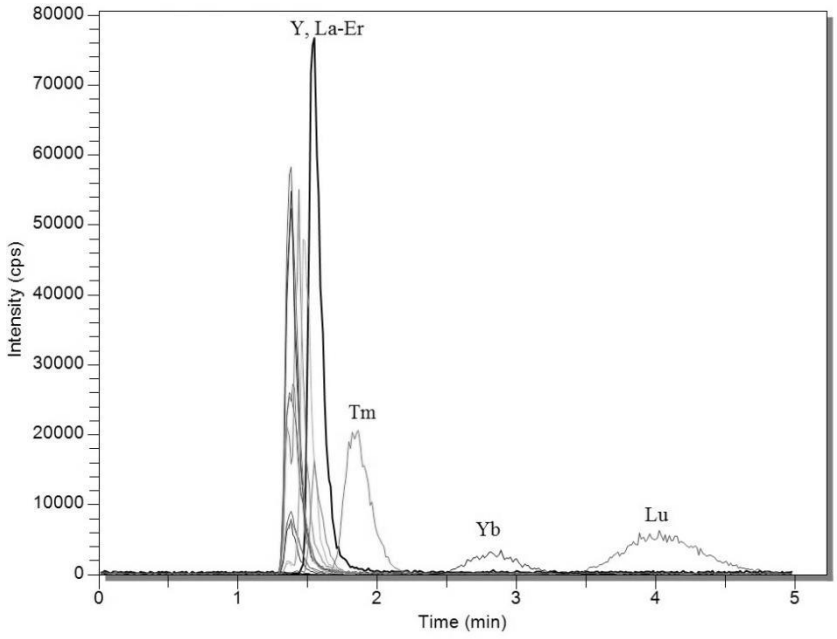

Figure 4.8.1: Chromatogram of the REEs (1 ng mL^{-1}) separated by an isocratic program of 5 minutes with 2.25 M HNO_3 on a C18-column (4.6 x 150 mm, 5 µm) impregnated with 0.16 mmole HDEHP. The mobile phase flow rate was set to 1 mL min^{-1}. Sc has been cropped out of the chromatogram due to high noise signals. The ICP-MS was operated under standard operational conditions and parameters.

The desired separation of Eu and Tm was achieved by the gradient program listed in table 4.8.1. Masses that were selected for monitoring were 153, 169, 174 and 175, which correspond to Eu, Tm, Yb and Lu, respectively. The gradient program consists of two steps.

The first step consists of 4 minutes with constant 1.125 M HNO_3, while the second step consists of 7 minutes with constant 2.25 M HNO_3, to ensure that Yb and Lu are fully eluted. The gradient curve between the two steps was set to 0.

Figure 4.8.2 shows that the separation of REEs at 2 ng mL^{-1} has ensured full elution of the remainder of REEs past Tm, mainly Yb and Lu, and full separation of Eu and Tm was. The time per analysis resulted in 16 minutes, which is relatively long, but the separation achieved by this system can be used as a diagnostic tool in order to determine the contribution of ^{153}EuO that is formed in the plasma to the signal intensity at mass 169 and its significance towards the determination of trace amounts of Tm in the diluted standard solution of Eu. The retention times of the selected REEs were 1.5 minutes for Eu, 5.7 minutes for Tm, 8.4 minutes for Yb and 9.7 minutes for Lu. The retention times were established by several repeated runs with the same chromatographic conditions. To ensure that the masses of 153 and 169 are sufficiently separated in order to distinguish the contribution of ^{153}EuO, which is formed in the plasma, to the signal intensity at mass 169 from Tm, a sample of 10 µg Eu mL^{-1} spiked with REEs at 1 ng mL^{-1} was subjected to the same gradient program (table 4.8.1). Figure 4.8.3 shows that mass 169 has two peaks, which is labelled as EuO and Tm in the figure, and are fully separated from each other. The peak labelled as EuO in the figure has the same retention time as mass 153, which represents Eu, and suggests that formation of ^{153}EuO occurs as the highly concentrated matrix element Eu is introduced into the plasma of the ICP-MS.

The separation achieved is able to determine the contribution of ^{153}EuO, which is formed in the plasma, to the signal intensity observed at mass 169. Determination of REEs as trace impurities in the standard solution of europium can be achieved by utilizing extraction chromatography with a C18-column (4.6 x 150 mm, 5 µm) impregnated with 0.16 mmole HDEHP with the gradient program listed in table 4.8.1. Eu and Tm are fully separated and their retention times are 1.5 and 5.6 minutes, respectively. The method developed can also be used as a diagnostic tool to determine whether the amount of Tm in a diluted standard solution of high-purity Eu significantly troubled by the formation of ^{153}EuO whose mass contributes to the signal intensity determined by the ICP-MS at mass 169. With further investigations, the total analysis time per sample could perhaps be shortened by several minutes since mass 153 and 169 are well separated (figure 4.8.2 and 4.8.3).

Reducing the signal intensity at mass 169 with altered plasma conditions was not tried as the results from the previous sections showed that the sensitivity was worsened for all of the

REEs in a sample of 10 µg mL^{-1} Yb. Section 4.2 also showed that the formation of oxides is more severe compared to the formation of hydrides.

Table 4.8.1: Gradient program for the separation of Eu and Tm by extraction chromatography with the HNO_3-HDEHP system on a C18-column (4.6 x 150 mm, 5 µm) impregnated with 0.16 mmole HDEHP.

Gradient program	Time	Mobile phase strength	Gradient curve	Mobile phase flow rate
Equilibration step	5 minutes	1.125 M HNO_3	-	1 mL min^{-1}
Gradient step 1	4 minutes	1.125 M HNO_3	-	1 mL min^{-1}
Gradient step 2	7 minutes	2.25 M HNO_3	0	1 mL min^{-1}

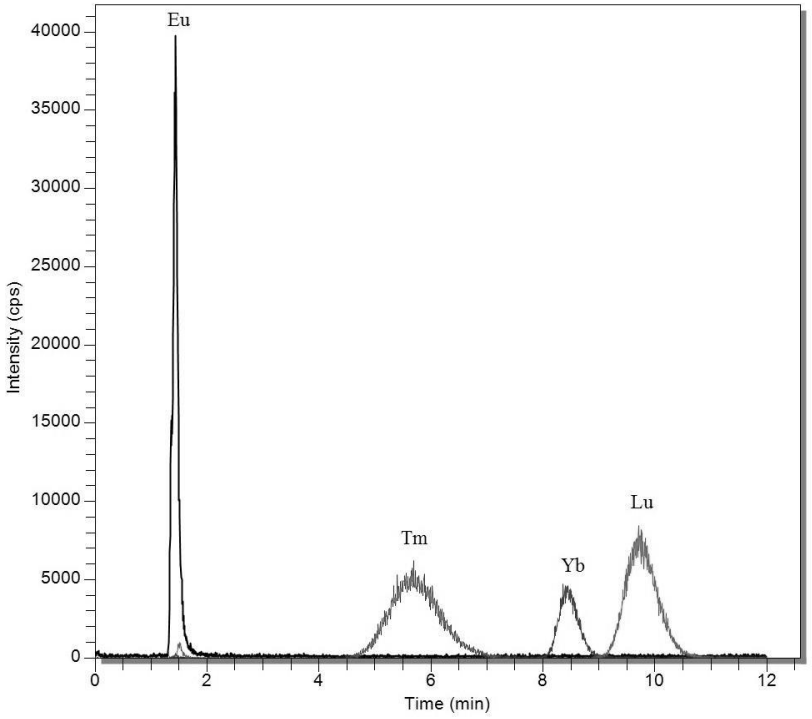

Figure 4.8.2: Chromatogram of REEs (1 ng mL^{-1}) separated by the gradient program listed in table 4.8.1 with HNO_3 as the mobile phase on a C18-column (4.6 x 150 mm, 5 µm) impregnated with 0.16 mmole HDEHP. The ICP-MS was operated under standard operational conditions and parameters. Masses selected for monitoring were 153, 169, 174 and 175, which correspond to Eu, Tm, Yb and Lu, respectively.

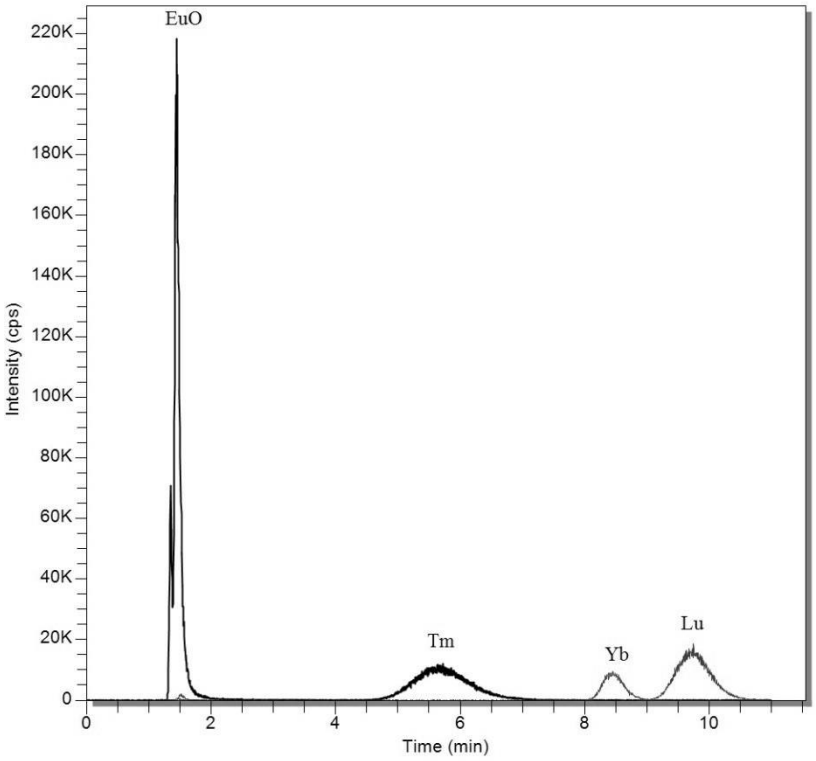

Figure 4.8.3: Chromatogram of 10 µg Eu mL^{-1} spiked with 2 ng of each REE separated by the gradient program listed in table 4.8.1 with HNO_3 as the mobile phase on a C18-column (4.6 x 150 mm, 5 µm) impregnated with 0.16 mmole HDEHP. The ICP-MS was operated under standard operational conditions and parameters. Masses selected for monitoring were 169, 174 and 175, which correspond to Tm, Yb and Lu, respectively. The peak labelled as EuO has the same mass of Tm, 169, and is formed as the matrix element Eu is introduced into the plasma.

4.8.1. Determination of REEs as trace impurities in standard solution of Eu by ICP-MS and HPLC-ICP-MS

In section 4.4, REEs as trace impurities in the standard solution of Eu, diluted to 10 µg mL^{-1}, were determined by external standardisation with ICP-MS with standard operational conditions and parameters. It was established that the high amount of Tm determined was due to the formation of ^{153}EuO, which can also be seen in the previous section. This section utilized the chromatographic conditions from the previous section in order to determine whether the presence of Tm in the diluted standard solution of Eu is above or below the detection limit and the contribution of ^{153}EuO to the signal intensity at mass 169.

As the desired separation between Eu and Tm was achieved with the HNO_3-HDEHP system from the previous section, purity of the standard solution of Eu, diluted to 10 µg mL^{-1}, was determined by the impurity approach. The sample and calibration solutions are presented in section 2.3.3 in chapter 2. Tm was determined with HPLC-ICP-MS by separating Eu from Tm with the HNO_3-HDEHP system as described in the previous section. The remaining REEs were already determined by the ICP-MS with standard operational conditions and parameters in section 4.4.

The chromatographic separation of Eu and Tm shows that Tm in the sample solution of 10 µg Eu mL^{-1} is below its detection limit and was not quantifiable. The peak area of Tm, which is supposed to elute at 5.6 minutes was below the detection limit, and integration for determining its peak area was not possible. The results can be seen in figure 4.8.6. Tm was below its detection limit in all of the three sample solutions that were determined. The only contribution to the signal intensity at mass 169 determined by the ICP-MS in section 4.4 was due to the formation of ^{153}EuO. The total impurities determined after separation of Eu and Tm by HPLC-ICP-MS is lower compared to determination solely by the ICP-MS. The results are presented in table 4.8.3. The purity of Eu was recalculated by removing the contribution of Tm as its concentration is below the detection and the observed signal intensity at its mass consists solely of ^{153}EuO. Purity of the standard solution of Eu was significantly increased when the contribution of ^{153}EuO was eliminated from mass 169 in order to the determine REEs as trace impurities. Its purity was found to be > 99.99 %, while its purity was determined in section 4.4 to be > 99.98 %, which included the contribution of ^{153}EuO. See section A.2.2 in the appendix for the calibration curves, statistics and calculations of LOD, and section A.4 for the chromatograms of the sample solutions of Eu.

The method developed can be used for other samples of high-purity Eu solutions or digested and diluted high-purity europium oxides as a diagnostic tool to determine the presence of Tm and the contribution of ^{153}EuO to the signal intensity at mass 169. Selecting methods for determining REEs as trace impurities would be dependent on the contribution of Tm. If Tm is above its detection limit, determining its concentration should be done by HPLC-ICP-MS. If Tm is below its detection limit, the determination of REEs as trace impurities in a concentrated sample solution of Eu is sufficient with the ICP-MS.

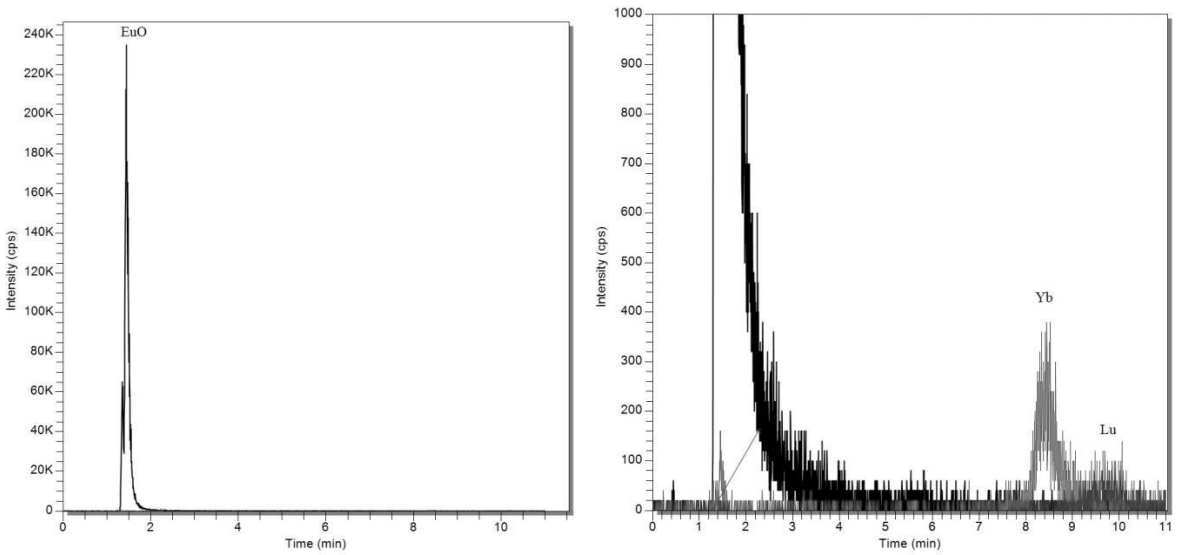

Figure 4.8.6: Chromatograms of a standard solution of Eu diluted to 10 µg mL^{-1} separated by the gradient program listed in table 4.8.2 with extraction chromatography. The peak labelled as EuO has mass 169, which represents the formation of ^{153}EuO as Eu is introduced into the plasma. The ICP-MS was operated with standard operational conditions and parameters. The remaining chromatograms are listed in section A.4 in the appendix.

Table 4.8.3: Average concentrations of REEs determined in the standard solution of Eu diluted to 10 µg mL^{-1} by ICP-MS. The values are in pg mL^{-1}. The ddjusted purity of the Eu standard solution is also presented as the contribution of ^{153}EuO was removed from the signal intensity at mass 169.

Analyte	Concentration*	Concentration**	LOD
^{45}Sc	< LOD		2.8
^{89}Y	6.0 ± 0.4		0.3
^{139}La	3.2 ± 0.3		0.2
^{140}Ce	1.0 ± 0.3		0.1
^{141}Pr	0.8 ± 0.2		0.1
^{143}Nd	2.9 ± 0.1		0.5
^{147}Sm	76 ± 2		0.6
^{157}Gd	459 ± 9		0.8
^{159}Tb	0.4 ± 0.1		0.1
^{163}Dy	1.30 ± 0.02		0.2
^{165}Ho	0.20 ± 0.04		0.03
^{166}Er	0.4 ± 0.1		0.1
Tm	1642 ± 70	< LOD	1.2
^{174}Yb	17 ± 5		3.3
^{175}Lu	0.6 ± 0.3		0.1
Total amount of REEs	2211 ± 70	569 ± 10	
Purity of Eu	99.9778 ± 0.0007 %	99.9943 ± 0.0001 %	

*Determined by ICP-MS with standard operational conditions and parameters.

**Determined by separation of Eu and Tm with HPLC-ICP-MS.

5. Concluding remarks

This study utilized two analytical techniques, ICP-MS and HPLC-ICP-MS, to develop methods for the purity determination of high-purity REEs and REOs by the impurity approach, which ideally can be used for routine analyses. Two different separation systems for online separation of REEs with HPLC hyphenated with the ICP-MS were tried; ion pair chromatography and extraction chromatography. Methods were developed in order to determine the purity of standard solutions of Yb and Eu, and high-purity Yb_2O_3, by determining the presence of REEs as trace impurities in these materials.

Due to the highly concentrated matrix element, spectral and non-spectral interferences were observed for the determination of REEs as trace impurities. It was found in the study that the signal suppression effects did not occur when the concentration of the matrix rare earth element is $\leq$ 10 μg mL^{-1}. However, formation of polyatomic ions did occur at this concentration level of the matrix element, which overlapped with certain REE-analytes. The determination of Lu (at mass 175) in sample solutions of $\leq$ 10 μg mL^{-1} Yb was affected by the formation of ^{174}YbH, which has the mass of 175, while determination of Tm (at mass 169) in a sample solution of 10 μg mL^{-1} Eu was affected by the formation of ^{153}EuO, which has the mass of 169. It was found that the formation of hydrides is less severe than the formation of oxides.

Several attempts were made in order to eliminate the contribution of polyatomic ions to the signal intensities observed at mass 169 and 175 in their respective sample solutions of Eu and Yb. By altering the plasma conditions via its ICP RF-power and nebulizer gas flow rate, the signal intensity of ^{174}YbH was reduced. The reduction was, however, caused by an overall worsened instrumental sensitivity. It was found that the determination of REEs as trace impurities by utilizing standard operational conditions and parameters of the ICP-MS versus increased ICP RF-power and decreased nebulizer gas flow rate did not significantly differ from each other. The overall instrumental sensitivity was worsened and the results obtained by the altered plasma conditions were less accurate compared to the standard operational conditions and parameters of the ICP-MS. Therefore, online separation by HPLC hyphenated with ICP-MS was investigated in order to separate the matrix element from the analytes, which are affected by mass overlaps due to the formation of polyatomic ions.

The separation systems that were investigated included ion pair chromatography and extraction chromatography, which were hyphenated with the ICP-MS. Ion pair chromatography with the OS-HIBA system and the HFBA-HIBA system proved to be either unsuccessful or unsuitable for online separation of Lu from the Yb matrix element. The OS-HIBA system did provide partial separation of Lu and Yb. Sharp and symmetrical peaks for the REEs of interest was also obtained with this system, but high amount of dissolved solids in the reagents led to deposition of solids on the entrance cones of the ICP-MS. Deposition of solids increases the frequency of which the cones must be cleaned, which is not ideal for a routine analysis method. The HFBA-HIBA system was therefore tried in hope that it is more suitable towards the hyphenation of HPLC with ICP-MS. HFBA is a more volatile ion pair reagent compared to OS and does not contain sodium. However, the mobile phase's pH was adjusted with NaOH, which also led to deposition of solids on the entrance cones. Although Lu and Yb was not able to be separated by this system, further investigations by using NH_4OH to adjust pH of the mobile phase should be made in order to determine its suitability towards online separation of Lu and Yb by HPLC hyphenated with ICP-MS. Extraction chromatography utilizing the HNO_3-HDEHP system was therefore investigated. The system does not contain any dissolved solids and may prove to be more suitable towards the hyphenation of HPLC with ICP-MS.

The purity of the standard solutions of Yb and Eu, and high-purity Yb_2O_3, were successfully determined by the impurity approach utilizing extraction chromatography with the HNO_3-HDEHP system hyphenated with ICP-MS. Purity of the Yb standard solution and high-purity Yb_2O_3 were found to be > 99.99 % by determining the concentration of Lu after it has been separated from the highly concentrated Yb matrix element with a gradient program by the HNO_3-HDEHP system, while the rest of the REEs were determined solely by the ICP-MS. The gradient program separated the REEs of interest with 1.8 – 2.25 M HNO_3 over 8 minutes on a C18 column (4.6 x 150 mm, 5 µm) impregnated with 0.16 mmole HDEHP at a mobile phase flow rate of 1 mL min^{-1}. The concentration of Lu in the standard solution of Yb determined by HPLC-ICP-MS was found to be significantly different compared to its concentration found solely by the ICP-MS. But its concentration in the digested and diluted sample of Yb_2O_3 was not significantly different when comparing the two methods. However, the significance of its contribution would not be possible to determine if Lu was not separated from the matrix element Yb. Purity of the standard solution of Eu was found to be > 99.99 %. The high concentration of Tm in the standard solution of Eu, which was determined solely by

the ICP-MS, was due to the formation of ^{153}EuO whose mass overlaps with the mono-isotopic Tm. By utilizing the HNO_3-HDEHP system, the masses of 153 and 169 were separated by a gradient program. The gradient program consisted of 4 minutes with constant 1.125 M HNO_3 and 7 minutes with constant 2.25 M HNO_3. The gradient curve between two steps was set to 0. Eu and Tm were separated over 11 minutes on a C18 column (4.6 x 150 mm, 5 µm) impregnated with 0.16 mmole HDEHP at a mobile phase flow rate of 1 mL min^{-1}. It was found that the presence of Tm in the standard solution of Eu, which was diluted to 10 µg mL^{-1}, was below its detection limit. The determination of REEs as trace impurities solely by ICP-MS is sufficient to determine its purity as the concentration of Tm initially found was due to the formation of polyatomic ions. The HNO_3-HDEHP system was used as a diagnostic tool in order to determine the contribution of ^{153}EuO to the observed signal intensity at mass 169. Purity of the Eu standard solution was then recalculated by removing the contribution of Tm as its presence in the 10 µg mL^{-1} Eu sample solution was below its detection limit.

The HNO_3-HDEHP system was proved to be more suitable towards the hyphenation with ICP-MS due to the absent of dissolved solids in the mobile phase. Successful separations were achieved for the sample solutions of Eu and Yb. It was found that the system can both be used to determine the concentration of analytes that are affected by formation of matrix-based polyatomic ions, and as a diagnostic tool in order to investigate the contribution of the polyatomic ions to the signal intensities observed at masses of interest. The overall low detection limits obtained with the quadrupole ICP-MS enables the determination of REEs as trace impurities in REEs and REOs that are > 99.999 % pure by utilizing the HNO_3-HDEHP to eliminate polyatomic spectral interferences.

6. References

1. Connelly, N.G., Damhus, T., Hartshorn, R.M. and Hutton, A.T., *Nomenclature of Inorganic Chemistry - IUPAC Recommendations 2005*. 2005, RSC Publishing. p. 51-52.
2. Rayner-Canham, G. and Overton, T., *Descriptive Inorganic Chemistry*. 2010 [cited 2013 03 Sep]; Available from: http://bcs.whfreeman.com/descriptive5e/default.asp#t_576047____.
3. Greenwood, N.N. and Earnshaw, A., *The Lanthanide Elements*, in *Chemistry of the Elements*. 1997, Reed Educational and Professional Publishing Ltd. p. 1227-1249.
4. Kanazawa, Y. and Kamitami, M., *Rare earth minerals and resources in the world.* Journal of Alloys and Compounds, 2006. **408-412**: p. 1339-1343.
5. Cotton, S., *Introduction to the Lanthanides*, in *Lanthanide and Actinide Chemistry*. 2007, John Wiley & Sons Ltd. p. 1-7.
6. Hurst, C., *China's rare earth elements industry: What can the West learn?* 2010.
7. Goonan, T.G., *Rare earth elements - End use and recyclability*. 2011, U.S. Geological Survey Scientific Investigations Report. p. 15.
8. Meyer, L. and Bras, B., *Rare Earth Metal Recycling*, in *Sustainable Systems and Technology (ISSST), 2011 IEEE Internation Symposium*. 2011: Chicago, IL. p. 6.
9. *Rare earths*, in *Materials for a sustainable future*, Letcher, T.M and Scott, J.L., Editors. 2012, The Royal Society of Chemistry. p. 60-89.
10. Aspinall, H.C., *Properties of the elements*, in *Chemistry of the f-block elements*. 2001, Gordon and Breach Science Publishers. p. 10-21.
11. Cotton, S., *Coordination chemistry of the lanthanides*, in *Lanthanide and Actinide Chemistry*. 2007, John Wiley & Sons, Ltd. p. 35-56.
12. Aspinall, H.C., *Coordination Chemistry*, in *Chemistry of the f-block elements*. 2001, Gordon and Breach Science Publishers. p. 63-83.
13. Cotton, S., *The Lanthanides - Principles and Energetics*, in *Lanthanide and Actinide Chemistry*. 2007, John Wiley & Sons Ltd. p. 9-19.
14. Rayner-Canham, G. and Overton, T., *Solvent Systems and Acid-Base Behavior*, in *Descriptive Inorganic Chemistry*. 2010, Clancy Marshall. p. 156-162.
15. Peppard, D.F., Mason G.W., and Lewey, S., *A tetrad effect in the liquid-liquid extraction ordering of lanthanides(III).* Journal of Inorganic and Nuclear Chemistry, 1969. **31**: p. 2271-2272.

16. Fidelis, I. and Siekierski, S., *On the regularities of tetrad effect in complex formation by f-electron elements. A double-double effect.* Journal of Inorganic and Nuclear Chemistry, 1971. **33**(9): p. 3191-3194.
17. Fuks, L. and Majdan, M., *Features of Solvent Extraction of Lanthanides and Actinides.* Mineral Processing and Extractive Metallurgy Review: An Internation Journal, 2000. **21**(1-5): p. 25-48.
18. Vodyanitskii, Y.N., *Geochemical Fractionation of Lanthanides in Soils and Rocks: A Review of Publications.* Eurasian Soil Science, 2012. **45**(1): p. 56-67.
19. Andersson, S., Eberhardt, K., Ekberg, C., Liljenzin, J.-O., Nilsson, M. and Skarnemark, G., *Determination of stability constants of lanthanide nitrate complex formation using a solvent extraction technique.* Radiochimica Acta, 2006. **94**: p. 469-474.
20. Ortner, H.M., Blodörn, W., Friedbacher, G., Grasserbauer, M., Krivan, V., Virag, A., Wilhartitz, P. and Wünsch, G., *High Performance Analytical Characterization of Refractory Metals.* Mikrochimica Acta, 1987. **91**(1-6): p. 233-260.
21. Balaram, V., *Recent developments in analytical techniques for characterization of ultra pure materials - An overview.* Bulletin of Material Science, 2005. **28**(4): p. 345-348.
22. Weber, M. and Wüthrich, J., *TraceCERT(TM) - Traceable Certified Reference Material. Part 3: Challenges in the characterization of high-purity starting materials*. 2007 [cited 2013 04 Sep]; Available from: http://www.sigmaaldrich.com/content/dam/sigma-aldrich/docs/Sigma/General_Information/analytix_2007_2_p12-14.pdf.
23. Bédard, L.P. and Linge, K.L., *GGR Biennial Review: Atomic Absorption, Inductively Coupled Plasma-Atomic Emission Spectrometry, Neutron Activation Analysis and X-Ray Fluorescence Spectrometry Review for 2008-2009.* Geostandards and Geoanalytical Research, 2010. **34**(4).
24. Balaram, V., *Recent trends in the instrumental analysis of rare earth elements in geological and industrial materials.* Trends in Analytical Chemistry, 1996. **15**(9): p. 475-486.
25. Duffield, J. and Gilmore, G.R., *An optimum method for the determination of rare earth elements by neutron activation analysis.* Journal of Radioanalytical Chemistry, 1979. **48**: p. 135-145.

26. Zawisza, B., Pytlakowska, K., Feist, B., Polowniak, M., Kita, A. and Sitko, R., *Determination of rare earth elements by spectroscopic techniques: a review.* Journal of Analytical Atomic Spectrometry, 2011. **26**(12): p. 2373-2390.
27. Sudersanan, M., *Role of analytical techniques for characterisation of advanced and high purity materials.* Progress in Crystal Growth and Characterization of Materials, 2002. **44**(3): p. 189-194.
28. Sitko, R. and Zawisza, B., *Quantification in X-Ray Fluorescence Spectrometry*, in *X-Ray Spectroscopy*, S.K. Sharma, Editor. 2012, InTech. p. 137-162.
29. Kolibarska, I., Velichkov, S. and Daskalova, N., *Spectral interferences in the determination of traces of scandium, yttrium and rare earth elements in "pure" rare earth matrices by inductively coupled plasma atomic emission spectrometry.* Spectrochimica Acta Part B, 2008. **63**: p. 603-606.
30. Shelpakova, I.R. and Saprykin, A.I., *Analysis of high-purity solids by atomic emission spectroscopy and mass spectrometry with atom excitation and ionisation in inductively coupled plasma.* Russian Chemical Reviews, 2005. **74**(11): p. 1015-1025.
31. Thomas, R., *Mass analyzers: Quadrupole Technology*, in *Practical guide to ICP-MS: A tutorial for beginners*. 2008, Taylor & Francis Group. p. 47-54.
32. Thomas, R., *Mass Analyzers: Double-Focusing Magnetic Sector Technology*, in *Practical guide to ICP-MS: A tutorial for beginners*. 2008, Taylor & Francis Group. p. 57-63.
33. Zhang, X., Yi, Y., Liu, Y., Li, X., Liu, J., Jiang, Y. and Su, Y., *Direct determination of rare earth impurities in high purity erbium oxide dissolved in nitric acid by inductively coupled plasma mass spectrometry.* Analytica Chimica Acta, 2005. **555**: p. 57-62.
34. Thomas, R., *Practical Guide To ICP-MS: A tutorial for beginners*. 2nd ed. Practical Spectroscopy Vol. 37. 2008: CRC Press: Taylor & Francis Group. 347.
35. McNaught, A.D. and Wilkinson, A., *IUPAC. Compendium of Chemical Terminology*. 1997: Blackwell Scientific Publications.
36. Thomas, R., *Abundance sensitivity*, in *Practical Guide To ICP-MS: A tutorial for beginners*. 2008, CR Press: Taylor & Francis Group. p. 52-53.
37. Zhang, A., Liu, X., and Zhang, W., *Determination of rare earth impurities in high purity europium oxide by inductively coupled plasma-mass spectrometry and evaluation of concentration values for europium oxide standard material.* European Journal of Mass Spectrometry, 2004. **10**: p. 589-598.

38. Kawabata, K., Kishi, Y., Kawaguchi, O., Watanabe, Y. and Inoue, Y., *Determination of Rare-Earth Elements by Inductively Coupled Plasma Mass Spectrometry with Ion Chromatography.* Analytical Chemical Society, 1991. **63**: p. 2137-2140.
39. Pedreira, W.R., de Silva Queiroz, C.A., Abrão, A. and Pimentel, M.M., *Quantification of trace amounts of rare earth elements in high purity gadolinium oxide by sector field inductively coupled plasma mass spectrometry.* Journal of Alloys and Compounds, 2004. **374**: p. 129-132.
40. Pedreira, W.R., Sarkis, J.E.S, de Silva Queiroz, C.A., Rodrigues, C., Tomiyoshi, I.A. and Abrão, A., *Determination of trace amounts of rare-earth elements in highly pure neodymium oxide by sectorfield inductively coupled plasma mass spectrometry (ICP-SFMS) and high-performance liquid chromatography (HPLC) techniques.* Journal of Solid State Chemistry, 2003. **171**: p. 3-6.
41. Pedreira, W.R., Sarkis, J.E.S., Rodrigues, C., Tomiyoshi, I.A., de Silva Queiroz, C.A. and Abrão, A., *Determination of trace amounts of rare earth elements in highly pure praseodymium by double focusing inductively coupled plasma mass spectrometry and high-performance liquid chromatography.* Journal of Alloys and Compounds, 2001. **323-324**: p. 49-52.
42. Pedreira, W.R., Sarkis, J.E.S., Rodrigues, C., Tomiyoshi, I.A., de Silva Queiroz, C.A. and Abrão, A., *Determination of rare earth elements in high pure lanthanum oxide by sector field inductively coupled plasma mass spectrometry (HR ICP-MS) and high-performance liquid chromatography (HPLC) techniques.* Journal of Alloys and Compounds, 2002. **344**: p. 17-20.
43. Li, B., Zhang, Y., and Yun, M., *Determination of Trace Amounts of Rare Earth Elements in High-purity Cerium Oxide by Inductively Coupled Plasma Mass Spectrometry After Separation by Solvent Extraction.* Analyst, 1997. **122**: p. 543-547.
44. Verma, S.P. and Santoyo, E., *High-Performance Liquid and Ion Chromatography: Separation and Quantification Analytical Techniques for Rare earth Elements.* Geostandards and Geoanalytical Research, 2007. **31**(3): p. 161-184.
45. Nash, K.L. and Jensen, M.P., *Analytical-scale separations of the lanthanides: A review of techniques and fundamentals.* Separation Science and Technology, 2007. **36**(5-6): p. 1257-1282.
46. Cecchi, T., *Ion Pairing Chromatography.* Critical Reviews in Analytical Chemistry, 2008. **38**(3): p. 161-213.

47. Dietz, M.L., Horwitz, E.P., and Bond, A.H., *Extraction Chromatography: Progress and Oppurtinities.* Metal-Ion Separation and Preconcentration, 1999. **716**: p. 234-250.
48. Braun, T. and Ghersini, G., *Extraction Chromatography*. Journal of Chromatography Library, volume 2. Vol. 2. 1975: American Elsevier Publishing Company, Inc. 565.
49. Thomas, R., *Contamination issues associated with sample preparation*, in *Practical Guide to ICP-MS: A tutorial for beginners*. 2008, Taylor & Francis Group. p. 137-149.
50. Nölte, J., *ICP Emission Spectroscopy: A practical guide*. 2003: Wiley-VCH Verlag GmbH & Co. KGaA, Weinheim. 267.
51. Miller, J.N. and Miller, J.C., *Statistics and Chemometrics for Analytical Chemistry*. Sixth ed. 2010: Pearson Education Limited. 278.
52. Kifle, D. and Wibetoe, G., *Selective liquid chromatographic separation of yttrium from rare earth elements using acetic acid as a novel eluent.* Journal of Chromatography A, 2013. **1307**: p. 86-90.
53. Thomas, R., *Optimizing conditions for low oxides*, in *Practical Guide to ICP-MS: A tutorial for beginners*. 2008, Taylor & Francis Group. p. 36.
54. Miller, J.N. and Miller, J.C., *Significance tests*, in *Statistics and Chemometrics for Analytical Chemistry*. 2010, Pearson Education Limited. p. 37-66.

Appendix

A.1. Preparation of sample and calibration solutions, and mobile phases

The following subsections describe the preparation procedures of all sample and calibration solutions along with the mobile phases in chapter 2.

A.1.1. Sample preparation

Sample solutions for the investigation of signal suppression of REEs in different concentrations of Yb were prepared from the standard solution of Yb (10041 ± 23 µg mL^{-1}) and the multi-elemental solution containing all REEs (100 ± 0.1 µg mL^{-1}). Calculations are shown below. The multi-elemental solution was firstly diluted to 1 µg mL^{-1} prior to further preparation. The addition of 1.5 mL 65 % (w/w) suprapur HNO_3 corresponds to 0.2 M HNO_3 when diluted to 100 mL.

- Molecular mass of HNO_3 = 63 g mol^{-1}
- ρ = 1.4 g mL^{-1}
- 1 L of 65 % (w/w) HNO_3 weighs 910 g = (1 L × 1400 g L^{-1} × 0.65)
- 14.4 M HNO_3 = (910 g / 63 g mol^{-1}) / 1 L
- (1.5 mL × 14.4 M HNO_3) / 100 mL type 1-water = 0.2 M HNO_3

Dilution of multi-elemental solution of all REEs (from 100 ± 0.1 µg mL^{-1}):

(100 µg mL^{-1} × 1000 µL) / 100 mL type 1-water = 1 µg mL^{-1}

Preparation of sample set 1 and 2 in section 2.3.1 followed equation (3) as shown below. The values for x (amount of standard solution of Yb) and y (amount of diluted multi-elemental solution of the REEs) for the different sample solutions in the sample sets are listed in table A.1.1 and A.1.2. One example is given of which the other sample solutions were prepared in the same manner.

((x µL × 10041 µg mL^{-1}) + (y µL × 1 µg mL^{-1}) + (1.5 mL 65 % HNO_3)) / 100 mL type-1 water (3)

100 µL of 10041 µg Yb mL^{-1} and 250 µL of multi-elemental solution with a concentration of 1 µL mL^{-1} along with 1.5 mL of 65 % HNO_3 were added in a 100 mL volumetric flask. Type 1-water was then used to dilute it to 100 mL. The final concentration of the sample solution is 10 µg of Yb and 2.5 ng of each REE per mL^{-1} present in 0.2 M HNO_3.

Table A.1.1: Sample set 1 listed in section 2.3.1 was prepared by following equation (3). The table lists the values of x and y and the final concentration of Yb and of each REE in a 100 mL volumetric flask, and the final concentration of HNO_3.

Sample set 1	**x**	**Concentration of Yb**	**y**	**Concentration of REEs**	**HNO_3**
Sample 1	0	0 µg mL^{-1}	250	2.5 ng mL^{-1}	0.2 M
Sample 2	50	5 µg mL^{-1}	250	2.5 ng mL^{-1}	0.2 M
Sample 3	100	10 µg mL^{-1}	250	2.5 ng mL^{-1}	0.2 M
Sample 4	500	50 µg mL^{-1}	250	2.5 ng mL^{-1}	0.2 M
Sample 5	1000	100 µg mL^{-1}	250	2.5 ng mL^{-1}	0.2 M

Table A.1.2: Sample set 2 listed in section 2.3.1 was prepared by following equation (3). The table lists the values of x and y and the final concentration of Yb and of each REE in a 100 mL volumetric flask, and the final concentration of HNO_3.

Sample set 2	**x**	**Concentration of Yb**	**y**	**Concentration of REEs**	**HNO_3**
Sample 1	0	0 µg mL^{-1}	0	0	0.2 M
Sample 2	50	5 µg mL^{-1}	0	0	0.2 M
Sample 3	100	10 µg mL^{-1}	0	0	0.2 M
Sample 4	500	50 µg mL^{-1}	0	0	0.2 M
Sample 5	1000	100 µg mL^{-1}	0	0	0.2 M

For the determination of REEs in the standard solution of Yb by method of standard addition and external standardisation, the multi-elemental solution containing all REEs was first diluted to 100 ng mL^{-1} prior to further sample preparation. Appropriate amounts of the diluted multi-elemental solution and standard solution of Yb were then transferred to their respective 100 mL-volumetric flasks and diluted with type 1-water. Calculations are shown below.

Dilution of multi-elemental solution containing all REEs:

(100 µg mL^{-1} × 100 µL) / 100 mL type 1-water = 100 ng of each REE mL^{-1}.

Preparation of sample and calibration solutions followed equation (4) as shown below. The values for x and y for the different sample and calibration solutions in section 2.3.2 and 2.3.3 are listed in table A.1.3 and A.1.4.

(x µL × 10041 µg mL^{-1} Yb) + (y µL × 100 ng mL^{-1} of each REE) + 1.5 mL 65 % HNO_3) / 100 mL type-1 water (4)

Table A.1.3: Sample and calibration solutions for the determination of REEs as trace impurities in the standard solution of Yb by method of standard addition with ICP-MS listed in section 2.3.2 were prepared by following equation (4). The table lists the values of x and y and the final concentration of Yb and of each REE in a 100 mL volumetric flask, and the final concentration of HNO_3.

	x	**Concentration of Yb**	**y**	**Concentration of REEs**	**HNO_3**
Blank	0	0	0	0	0.2 M
Calibration 1	100	10 µg mL^{-1}	50	50 ng mL^{-1}	0.2 M
Calibration 2	100	10 µg mL^{-1}	150	150 ng mL^{-1}	0.2 M
Calibration 3	100	10 µg mL^{-1}	250	250 ng mL^{-1}	0.2 M
Sample 1, 2 and 3	100	10 µg mL^{-1}	0	0	0.2 M

Sample solutions of Eu for the determination of REEs as trace impurities in the Eu standard solution was prepared by following equation (7) as shown below. The calibration solutions for were prepared in the same manner. Table A.1.4 and A.1.5 shows the x-values (amount of standard solution of Eu) and y-values (amount of diluted multi-elemental solution of REEs) for the different sample and calibration solutions.

(x µL × 1000 µg mL^{-1}) + (y µL × 100 ng mL^{-1} of each REE) + 1.5 mL 65 % HNO_3) / 100 mL type-1 water (5)

In order to avoid further unnecessary repetitions, the preparation of sample solutions listed in section 2.3.4, which were used for separation with ion pair chromatography and extraction chromatography, followed the same manner as the above-mentioned sample solutions, where appropriate amounts of the standard solutions of Eu and Yb and the multi-elemental solution were added to their respective volumetric flasks and diluted with 0.2 M HNO_3.

Table A.1.4: Sample and calibration solutions for the determination of REEs as trace impurities in the standard solutions of Yb and Eu by external standardization with ICP-MS and HPLC-ICP-MS as listed in section 2.3.3 were prepared by following equation (4) for Yb and (5) for Eu. The table lists the values of x and y and the final concentrations of Yb, Eu and of each REE in a 100 mL volumetric flask, and the final concentration of HNO_3.

	x	**Concentration of Yb**	**y**	**Concentration of REEs**	**HNO_3**
Blank	0	0	0	0	0.2 M
Calibration 1	0	0	25	25 ng mL^{-1}	0.2 M
Calibration 2	0	0	75	75 ng mL^{-1}	0.2 M
Calibration 3	0	0	150	150 ng mL^{-1}	0.2 M
Calibration 4	0	0	250	250 ng mL^{-1}	0.2 M
Sample 1	100	10 µg mL^{-1}	0	0	0.2 M
Sample 2	100	10 µg mL^{-1}	0	0	0.2 M
Sample 3	100	10 µg mL^{-1}	0	0	0.2 M
	x	**Concentration of Eu**	**y**	**Concentration of REEs**	**HNO_3**
Sample 1	1000	10 µg mL^{-1}	0	0	0.2 M
Sample 2	1000	10 µg mL^{-1}	0	0	0.2 M
Sample 3	1000	10 µg mL^{-1}	0	0	0.2 M

A.1.2. Preparation of mobile phases for HPLC-ICP-MS

The mobile phase of the OS-HIBA system consisted of two reservoirs as shown in section 2.3.5. 5.4 g of OS was weighed and added to the respective 1000 mL bottles for mobile phase reservoir A (MP:A) and B (MP:B). The 1000 mL bottle of MP:B was also added 52 g of HIBA. Both bottles were diluted to 1000 mL with type 1-water. The pH of MP:B was adjusted by careful addition of 10 M NaOH while changes of its pH were monitored by a pH-meter.

The mobile phase of the HFBA-HIBA system also consisted of two mobile phase reservoirs, A and B. The 1000 mL bottles for MP:A and MP:B was added 2.6 mL of HFBA, respectively. MP:B was also added 52 g of HIBA. Both mobile phase reservoirs were then diluted to 1000 mL with type 1-water. The pH of MP:B was adjusted by careful addition of 10 M NaOH while changes of its pH were monitored by a pH-meter.

The mobile phase of the HNO_3-HDEHP system consisted of two mobile phase reservoirs, A and B. MP:A consisted only of type 1-water, while MP:B was added 156 mL of 65 % HNO_3 and diluted to 1000 mL with type 1-water.

A.1.3. Sample decomposition of 99.9 % pure Yb_2O_3

Yb was prepared from 99.9 % pure Yb_2O_3 (see section 2.4 for sample decomposition procedure) and had a final concentration of 8.7 µg mL^{-1} that were used for analysis. Calculations for the first sample were chosen as an example. The other samples were calculated in the same manner. Table A.1.5 lists the final concentrations of Yb obtained from digestion and dilution of 99.9 % pure Yb_2O_3.

- Molecular mass of Yb_2O_3 = (2 × 173) + (3 × 16) = 394 g mol^{-1}.
- Amount of Yb_2O_3 weighed into a PTFE-vessel: 0.4959 g Yb_2O_3.
- 0.4959 g Yb_2O_3 / 394 g mol^{-1} = 1.26 × 10^{-3} mol.
- 1.26 ×10^{-3} mol × (2 × 173 g mol^{-1}) = 0.4355 g Yb.
- 0.4355 g Yb diluted to 100 mL = 4355 µg mL^{-1} Yb.
- 100 µL of Yb (4355 µg mL^{-1}) was further diluted to 50 mL with 0.2 M HNO_3:
    - (4355 µg mL^{-1} × 0.100 mL) / 50 mL = 8.71 µg mL^{-1}.

Table A.1.5: Amount of Yb_2O_3 that was weighed into their respective vessels for decomposition by the microwave oven and the final concentration of Yb in the sample solutions.

Sample	**Yb_2O_3 weighed (g)**	**Concentration of Yb (µg mL^{-1})**
Sample 1	0.4959	8.71
Sample 2	0.4931	8.66
Sample 3	0.4959	8.71
Average	0.4950 ± 0.0016	8.69 ± 0.03

A.2. ICP-MS method development

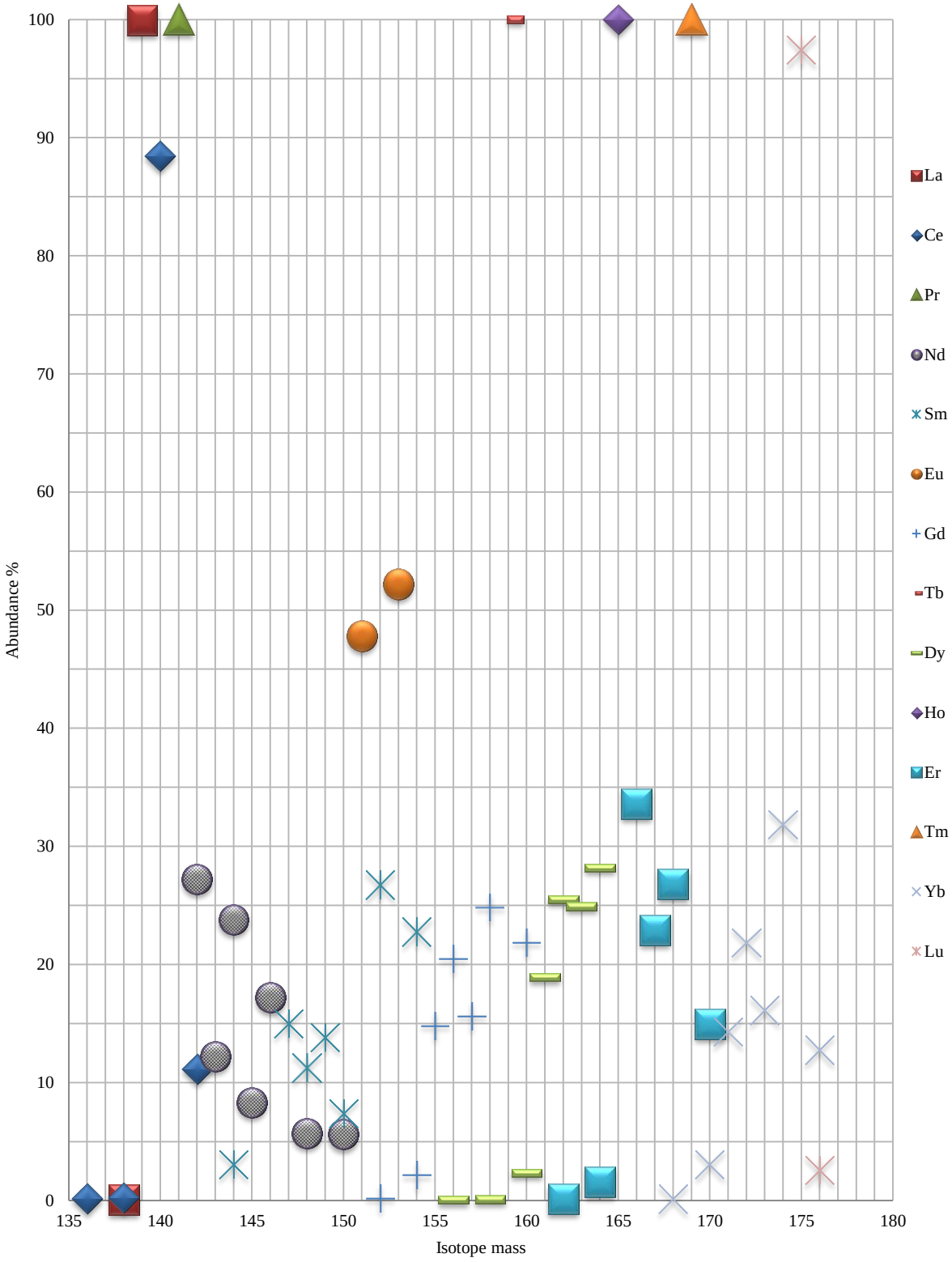

Figure A.2.1: An overview of all naturally occurring stable isotopes of the Lns and their natural abundances. ^{45}Sc and ^{89}Y are mono-isotopic with masses 45 and 89, respectively, and are not included in the figure.

A.2.1. Calibration curves, statistics for the determination of REEs as trace impurities in standard solution of Yb with ICP-MS by the method of standard addition

The concentration of REEs as trace impurities in Yb determined in section 4.3 was obtained by the method of standard addition. The calibration curve and statistics are shown in the figures below. The calibration curves were established by analysing the calibration solutions containing Yb at 10 µg mL^{-1} spiked with known concentrations of REEs. Three sample solutions of Yb were than analysed and the results from each sample solution were plotted in the calibration curve, where the calibration line was extrapolated to y = 0. This procedure resulted in three calibration curve statistics per REE, which are presented in the figures below.

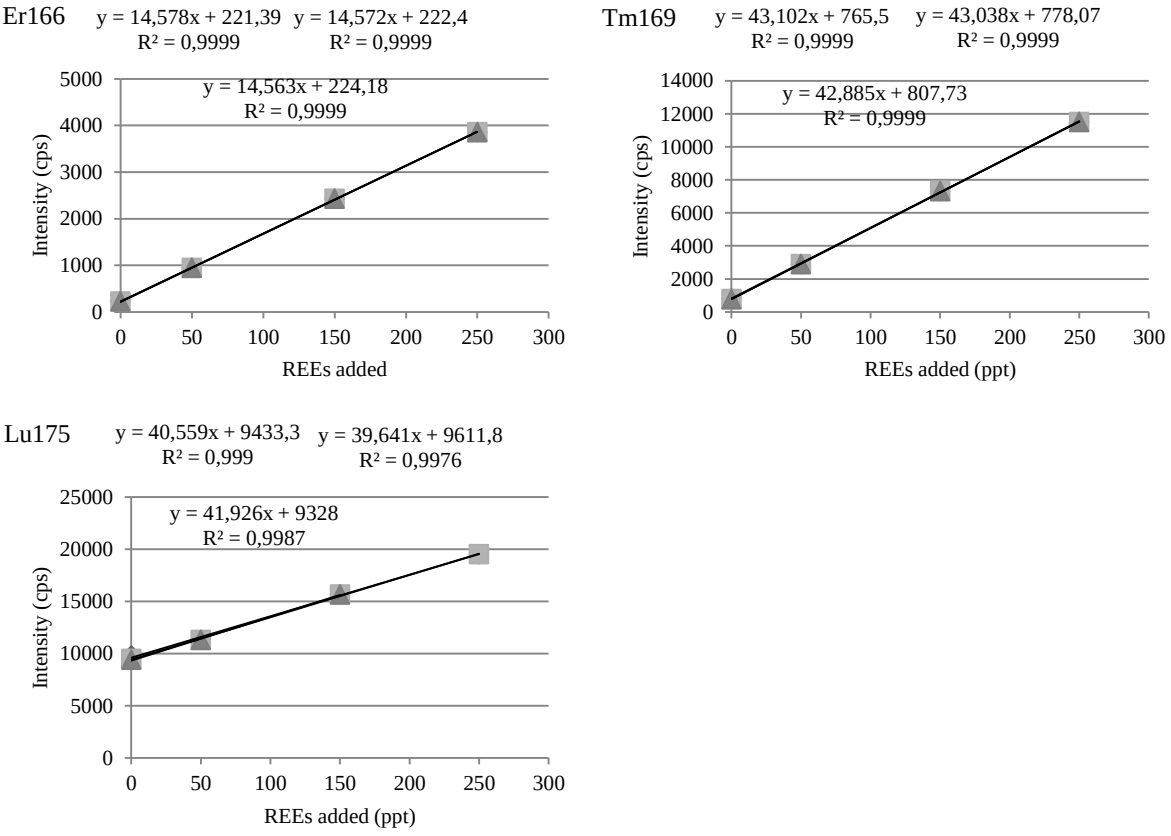

Figure A.2.2: Calibration curves of Er, Tm and Lu for the determination of REEs in the standard solution of Yb, diluted to 10 µg mL^{-1}, by standard addition with ICP-MS. The calibration curve statistics can be seen in the figures.

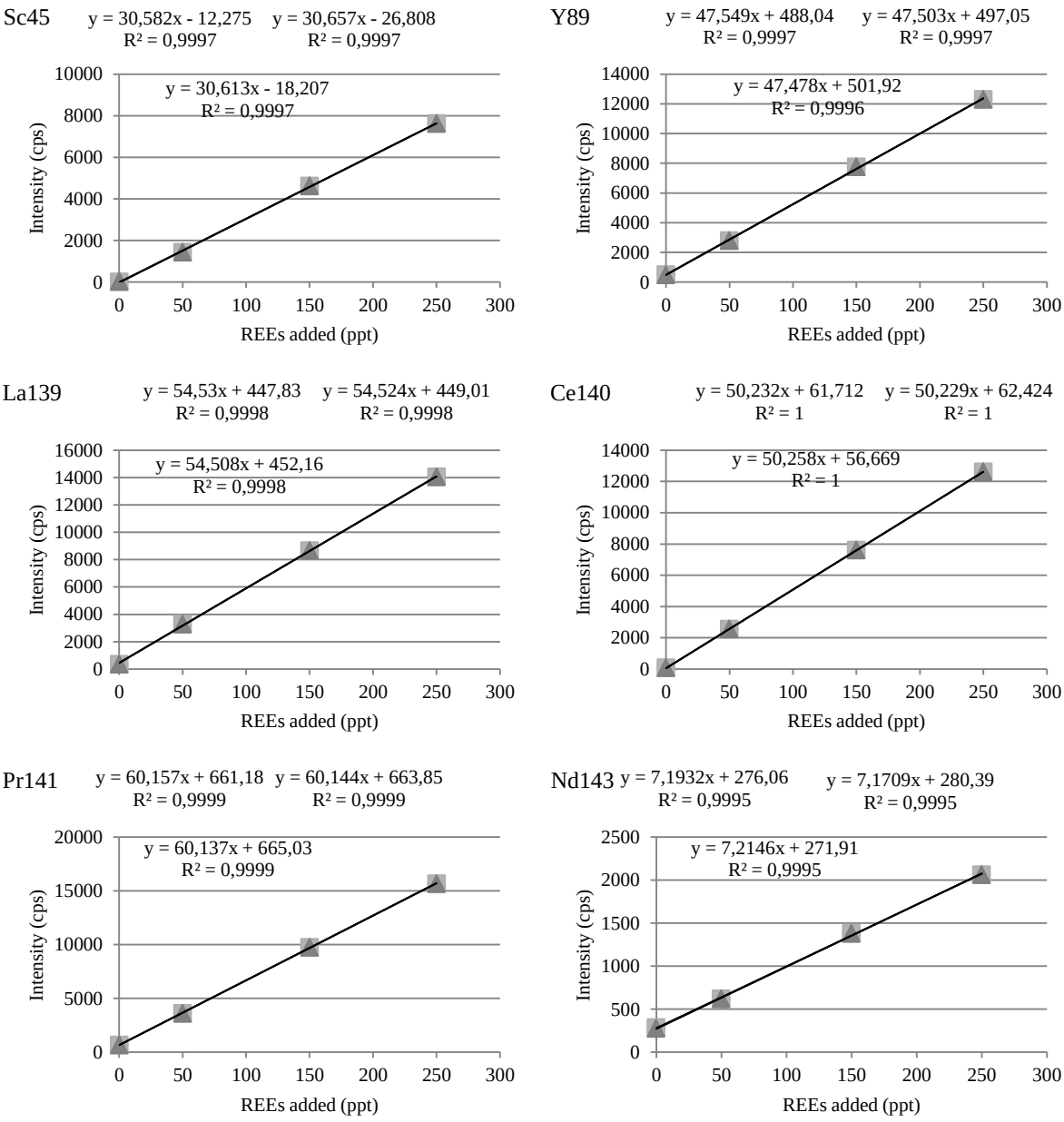

Figure A.2.3: Calibration curves of Y, Sc, La, Ce, Pr and Nd for the determination of REEs in the standard solution of Yb, diluted to 10 µg mL^{-1}, by standard addition with ICP-MS. The calibration curve statistics can be seen in the figures.

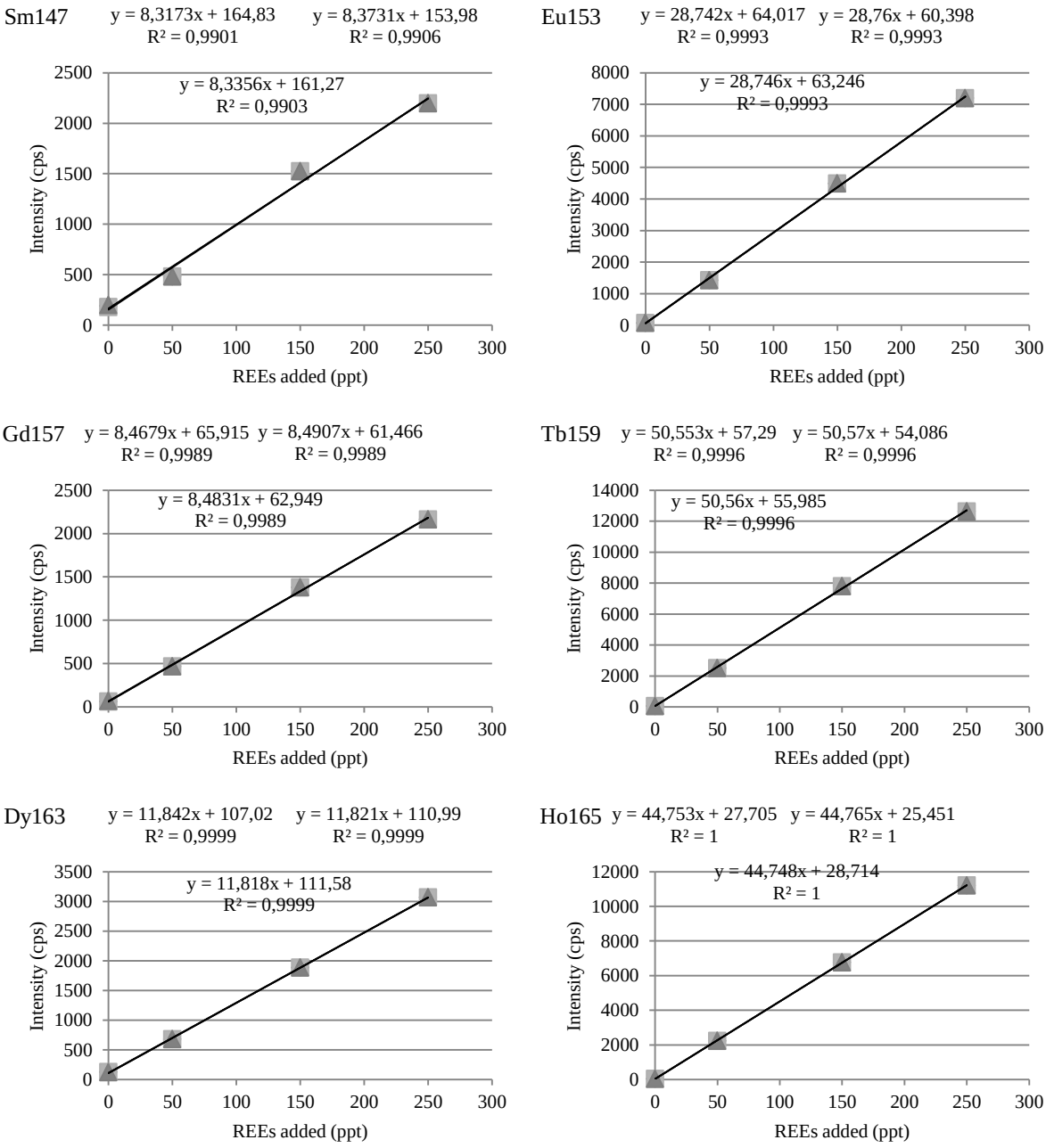

Figure A.2.4: Calibration curves for Sm, Eu, Gd, Tb, Dy and Ho for the determination of REEs in the standard solution of Yb, diluted to 10 µg mL^{-1}, by standard addition with ICP-MS. The calibration curve statistics can be seen in the figures.

A.2.2. Calibration curves, statistics, and LOD for the determination of REEs as trace impurities in standard solution of Eu with ICP-MS by external standardisation

The concentration of REEs as trace impurities in Eu determined in section 4.4 was obtained by external standardisation. The calibration curves in figure A.2.5 were obtained by analysing the calibration solutions with known concentrations of REEs. Linearity of the calibration lines was forced through x = 0 and y = 0.

Table A.2.1 shows the raw data for ten readings of the blank solution in the ICP-MS. The blank solution was analysed after the sample solutions. Detection limits of the REEs were calculated based on the results in table A.2.1 and are presented in table A.2.2.

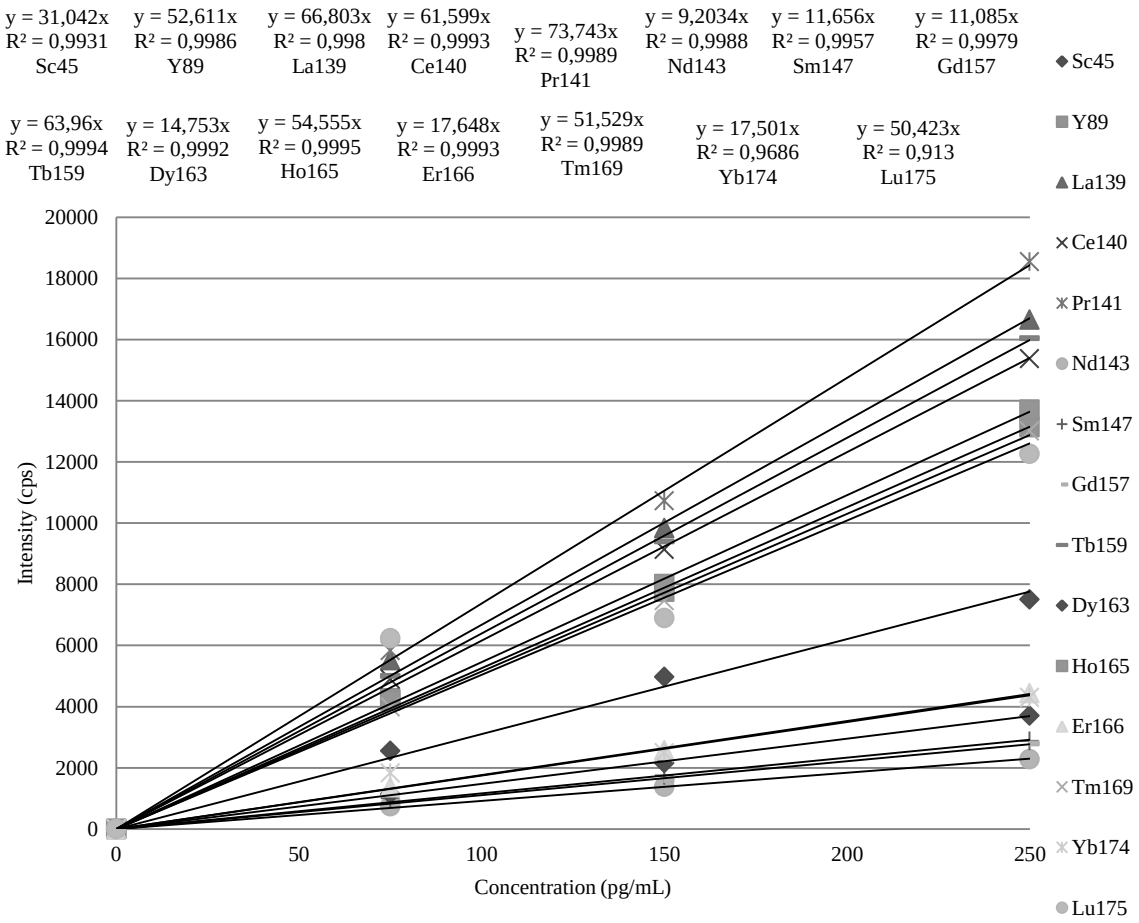

Figure A.2.5: Calibration curve of 15 REEs for the determination of REEs as trace impurities in standard solution of Eu by external standardisation with ICP-MS. The calibration statistics for the REEs can be seen in the figure.

Table A.2.1: Determination of LOD by the blank method. The table shows concentrations (pg mL^{-1}) of REEs found in the blank solution used for the determination of REEs as trace impurities in standard solution of Eu.

	LOD1	LOD2	LOD3	LOD4	LOD5	LOD6	LOD7	LOD8	LOD9	LOD10
Sc	-0.86	-0.19	-1.93	-1.21	-2.66	-1.99	-1.33	-2.78	-3.00	-2.46
Y	-0.01	-0.14	-0.03	-0.11	-0.06	0.00	0.10	-0.01	-0.18	0.10
La	0.04	0.00	0.00	0.03	-0.01	0.06	0.13	0.07	0.18	0.13
Ce	0.01	0.03	0.04	0.01	0.00	0.02	-0.02	-0.03	0.02	-0.06
Pr	0.03	0.03	0.01	0.01	0.05	0.06	0.01	0.01	0.02	0.05
Nd	0.33	0.14	0.40	0.11	0.18	0.00	0.43	0.22	0.00	0.11
Sm	-0.15	0.06	0.09	-0.11	0.23	0.15	-0.09	0.45	-0.11	0.28
Gd	0.63	0.32	0.27	-0.09	-0.13	0.03	0.03	0.09	-0.18	-0.09
Tb	0.06	0.02	0.00	0.01	0.05	0.01	0.00	0.04	0.00	0.00
Dy	-0.09	0.02	-0.09	-0.05	0.04	0.09	-0.03	-0.07	0.14	-0.07
Ho	165	0.01	0.01	0.03	0.00	0.02	0.02	0.01	0.00	0.03
Er	166	-0.05	0.01	0.05	0.01	0.03	0.03	0.01	-0.03	-0.01
Tm	169	1.44	0.70	0.46	0.37	0.30	0.25	0.32	0.29	0.21
Yb	174	-0.06	-0.25	-0.32	-0.43	-0.51	3.18	-0.32	0.21	-0.42
Lu	175	-0.01	0.00	0.00	0.01	0.04	0.02	0.02	0.04	0.00

Table A.2.2: LOD and LOQ of the REEs calculated from the results in table A.2.1. The values are in pg mL^{-1}.

	Average	Standard deviation	LOD	LOQ
Sc	-1.84	0.92	2.76	9.21
Y	-0.03	0.09	0.27	0.91
La	0.06	0.07	0.20	0.66
Ce	0.00	0.03	0.09	0.29
Pr	0.03	0.02	0.06	0.20
Nd	0.19	0.15	0.46	1.53
Sm	0.08	0.20	0.60	2.00
Gd	0.09	0.25	0.76	2.52
Tb	0.02	0.02	0.07	0.23
Dy	-0.01	0.08	0.24	0.80
Ho	0.02	0.01	0.03	0.10
Er	0.01	0.03	0.10	0.34
Tm	0.45	0.38	1.15	3.82
Yb	0.10	1.10	3.31	11.04
Lu	0.02	0.02	0.05	0.18

A.3. Chromatograms of mass 168 and 175 and their signal intensities with various combinations of ICP RF-power and nebulizer gas flow rate in diluted standard solution of Yb

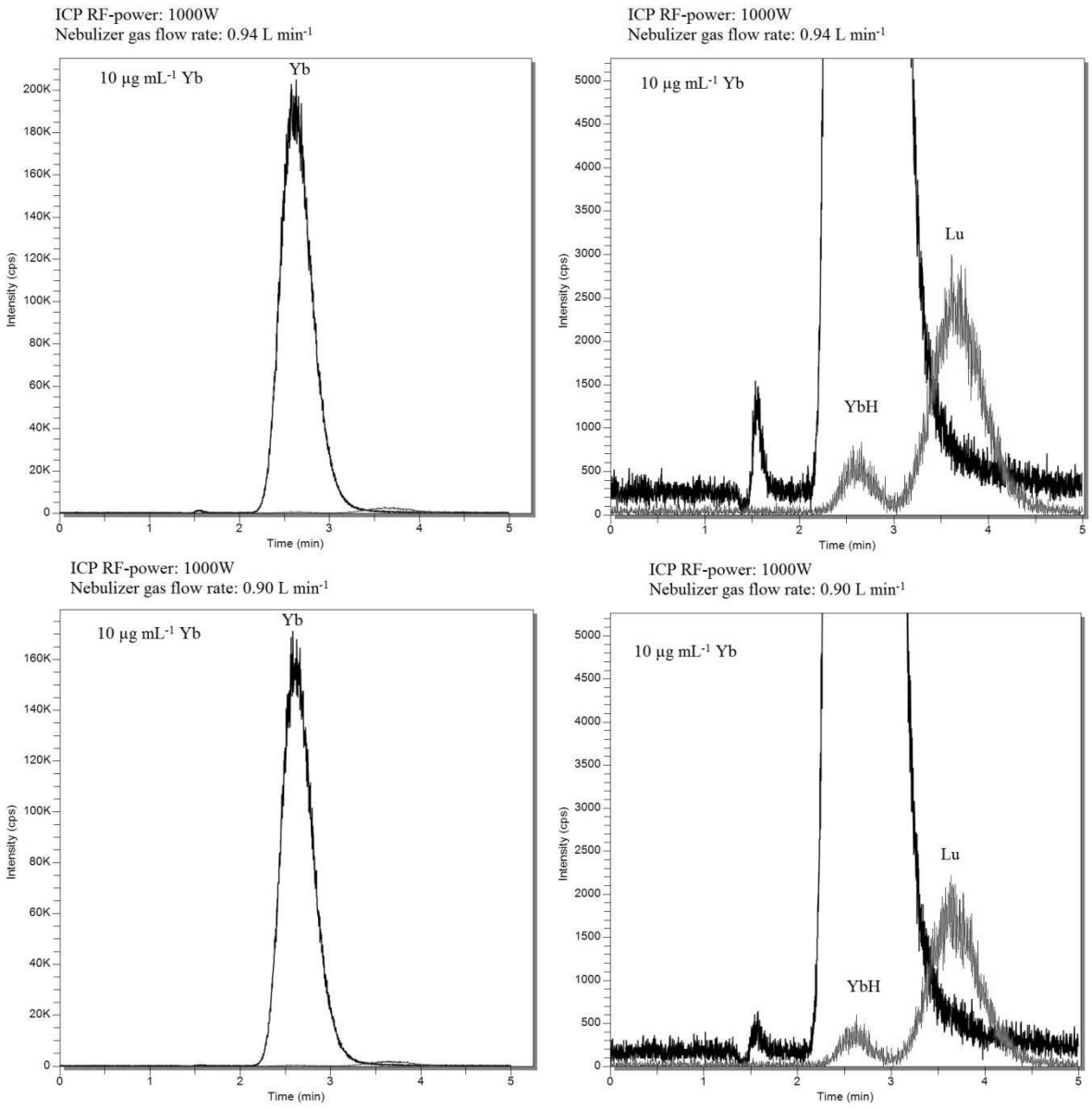

Figure A.3.1: Mass 168 is labelled as Yb, while mass 175 are labelled as YbH and Lu in the chromatograms.

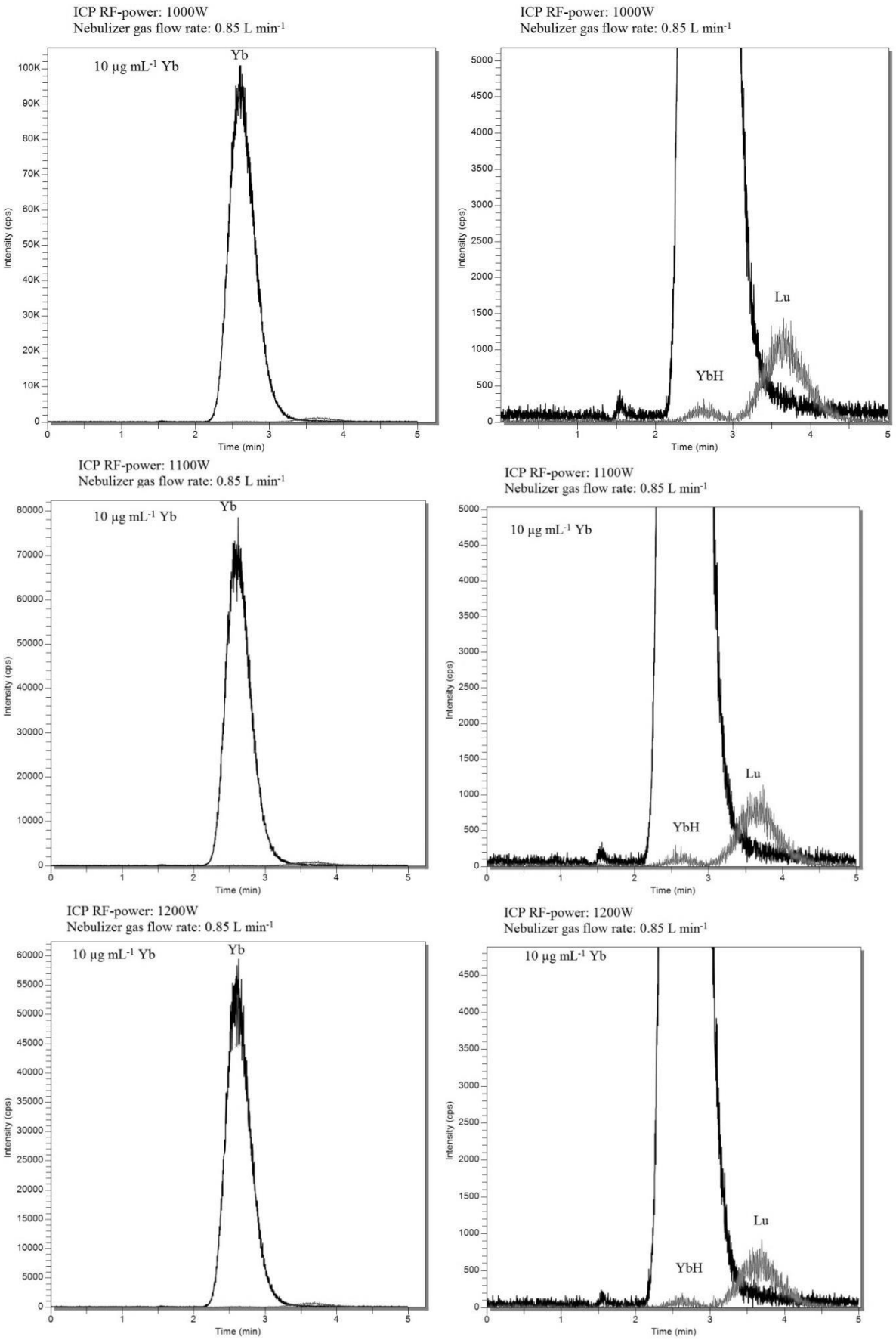

Figure A.3.2: Mass 168 is labelled as Yb, while mass 175 are labelled as YbH and Lu in the chromatograms.

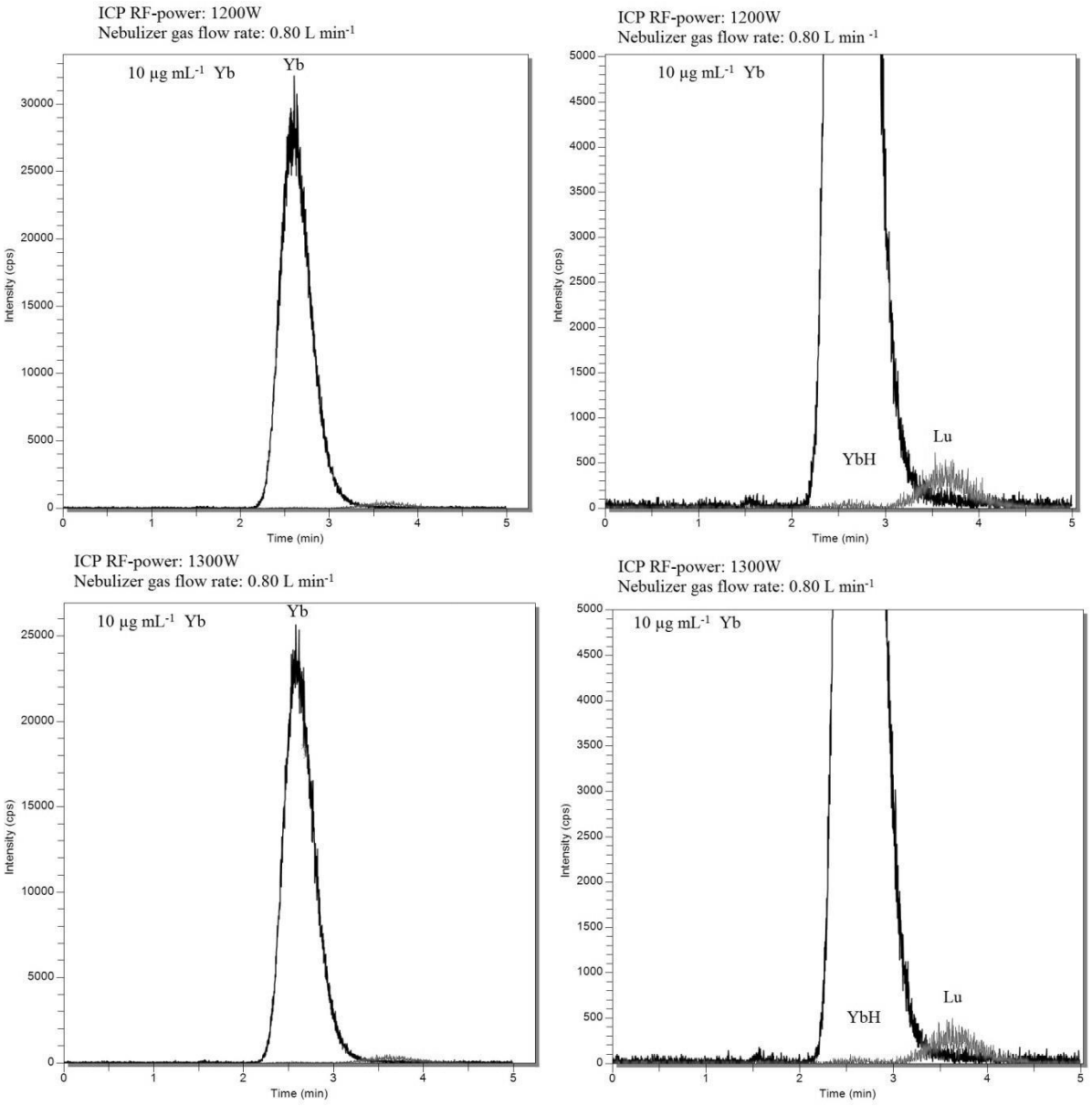

Figure A.3.3: Mass 168 is labelled as Yb, while mass 175 are labelled as YbH and Lu in the chromatograms.

A.4. Chromatograms of three sample solutions of Eu diluted from the standard solution to 10 µg mL^{-1}

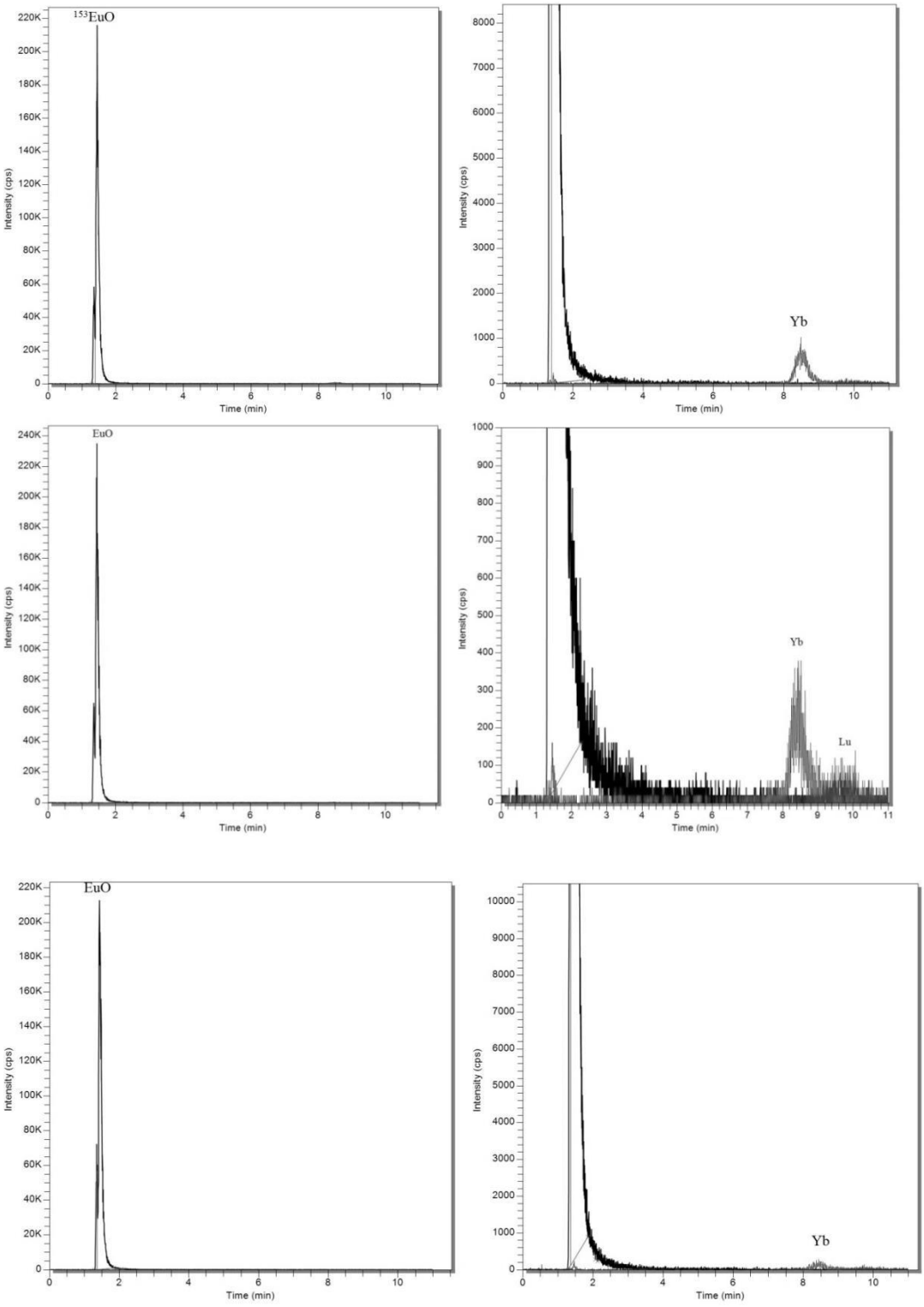

Figure A.3.4: Mass 169, 174 and 175 are labelled as EuO, Yb and Lu, respectively, in the chromatograms.

A.5. Calibration curves, statistics, and LOD for the determination of REEs as trace impurities in the standard solution of Yb and 99.9 % pure Yb_2O_3

The concentration of REEs in the standard solution of Yb, diluted to 10 µg mL^{-1}, and in Yb_2O_3, which was digested and diluted, determined in sections 4.7.2 and 4.7.3 were obtained by external standardisation. Their calibration curves and statistics are shown below.

In order to compare the results obtained from the different methods used in section 4.7.2 and 4.7.3, a t-test [54] was performed to compare two sample means. The null hypothesis is that the two methods give the same result, i.e. H_0: $\mu_1 = \mu_2$. But prior to the t-test, a two-sided F-test was performed to compare whether there is any significance between the two standard deviations of the methods.

An F-test for section 4.7.2 was performed in order to determine the precision of the standard operational plasma conditions versus altered plasma conditions. The null hypothesis of the F-test is that there is no significant difference between the precision of the two methods. The critical value of the two-sided F-test was taken from [51]. Three sample solutions were determined for each method and the degrees of freedom is therefore 2 for both numerator and denominator. s_1 and s_2 are the standard deviations of method 1 and 2, respectively.

- $F = s^2_1 / s^2_2 = 12^2/3^2 = 16$
- $F_{2,2}$ (P = 0.05) = 39
- $F_{2,2} > F$ and the null hypothesis is accepted, there is no significant difference between the two variances at a significance level of P = 0.05.

Since the F-test has established that there is no significance in the standard deviations of the total REEs determined by the two methods, a t-test was performed in order to compare whether the results obtained by the two methods give the same result. The null-hypothesis of the t-test is that the results are the same.

- $t = (x_1 – x_2) / (s \sqrt{((1/n_1) + (1/n_2))})$, x_1 is the experimental mean of method 1, and x_2 is the experimental mean of method 2. n_1 and n_2 are the sample sizes of method 1 and 2, respectively. s is the pooled estimate of the standard deviations, given that they do not differ from each other.

- $s^2 = ((n_1-1)s_1^2 + (n_2-1)s_2^2) / (n_1 + n_2 - 2)$, $s = 8.75$

- $t = (528-520) / (8.75 \sqrt{((1/3) + (1/3))}) = 1.12$.
- t_4 ($P = 0.05$) = 2.78.
- $t < t_4$, the null hypothesis is accepted. Both the methods give the same results.

The calculations above calculated the differences of the standard deviations and the total amount of REEs determined by the method with standard operational conditions and parameters of the ICP-MS versus the altered plasma conditions in section 4.7.2. The other F- and t-tests in section 4.7.2 and 4.7.3 were calculated in the same manner.

A.5.1. Calibration curves, statistics, LOD and chromatograms of diluted standard solution of Yb

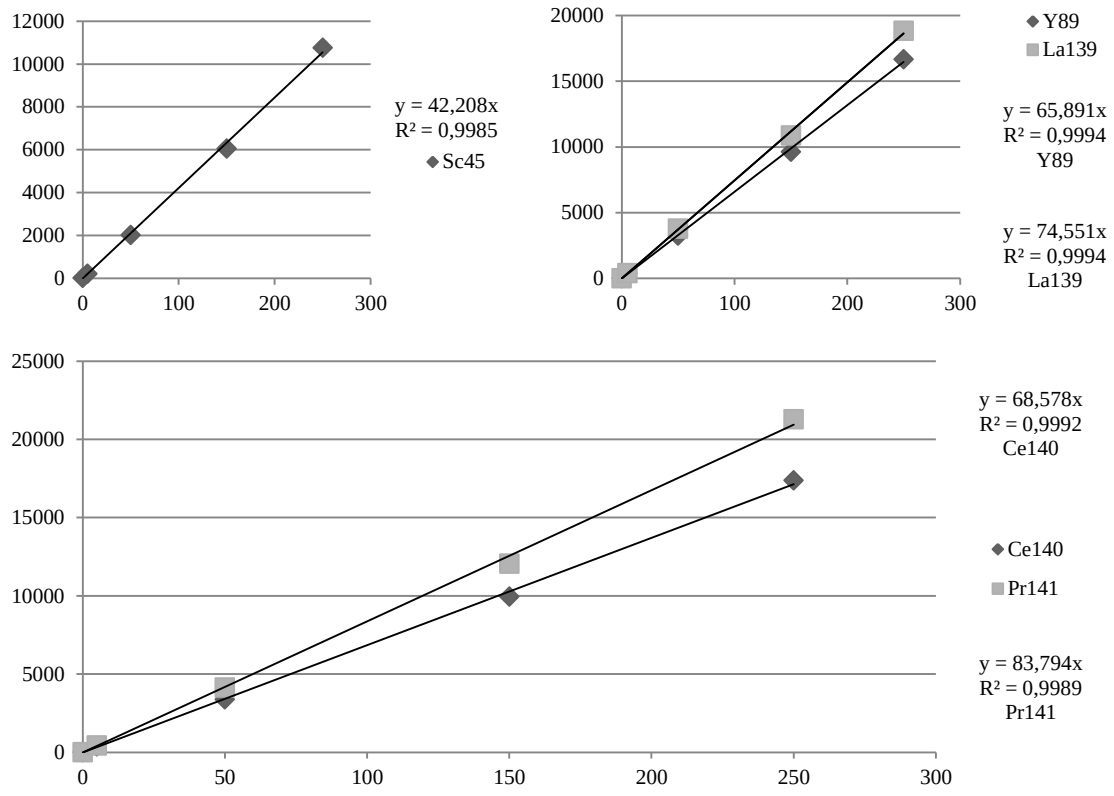

Figure A.5.1: Calibration curves of Sc, Y, La, Ce and Pr for the determination of REEs in the diluted standard solution of Yb by external standardisation with ICP-MS. The calibration curve statistics can be seen in the figures. The y-axis is signal intensity (cps) and the x-axis is the amount of REEs added (pg mL^{-1}).

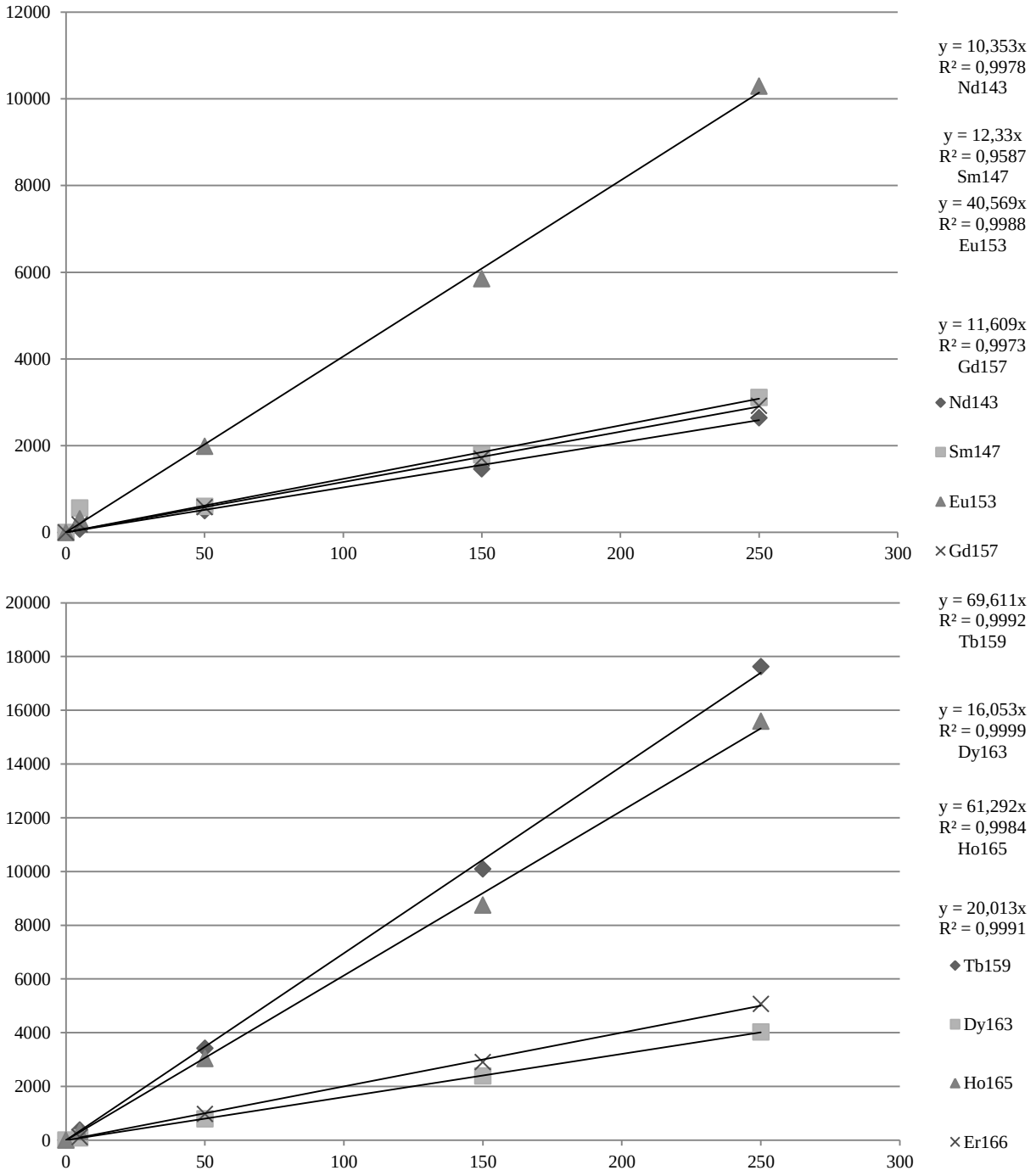

Figure A.5.2: Calibration curves of Nd, Sm, Eu, Gd, Tb, Dy, Ho and Er for the determination of REEs in the diluted standard solution of Yb by external standardisation with ICP-MS. The calibration curve statistics can be seen in the figures. The y-axis is signal intensity (cps) and the x-axis is the amount of REEs added (pg mL^{-1}).

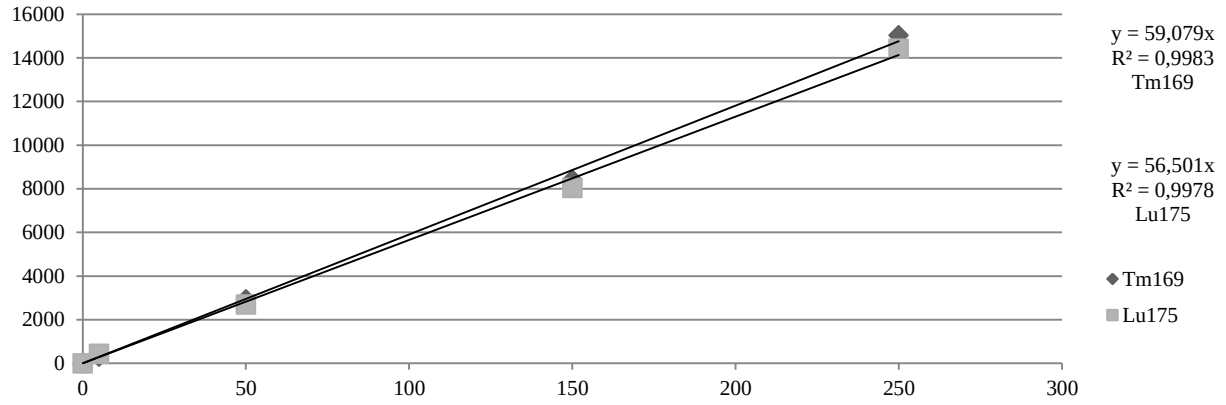

Figure A.5.3: Calibration curves of Tm and Lu for the determination of REEs in the diluted standard solution of Yb by external standardisation with ICP-MS. The calibration curve statistics can be seen in the figures. The y-axis is signal intensity (cps) and the x-axis is the amount of REEs added (pg mL^{-1}).

Table A.5.1: Determination of LOD by the blank method. The table shows concentrations (pg mL^{-1}) of REEs found in the calibration blank used for the purity determination of standard solution Yb.

	LOD1	**LOD2**	**LOD3**	**LOD4**	**LOD5**	**LOD6**	**LOD7**	**LOD8**	**LOD9**	**LOD10**
Sc	1.01	0.22	0.57	0.41	1.1	1.19	0.44	1.1	0.35	0.87
Y	1.37	1.38	1.41	1.36	1.32	1.31	1.32	1.36	1.29	1.42
La	0.97	1.09	1.31	1.3	1.37	1.48	1.66	1.78	1.86	2.05
Ce	1.47	1.42	1.44	1.43	1.4	1.47	1.42	1.44	1.45	1.47
Pr	1.67	1.66	1.66	1.67	1.66	1.67	1.67	1.66	1.68	1.66
Nd	1.38	1.43	1.52	1.28	1.22	1.41	1.51	1.36	1.38	1.33
Sm	-26.38	-26.21	-26.23	-25.8	-26	-25.71	-25.3	-25.86	-26.05	-25.88
Eu	0.03	0.01	0.16	0.13	0.14	0.14	0.12	0.01	0.11	0.1
Gd	-5.8	-5.9	-5.8	-5.95	-5.87	-5.89	-5.86	-5.86	-5.68	-5.9
Tb	1.32	1.32	1.29	1.32	1.34	1.35	1.36	1.3	1.31	1.31
Dy	0.32	0.23	0.22	0.4	0.38	0.38	0.35	0.28	0.28	0.42
Ho	1.82	1.82	1.81	1.8	1.83	1.82	1.82	1.81	1.81	1.8
Er	1.5	1.5	1.45	1.5	1.54	1.54	1.5	1.51	1.5	1.52
Tm	1.81	1.8	1.8	1.83	1.83	1.8	1.82	1.81	1.8	1.8
Lu	0	0.04	-0.01	0.06	-0.01	0.01	0.05	0.06	0.04	0.02

Table A.5.2: LOD and LOQ calculated from table A.5.1. The values are in pg mL^{-1}.

	Average	Standard deviation	LOD	LOQ
Sc	0.73	0.37	1.10	3.65
Y	1.35	0.04	0.13	0.43
La	1.49	0.35	1.04	3.46
Ce	1.44	0.02	0.07	0.24
Pr	1.67	0.01	0.02	0.07
Nd	1.38	0.09	0.28	0.93
Sm	-25.94	0.31	0.93	3.09
Eu	0.10	0.06	0.17	0.57
Gd	-5.85	0.08	0.23	0.75
Tb	1.32	0.02	0.07	0.22
Dy	0.33	0.07	0.21	0.71
Ho	1.81	0.01	0.03	0.10
Er	1.51	0.03	0.08	0.25
Tm	1.81	0.01	0.04	0.12
Lu	0.03	0.03	0.08	0.28

a) b) c)

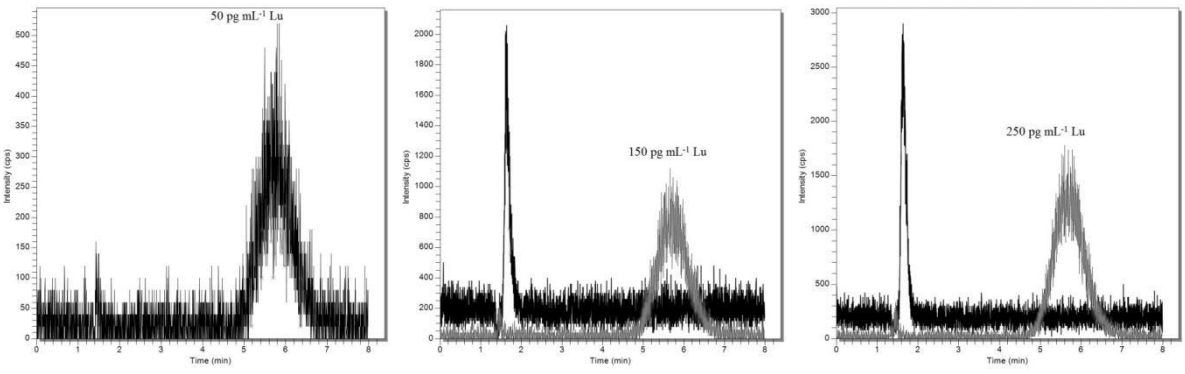

Figure A.5.4: Chromatograms of the calibration solutions of REEs at a) 50, b) 150 and c) 250 pg mL^{-1} for the determination of Lu in the diluted standard solution of Yb. The peak labelled as Lu corresponds to mass 175.

Table A.5.3: Peak areas of mass 175 in the calibration solutions of the REEs from figure A.4.4 found by integration via the Chromera software.

Calibration solution	Peak area of mass 175
50 pg mL^{-1}	17757
150 pg mL^{-1}	45580
250 pg mL^{-1}	75037

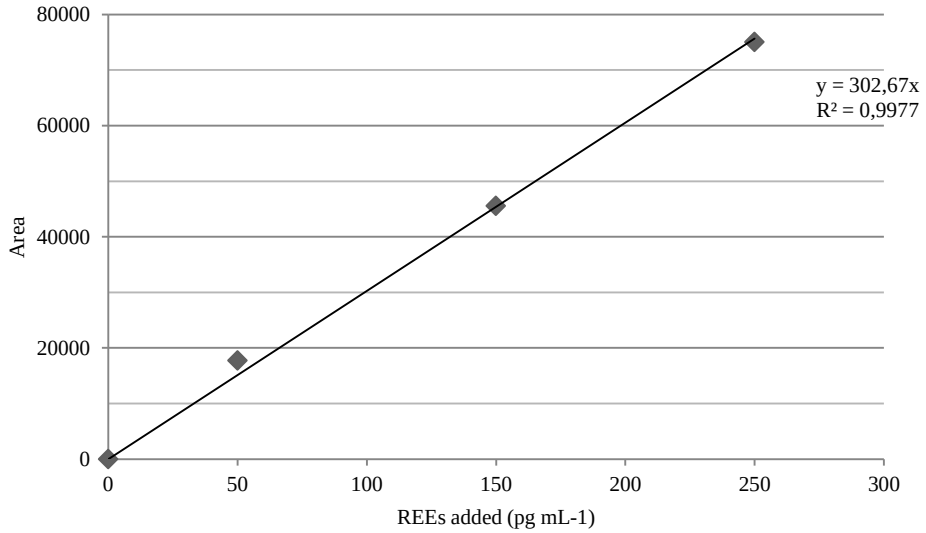

Figure A.5.5: Calibration curve and statistic of mass 175 (Lu) obtained by integrating the peak areas in figure A.4.3 via the Chromera software.

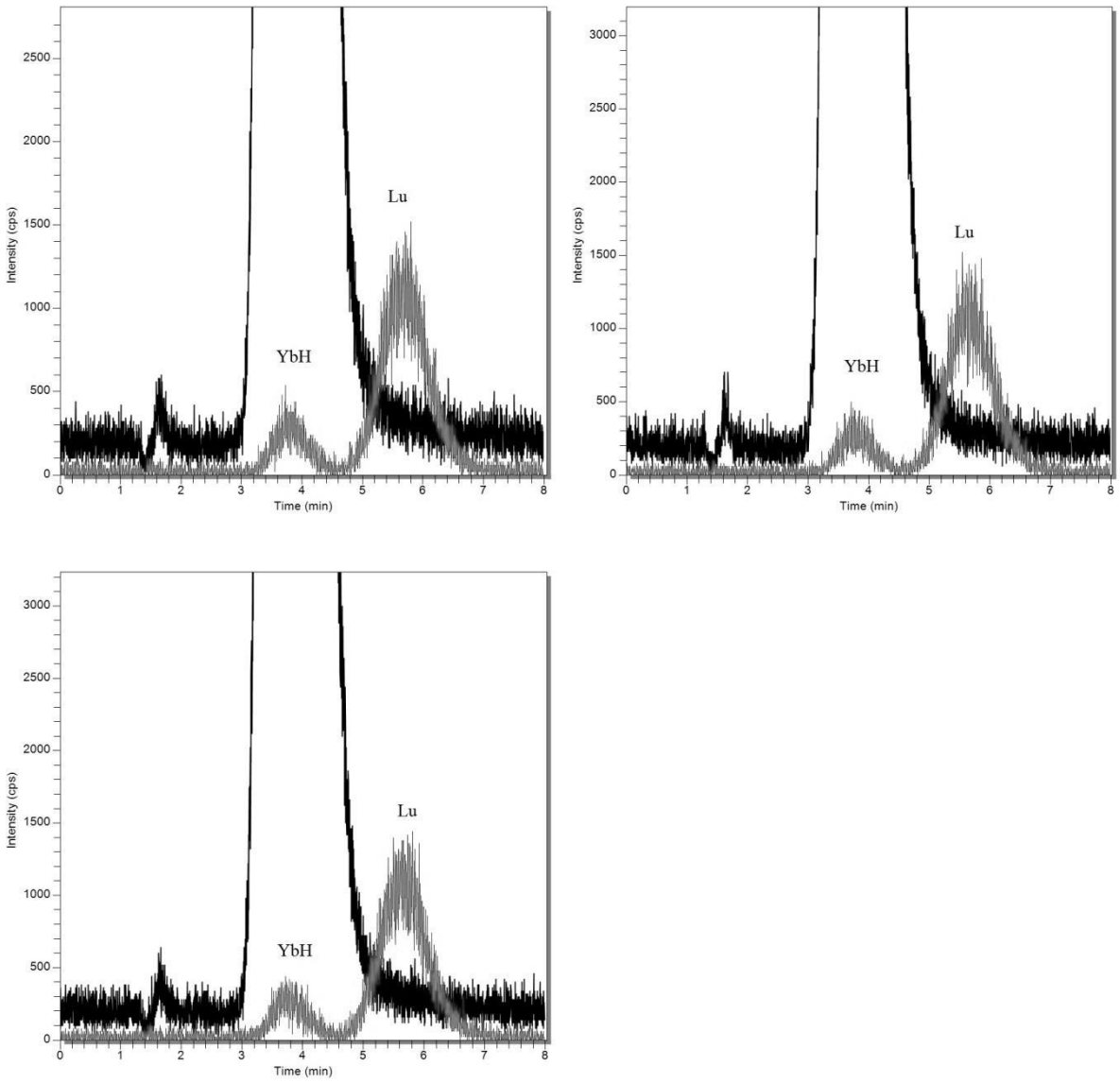

Figure A.5.6: Chromatograms of the three sample solutions of the standard solution of Yb, diluted to 10 µg mL^{-1}. Mass 175 is labelled as both YbH and Lu in the chromatograms.

Table A.5.4: Peak areas of mass 175 labelled as Lu in figure A.5.6 found by integration via the Chromera software.

Yb sample solution	Peak area of mass 175 labelled as Lu
Sample 1	64282
Sample 2	63026
Sample 3	63126

A.5.2. Calibration curves, statistics, and LOD of Yb standard solution determined with altered plasma conditions

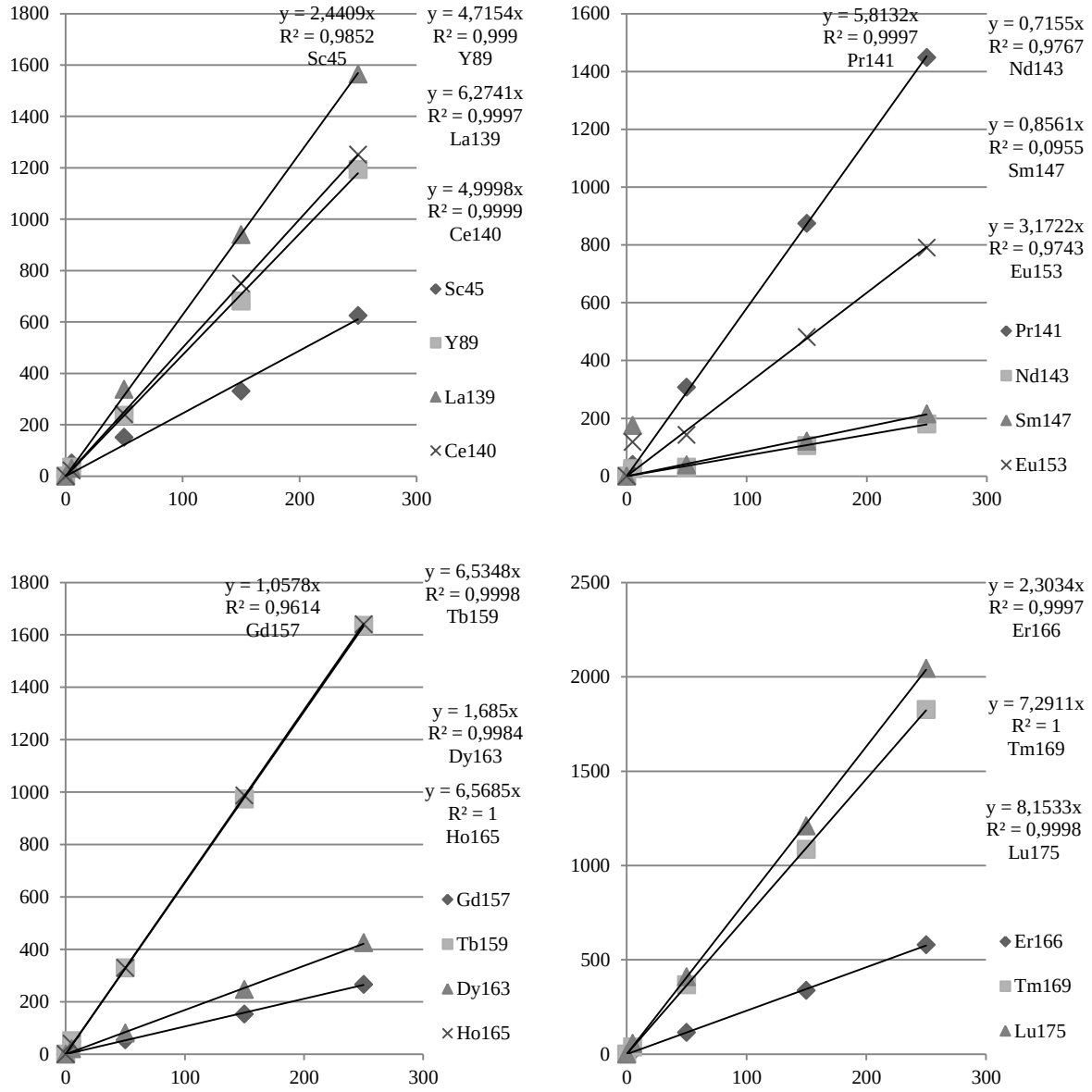

Figure A.5.7: Calibration curves of the REEs for their determination as trace impurities in the standard solution of Yb, diluted to 10 µg mL^{-1} external standardisation with ICP-MS, where the ICP RF-power is 1300W and the nebulizer gas flow rate 0.80 L min^{-1}. The calibration curve statistics can be seen in the figures. The y-axis is signal intensity (cps) and the x-axis is the amount of REEs added (pg mL^{-1}).

Table A.5.5: Determination of LOD by the blank method. The table shows concentrations (pg mL^{-1}) of REEs found in the calibration blank used for the purity determination of standard solution Yb.

	LOD1	LOD2	LOD3	LOD4	LOD5	LOD6	LOD7	LOD8	LOD9	LOD10
Sc	-4,62	-3,9	-7,97	-5,93	-15,31	-7,9	-2,01	-4,77	-6,08	-18
Y	0,07	0,21	-0,57	-0,21	-0,28	-0,32	-0,21	0,11	-0,64	0
La	-2,13	-2,05	-2,02	-1,6	-2,1	-1,89	-2,05	-2,32	-1,92	-2,24
Ce	0,69	0,78	0,95	0,32	0,72	0,98	0,42	0,62	0,75	0,78
Pr	-2,27	-2,24	-2,27	-2,42	-2,33	-2,04	-2,33	-2,68	-2,59	-2,07
Nd	-13,38	-14,9	-17,16	-12,63	-17,67	-14,9	-13,13	-15,15	-13,38	-15,9
Sm	-311,1	-308,6	-309,2	-304,2	-309,6	-302,2	-311,1	-311,1	-309,2	-310,6
Eu	-19,55	-19,67	-19,09	-20,24	-19,2	-19,55	-19,55	-20,01	-19,67	-19,26
Gd	-29,02	-29,56	-26,7	-26,34	-28,31	-26,16	-27,24	-28,31	-27,59	-29,38
Tb	-1,81	-1,76	-1,76	-1,66	-1,61	-2,04	-1,76	-1,61	-1,68	-1,86
Dy	-2,68	-3,49	-2,48	-2,28	-2,18	-2,58	-2,58	-2,68	-2,38	-2,38
Ho	-0,65	-1,16	-0,65	-0,8	-0,98	-0,62	-0,75	-0,44	-0,7	-0,95
Er	-0,36	-0,29	-0,29	0,65	-0,8	-0,51	0,14	0,36	-0,51	-0,07
Tm	0,02	-0,48	-0,41	-0,14	-0,27	-0,41	-0,05	-0,3	-0,39	-0,18
Lu	0,39	0,16	0,08	-0,33	-0,14	0,04	0,12	-0,14	0,1	0,2

Table A.5.6: LOD and LOQ calculated from table A.5.5. The values are in pg mL^{-1}.

	Average	Standard deviation	LOD	LOQ
Sc	-7.65	5.11	15.32	51.07
Y	-0.18	0.28	0.85	2.84
La	-2.03	0.20	0.60	2.00
Ce	0.70	0.21	0.62	2.07
Pr	-2.32	0.20	0.60	2.01
Nd	-14.82	1.72	5.17	17.22
Sm	-308.70	3.06	9.19	30.63
Eu	-19.58	0.35	1.06	3.54
Gd	-27.86	1.25	3.74	12.45
Tb	-1.76	0.13	0.39	1.30
Dy	-2.57	0.36	1.09	3.63
Ho	-0.77	0.21	0.63	2.09
Er	-0.17	0.44	1.32	4.41
Tm	-0.26	0.17	0.51	1.68
Lu	0.05	0.20	0.61	2.04

A.5.3. Calibration curves, statistics. LOD and chromatograms of Yb_2O_3 digested and diluted to 8.7 µg Yb mL^{-1}

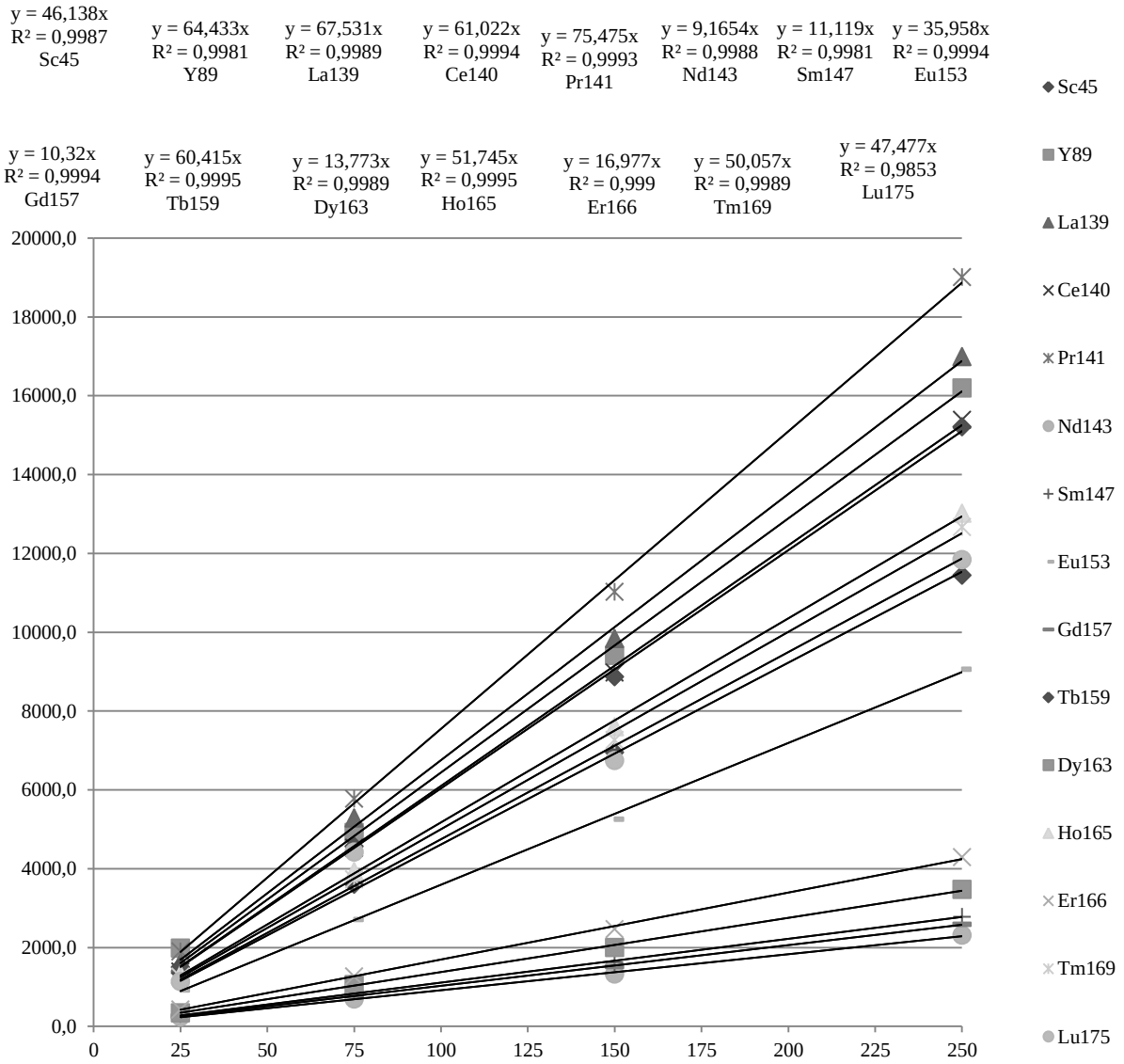

Figure A.5.8: Calibration curve of 15 REEs for the purity determination of digested and diluted Yb_2O_3 by external standardisation with ICP-MS. The calibration statistics can be seen in the figure. The y-axis is signal intensity (cps) and the x-axis is added REEs (pg mL^{-1}).

Table A.5.7: Determination of LOD and LOQ by the blank method. The table shows LOD and LOQ (pg mL^{-1}) of REEs found in three calibration blanks used for the purity determination of Yb_2O_3 that went through the same procedures as the digested sample of Yb. The LOD and LOQ were then calculated as an average of the three samples.

	LOD of blank 1	LOD of blank 2	LOD of blank 3	LOQ of blank 1	LOQ of blank 2	LOQ of blank 3	Average LOD	Average LOQ
Sc	2.03	2.43	1.28	6.78	8.11	4.25	1.9 ± 0.6	6 ± 2
Y	3.17	1.61	0.63	10.57	5.36	2.11	1.8 ± 1.3	6 ± 4
La	7.51	0.31	0.56	25.03	1.05	1.85	2.8 ± 4.1	9 ± 14
Ce	0.26	2.95	1.19	0.87	9.82	3.96	1.5 ± 1.4	5 ± 5
Pr	0.05	0.02	0.04	0.18	0.07	0.13	0.04 ± 0.02	0.13 ± 0.01
Nd	0.66	0.81	1.01	2.19	2.69	3.38	0.8 ± 0.2	2.8 ± 0.6
Sm	2.65	2.07	3.66	8.83	6.91	12.19	2.8 ± 0.8	9 ± 3
Eu	0.77	0.50	0.36	2.56	1.67	1.20	0.5 ± 0.2	1.8 ± 0.7
Gd	0.73	0.59	0.90	2.43	1.97	3.01	0.7 ± 0.2	2.5 ± 0.5
Tb	0.12	0.06	0.10	0.40	0.20	0.34	0.09 ± 0.03	0.3 ± 0.1
Dy	0.35	0.34	0.36	1.16	1.13	1.20	0.35 ± 0.01	1.16 ± 0.03
Ho	0.08	0.07	0.09	0.26	0.23	0.29	0.08 ± 0.01	0.26 ± 0.03
Er	0.17	0.10	0.05	0.55	0.32	0.16	0.10 ± 0.06	0.3 ± 0.2
Tm	0.09	0.02	0.03	0.29	0.08	0.09	0.05 ± 0.04	0.1 ± 0.1
Lu	0.15	0.33	0.36	0.49	1.10	1.19	0.3 ± 0.1	0.9 ± 0.4

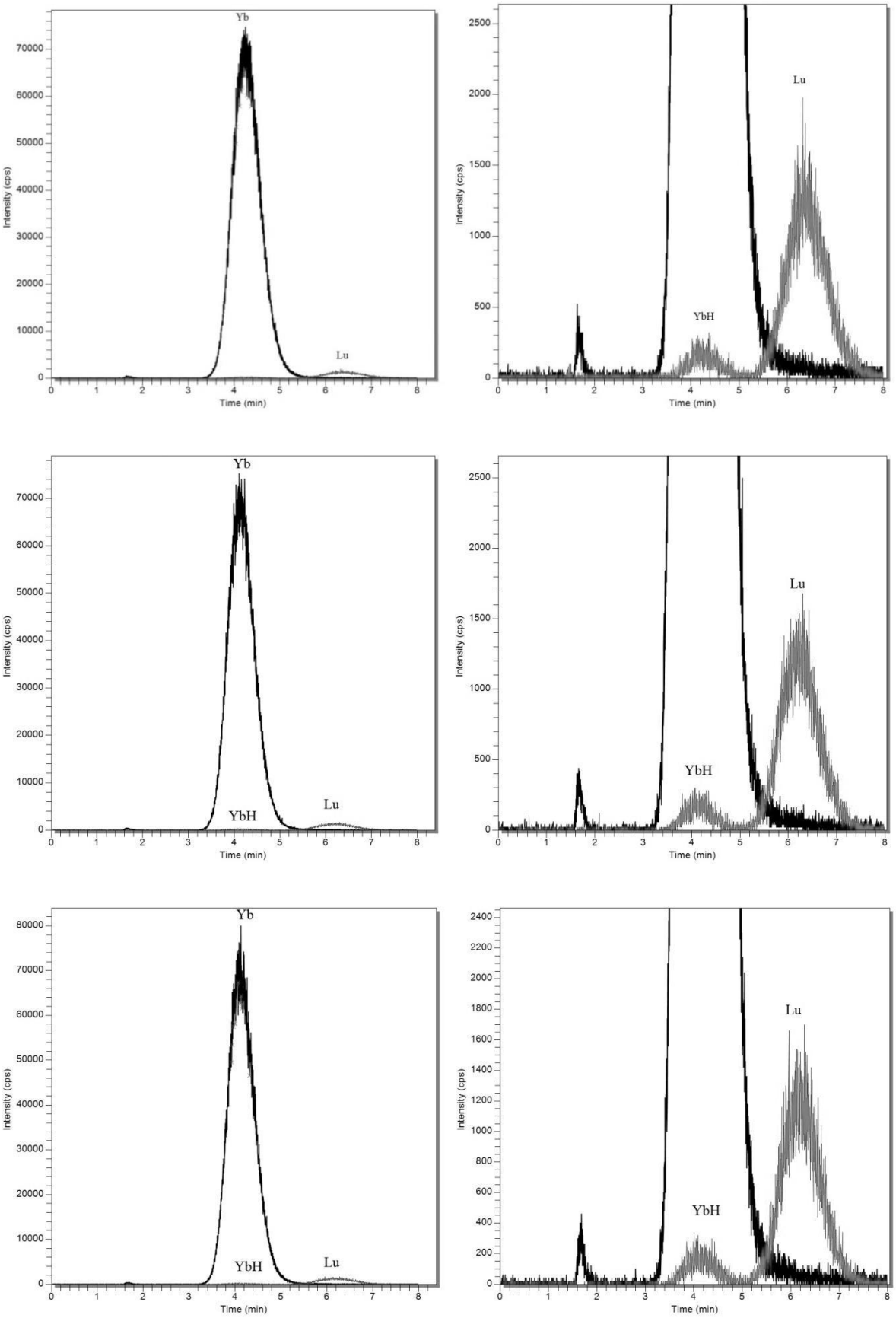

Figure A.5.9: Chromatograms of three digested samples of Yb_2O_3. Mass 168 is labelled as Yb, while mass 175 is labelled as YbH and Lu in the chromatograms.

a) b) c)

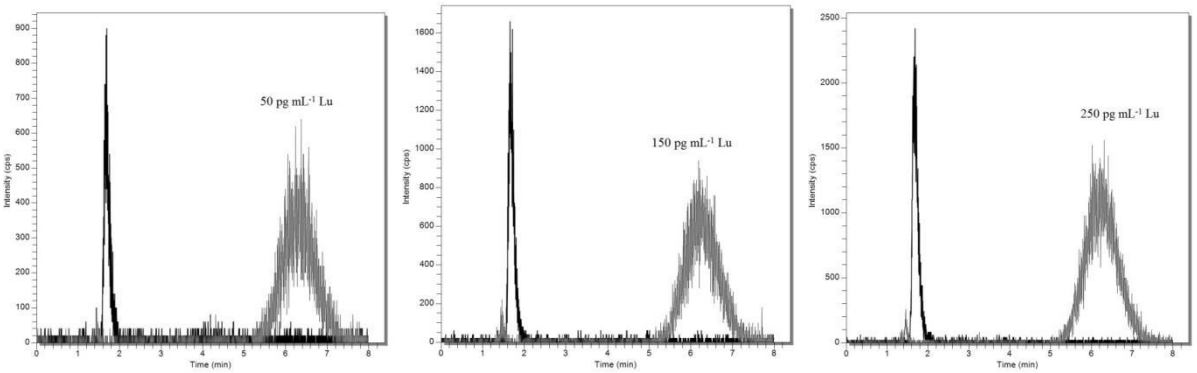

Figure A.5.10: Chromatograms of standard solutions with a) 50, b) 150 and c) 250 pg REEs mL^{-1} for the determination of Lu in the three digested and diluted samples of Yb_2O_3. Mass 175 is labelled as Lu in the chromatograms.

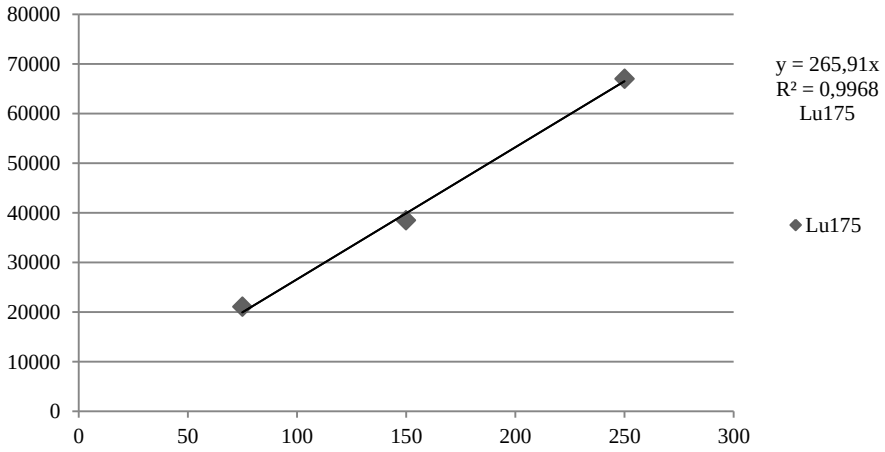

Figure A.5.9: Calibration curve of Lu found by HPLC-ICP-MS. The y-axis is the integrated area of Lu and x-axis is the amount of REEs added (pg mL^{-1}).